Bulgarian Academy of Sciences. Space Research Institute
Aerospace Research in Bulgaria. 17. 2003. Sofia

AEROSPACE RESEARCH IN BULGARIA
Volume 17 • Sofia • 2003
Space Research Institute
Bulgarian Academy of Sciences

Address
AEROSPACE RESEARCH IN BULGARIA
Space Research Institute
6, Moskovska St., Sofia 1000
Bulgaria
E- mail: office@space.bac.bg
http://www.space.bas.bg

Editor & Translation
Lubomira Kraleva

Technical Editor
Valeri Vassev

Aerospace Research in Bulgaria

17

Sofia, 2003

Contents

СЪДЪРЖАНИЕ

Bulgarian Academy of Sciences. Space Research Institute
Aerospace Research in Bulgaria. 17.2003. Sofia

THE ROLE OF AEROSPACE TECHNOLOGIES AND THE MILITARY FACTOR FOR NATIONAL SECURITY

Petar Getsov, Pavel Penev***

** Director of the Space Research Institute-Bulgarian Academy of Sciences*
*** Military Academy "G.S.Rakovski"*

Abstract

In the paper, the current state of using aerospace data in the Bulgarian Army is discussed. The potential application areas of aeropace images in military affairs are outlined. Peacetime, pre-war and wartime tasks are identified and classified. A National Centre for Aerospace Data and a Unit at the Bulgarian Army are suggested to be established to enhance the preventive factor in national security.

Currently, the Bulgarian army does not have in its disposition data from remote sensing Artificial Earth Satellites (AES) – military or civil. However, there is some experience with the use of two communication satellite systems, including "Inmarsat", the global satellite navigation system "NAVSTAR" by the Aviation and the Navy; the satellite meteorological system "Meteosat" for the needs of the Air Force; as well as the station of the military-topographic service of the Bulgarian Army (BA) for monitoring of AES by the system "NAVSTAR".

In the Military Doctrine of the Republic of Bulgaria, the following text was incorporated envisaging the future use of the space segment in military affairs:

"In modernization of the armed forces, priority shall be given to the systems for command, control, observation, investigation, communication, mutual acquaintance, computerization, navigation, **including space systems, equipment, and technologies** providing for compatibility with the armed forces of the NATO member-countries and transition to national information society."

By Order No.9/19.01.1998 of the Head of the General Staff (GS) of the BA, a work group was instituted to assess the need of aerospace data for the BA. At the GS, the Ministry of Defence (MD), and the various types of armed forces, archive space images from civil (American, French, and Russian) satellites for remote sensing of the Earth from Space were shown with resolution of 30 to 2 meters.

This analysis revealed that the army needs a unit to acquire, process, analyze, and distribute the necessary space data among all users from the corps. This unit is an affiliate of the National Centre for Aerospace Data (NCAD), which is intended to serve all users in the country (Fig.1).

The major prospective military areas where space images could be implemented are the following (Fig.2):

- assisting decision-taking based on models and data bases;
- digital cartographing and Geographic Information Systems (GIS);
- digital modelling of terrain, simulation, and training equipment.

According to current information war theory currently, the **decision-taking** process is a cognitive one. It takes place at all levels of military hierarchy: strategic, operative, and tactic, through the data-decision-action cycle. The sufficient amount of available correct data at each of these levels provides for the normal course of the cognitive cycle. If image data from the arena of military activity (AMA) is sent by a satellite almost on-line and the opponent does not have such data, a data superiority is available from the viewpoint of data provision of the actions of the armed forces. The implementation of this approach provides for a more expedient data-decision-action cognitive cycle. Thus, the actions of the corps and forces will be more expedient, too, and hopefully, they will be used in the most rational way.

In this direction, the unit shall have to solve the following specific problems:

a) with respect to the potential opponent
   - revealing, identification, and determination of the coordinates of military objects;
   - collecting data about the dislocation and composition of the Infantry, Air Forces, and Navy of the neighbouring countries;
   - controlling the observation of bilateral or multilateral military agreements on near-frontier zones;

- collecting data about the military-economic potential of the opponent;
- control of AMA equipment;
- collecting data about the accessibility and capacity of operative or technical directions;
- early identification of preparatory activities for aggression;
- monitoring of the progress of the troops of potential aggressors;
- collection of operative-technical data for planning of military actions.

b) with respect to one's one troops
  - control and assessment of operative masking;
  - updating of cartographic data for the country's territory and the pertaining territories of the neighbouring countries;
  - preparation and timely communication of topogeodetic data to the troops for the purpose of study and assessment of the AMA;
  - integral coordinate-time provision of the forces and equipment of the BA;
  - preparation of initial data with a view to the effective use of armament and military equipment;
  - coordination of satellite communication systems;
  - coordination of AMA real-time meteorological data and weather forecast for a couple-of-days period;
  - providing for the search and rescue of crews, aircraft, ships, and people in calamitous situations;
  - collection of data about the locality's pollution, radioactive pollution including, caused by great industrial failures and assessing their effect on the troops grouping;
  - monitoring of the state of water catchments and assessing the risk of potential floods;
  - assessing the effect of peace-time activity of the BA's garrisons on regional ecosystems;
  - provision of the forces and equipment participating in humanitarian or peace-establishing operations.

If, however, the opponent has already gained data superiority, the effort may be aimed at its reduction.

The above-listed tasks may be also classified as peace-time tasks, tasks in a period of threat, and war-time tasks. Regardless of the used classification, their analysis reveals that the nature of these tasks is mostly informative. Their accomplishment assumes the solution of a complex of technical, organizational, and financial problems, the timely preparation of dedicated military staff including.

Digital cartographing based on satellite images allows to make **digital maps** and to develop **geoinformation systems** referencing the individual activities, objects, and plans to geographic coordinates. Thus, various sections depending on the chosen symptom may be obtained providing invaluable data to military activity.

Digital terrain modelling allows to create data arrays for control of high-precision weapons, aviation, and unmanned aircraft. They can also be used to train crews by creating **virtual media** close to the real one thereby providing for the accomplishment of economical and highly effective **staff instruction and training**.

To implement these tasks in the strategic and operative units of the BA, three kinds of satellite data are needed: archive data, requested data, and current data.

Archive data is fundamental to assessment of the AMA, collection of additional cartographic data etc.

Requested data (up to several days) may be used to identify preparatory activities for potential aggression, to assess the masking of one's own troops, and to plan future battles.

Current data provides a nearly on-line assessment of the military-strategic circumstances in the region, including monitoring of the development of potential critical situations on the Balkans.

While the first two types of information can be provided for a compensation by distributing organizations, current data assumes the use of a ground-based station for receiving of images from remote sensing AES. In most countries, this equipment feed such data not to one institution, but to all concerned users related with economy, ecology, infrastructures, defence, and security.Albeit the current unfavourable economic circumstances, the Republic of Bulgaria can use data from various spacecraft with Bulgarian equipment on board.

Accounting for the expanding market of satellite data, for the purpose of this data's wholesome utilization for the needs of defence and other public activity areas, two approaches are possible:

a) through distributing organizations – regular obtaining of archive and requested data;
b) through construction of stations for data acquisition from remote sensing AES – obtaining of current data.

In Bulgaria, image data is distributed by the French firm "Spot Image", the Russian firm "Sovinformsputnik" and the Greek firm "Space

Imaging Europe" s.a. Professionals are also available who process these images by modern computer equipment, including by Silicon Graphics and Sun stations and develop GIS. This will be helpful in accomplishing both the first and the second version.To implement the second version for the needs of the country, a satellite data acquisition system should be bought which will supply images to the aerospace data unit of the MD as well. Suitable for the purpose are the mobile satellite data acquisition systems, which appeared recently on the market. They feature good enough characteristics and relatively low prices (about US$500,000). An example of such station is the Dutch system "RAPIDS" (Figs.3.1, 3.2, 3.3). The diagram of the joint Bulgarian-Dutch experiment is shown in Fig.4.

Accounting for the achievements and traditions of our country in Space use, by Decree of the Council of Ministers (CM) No.462/12.12.1997, an Interinstitutional Committee on Space Studies (Fig.5) was established. It accounts for and implements the interests and suggestions of the institutions, organizations, and private companies, among which the MD occupies a central place.The choice of the proper version lies within the competence of the Interinstitutional Committee on Space Studies. The solution of this problem is indispensable in view of the fact that the Republic of Bulgaria is winning recognition as an infrastructural joint on the Balkans comprising transportation corridors, petrol-, gas- and electricity-conducting networks, and a host-state to the staff of the multinational corps in South-East Europe.

Depending on its capacity, the prospective NCAD will provide data not only to the military, state, and private institutions, but to the state's leadership as well – the Advisory Council on National Security at the President's Office and the Council at the CM.The foundation of the NCAD at the BA is an essential prerequisite for strengthening of the preventive factor of national security, which becomes of essential importance now that the quantitative-qualitative features of the armament, military equipment, and the BA as a whole have dropped.

References

1. Михов М., Ролята и задачите на българската армия в системата за сигурност. Военен журнал No. 6, 1998.

2. Пенев П. Б., Спътниковата информация и борбата за информационно превъзходство, Военен журнал No. 6, 1998.

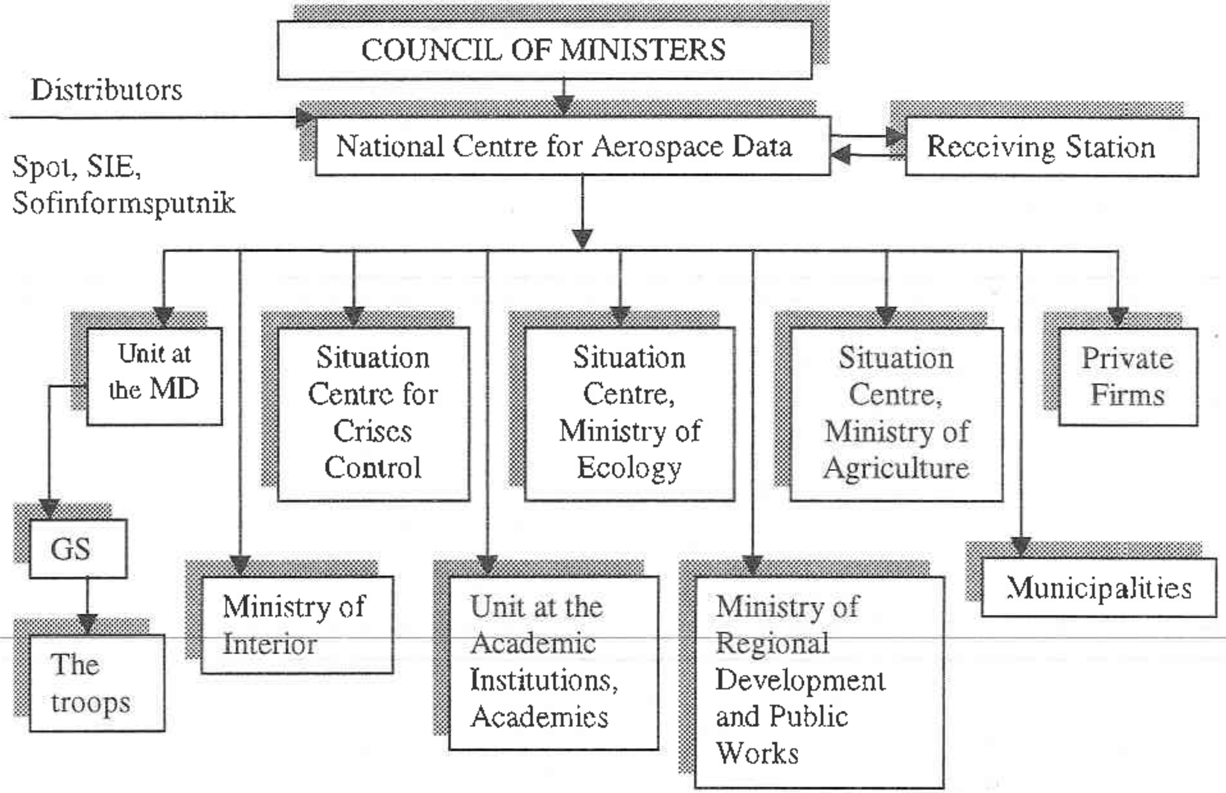
COUNCIL OF MINISTERS
Distributors
Spot, SIE, Sofinformsputnik
National Centre for Aerospace Data
Receiving Station
Unit at the MD
GS
The troops
Ministry of Interior
Situation Centre for Crises Control
Unit at the Academic Institutions, Academies
Situation Centre, Ministry of Ecology
Ministry of Regional Development and Public Works
Situation Centre, Ministry of Agriculture
Municipalities
Private Firms

Fig.1

UTILIZATION OF AEROSPACE IMAGES

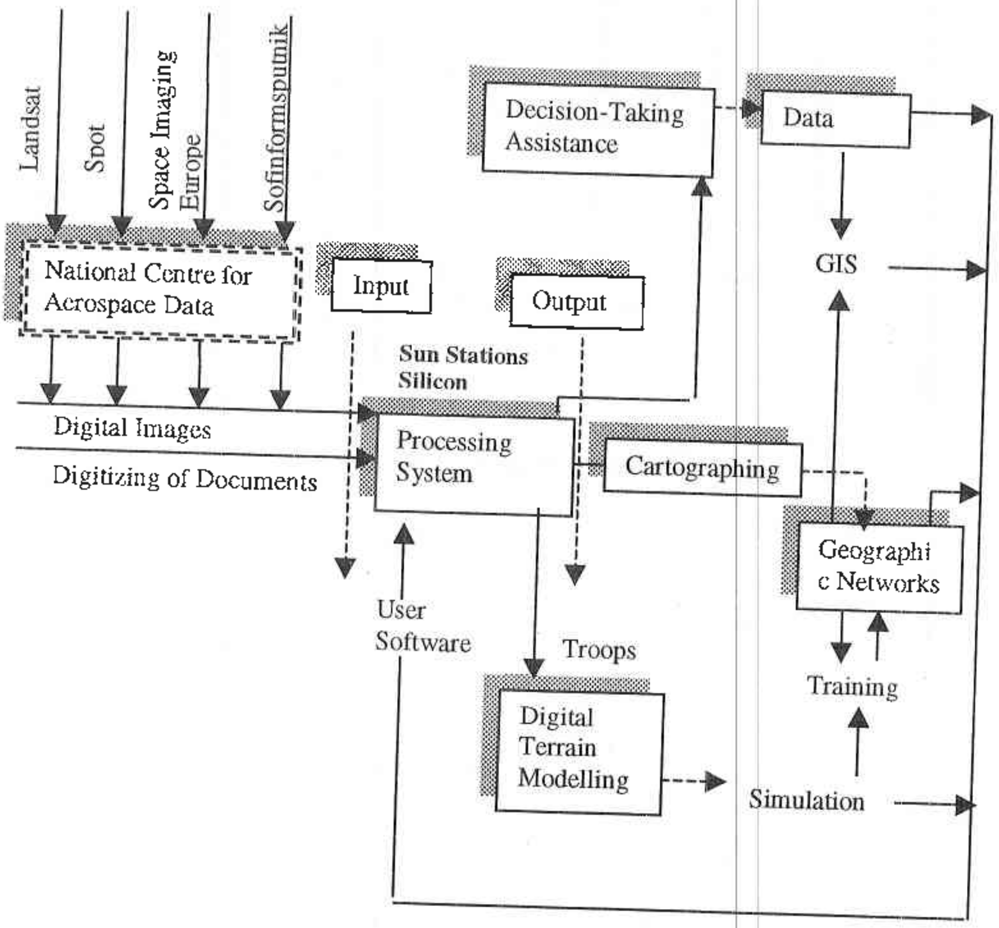

Fig. 2

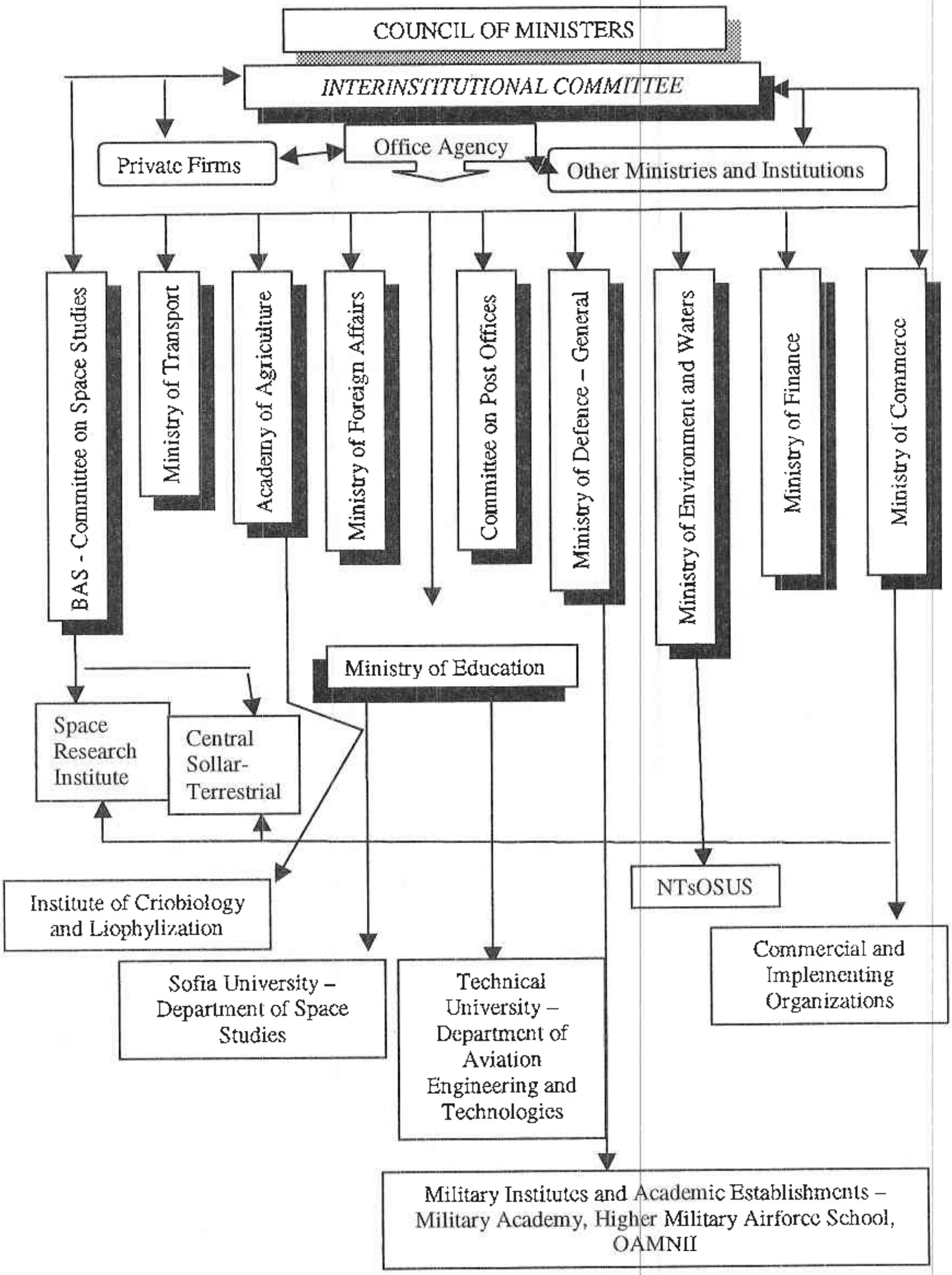
COUNCIL OF MINISTERS
INTERINSTITUTIONAL COMMITTEE
Private Firms
Office Agency
Other Ministries and Institutions
BAS - Committee on Space Studies
Ministry of Transport
Academy of Agriculture
Ministry of Foreign Affairs
Committee on Post Offices
Ministry of Defence – General
Ministry of Environment and Waters
Ministry of Finance
Ministry of Commerce
Ministry of Education
Space Research Institute
Central Sollar-Terrestrial
Institute of Criobiology and Liophylization
NTsOSUS
Commercial and Implementing Organizations
Sofia University – Department of Space Studies
Technical University – Department of Aviation Engineering and Technologies
Military Institutes and Academic Establishments – Military Academy, Higher Military Airforce School, OAMNII

Fig. 5

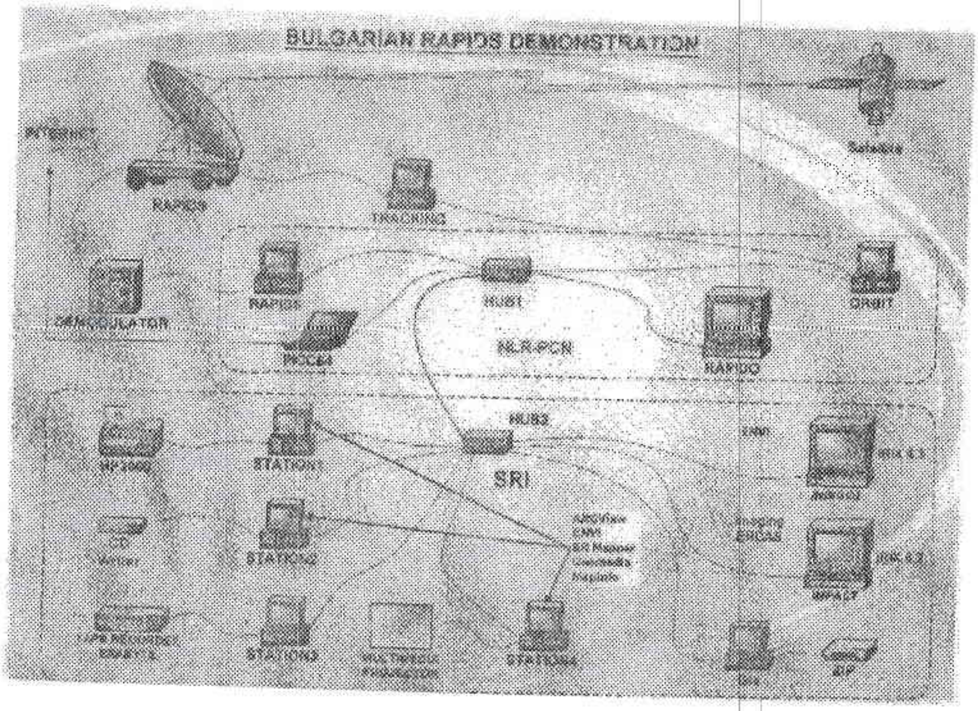
BULGARIAN RAPIDS DEMONSTRATION
INTERNET
Satellite
RAPIDS
TRACKING
DEMODULATOR
RAPIDS
HUB1
ORBIT
NLR-PCN
RAPIDO
HUB3
SRI
STATION1
STATION2
STATION3
STATION4
CD Writer
ArcView
ENVI
ER Mapper

Fig.3.1

Fig.4

RAPIDS

WHAT IS RAPIDS?

RAPIDS is a ground-based receiving station for receiving and processing of data from remote sensing satellites – ERS and SPOT

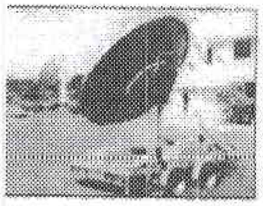

SYSTEM ADVANTAGES

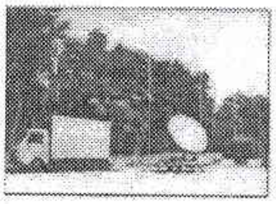

- Optional autonomous receiving of local data
- within an area with radius of 1,000 km.
- Easy transportation and installation.
- Automatic monitoring of satellites, collection and processing of data.
- Processing and archiving of data from optic and radar sensors.

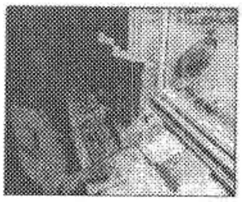

- Using standard PCs and software.
- Automatic check-in, easy maintenance,
- and prospects for development.
- Standard data source format compatible with various applications and technical equipment.

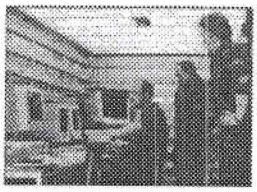

- Potential for system development with a view to receiving data from other satellites – LANDSAT, IRS, RADARSAT, EROS etc.
- Mission planning, education, training and simulation.

Joint project

Organized by the Ministry of Defence of the Republic of Bulgaria

and the Kingdom of Netherlands

Fig.3.2

RAPIDS

POTENTIAL APPLICATIONS OF THE OBTAINED DATA

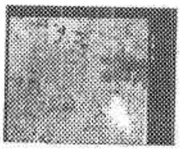

- Classification of the types of land cover for the purpose of updating the data from the project CORINE LANDCOVER.
- Mapping by using high-resolution data.

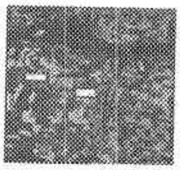

- Topical mapping and monitoring of forest massifs by optical and radar data combined with ground studies.
- Monitoring of natural disasters and failures. Effective identification of forest fires and floods, monitoring of their activity.

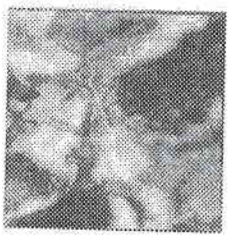

- Monitoring of areas with seismic activity.
- Working out of digital topographic maps.

- Obtaining of stereo images and deriving of digital models of the locality.
- 3D modelling for the purpose of terrain mapping and representing from various view angles and positions.
- Development of training complexes and simulation data bases.

Joint project

Organized by the Ministry of Defence of the Republic of Bulgaria
and the Kingdom of Netherlands

Fig.3.3

РОЛЯТА НА АЕРОКОСМИЧЕСКИТЕ ТЕХНОЛОГИИ И НА ВОЕННИЯ ФАКТОР ЗА НАЦИОНАЛНАТА СИГУРНОСТ

Петър Гецов, Павел Пенев

Резюме

В доклада се разглежда съвременното състояние на използването на аерокосмическа информация в Българската армия. Дефинирани са основните възможни области на приложение на аерокосмическите изображения във военното дело. Посочени и класифицирани са задачите в мирно време, в застрашаващия период и във военно време. Предлага се да бъде създаден национален център за аерокосмическа информация и звено към БАН с цел засилване на превантивния фактор в националната сигурност.

Bulgarian Academy of Sciences. Space Research Institute
Aerospace Research in Bulgaria. 17. 2003. Sofia

ONE POSSIBLE SIMPLIFICATION OF THE DYNAMICAL EQUATION GOVERNING THE EVOLUTION OF ELLIPTICAL ACCRETION DISCS

Dimitar Dimitrov

Space Research Institute - Bulgarian Academy of Sciences

Abstract

It is shown that, under the assumption of the viscosity law $\eta = \beta\Sigma^n$, the integrals involved in the equation describing the dynamics of the disc, may be replaced by polynomials and exponential functions of the eccentricity e, its derivative $\dot{e} = \partial e/\partial(\ln p)$ with respect to the focal parameter p, and the power index n. This transformation is useful for numerical solving of the dynamical second-order differential equation, because it avoids numerical evaluation of the integrals and, possibly, contributes to a more stable computational procedure. Our consideration of the problem is limited to the case when the values of the parameter n are not integers.

Observations and theoretical studies give evidences that the accretion discs around compact objects (in the Newtonian approach) are not only circular in shape, but may also have elongated structure. In the later case it is possible the eccentricity e of the particle orbits to vary with the focal parameter p $(e = e(p))$; e.g., the outer parts of the disc are more elongated than the inner ones. We shall consider smooth accretion discs in the sense that the possible spiral structures into the disc are not taken into account. The present paper is based on the theory of elliptical accretion discs developed by Lyubarskij et al. [1] and in what follows we shall use their approach and notations. These authors have obtained the dynamical equation governing the motion of particles alone elliptical streamlines and determining the functional dependence $e = e(p)$ for *a priori* assumed viscosity law $\eta = \beta\Sigma^n$. Here η is the viscosity coefficient, $\Sigma = \Sigma(p)$ is the disc surface density, β and n are parameters independent of p. They have also solved this equation (using numerical methods) for some values of the power index n.

The case of constant eccentricity e (when e does not depend on p and azimuthal angle φ for all points of the accretion disc) is a particular case of the set of solutions of the dynamical equation. It was treated in details in [2]. In this paper we concentrate on the case $e = e(p)$ and show that the dynamical equation may be simplified to some extend, avoiding numerical computation of the integrals involved in it. Following Lyubarskij et al. [1], we introduce a new variable $u = \ln p$ and write $e = e(u)$ instead of $e = e(p)$. Correspondingly, we denote by $\dot{e}$ the derivative $\dot{e} = \partial e/\partial u$. The streamlines of the fluid particles are described by the equation [1]:

$$\text{(1)}\qquad [\, Y\,(\partial Z/\partial \dot{e}) - Z\,(\partial Y/\partial \dot{e})\,]\,\ddot{e} + [\, Y\,(\partial Z/\partial e) - Z\,(\partial Y/\partial e) - Y^{2} e\,]\,\dot{e} + Y\,[\,(3/2)W - Z - (1/2)(1 - e^{2})\,Y\,] = 0\,.$$

In the above equation the auxiliary functions Y, Z and W (angle averaging with respect to φ has already been performed) are represented by the relations:

$$\text{(2)}\qquad 3Y(e, \dot{e}, n) = (1/2\pi)(p/GM)^{n/2}\,[\,(3 + e^{2} + 2e\dot{e})I_0 + (7e + e^{3} - 4\dot{e} - 2e^{3}\dot{e})I_1 + (4e^{2} - 8e\dot{e})I_2\,]\,,$$

$$\text{(3)}\qquad 3Z(e, \dot{e}, n) = (1/2\pi)(p/GM)^{n/2}\,[\,(3 + e^{4} - 2e\dot{e} - 2e^{3}\dot{e})I_0 + (13e + 2e^{3} + e^{5} - 4\dot{e} - 6e^{2}\dot{e} - 2e^{4}\dot{e})I_1 + (22e^{2} + 2e^{4} - 12e\dot{e} - 4e^{3}\dot{e})I_2 + (16e^{3} - 12e^{2}\dot{e})I_3 + (4e^{4} - 4e^{3}\dot{e})I_4\,]\,,$$

$$\text{(4)}\qquad 9W(e, \dot{e}, n) = (1/2\pi)(p/GM)^{n/2}\,[\,(9 - 2e^{2} + e^{4} + 4e\dot{e} - 4e^{3}\dot{e} + 8\dot{e}^{2} + 4e^{2}\dot{e}^{2})I_0 + (33e - 2e^{3} + e^{5} - 24\dot{e} + 4e^{2}\dot{e} - 4e^{4}\dot{e} + 8e\dot{e}^{2} + 4e^{3}\dot{e}^{2})I_1 + (48e^{2} - 72e\dot{e} + 8\dot{e}^{2})I_2 + (32e^{3} - 72e^{2}\dot{e} + 24e\dot{e}^{2})I_3 + (8e^{4} - 24e^{3}\dot{e} + 16e^{2}\dot{e}^{2})I_4\,]\,.$$

In such a way, at the very beginning of the problem for finding the dependence $e = e(p)$ by solving the dynamical equation (1), there arises a difficulty due to the inevitable appearance of 7 integrals defined as:

$$\text{(5)}\qquad I_k(e, \dot{e}, n) = \int_0^{2\pi} \cos^{k}\varphi\,(1 + e\cos\varphi)^{n-2}\,[1 + (e - \dot{e})\cos\varphi]^{-n-1}\,d\varphi\,,$$

$$k = 0, 1, \ldots, 4\,,$$

(6) $$I_{0-}(e, \dot{e}, n) = \int_0^{2\pi} (1 + e\cos\varphi)^{n-3} [1 + (e - \dot{e})\cos\varphi]^{-n-1}\, d\varphi ,$$

(7) $$I_{0+}(e, \dot{e}, n) = \int_0^{2\pi} (1 + e\cos\varphi)^{n-2} [1 + (e - \dot{e})\cos\varphi]^{-n-2}\, d\varphi .$$

Integration over φ describes the angle averaging along the streamlines. Coefficients of the equation (1) depend on $e = e(u \equiv ln\ p)$, $\dot{e} = \dot{e}(u \equiv ln\ p)$ and the power index n, which is assumed to be independent of p and φ. The above integrals (5) - (7) are considered for values of $e(u)$ and $\dot{e}(u)$ which satisfy the restriction $|e - \dot{e}| < 1$, so no singularities arise during the integration. This requirement is connected to the condition that the metric in the curvilinear coordinates (p, φ) must be nonsingular and self-adjoint orbits do not intersect. Finding the solution of equation (1) is complicated by the fact that the unknown function $e(u)$ and its derivative $\dot{e}(u)$ enter into the integrands of (5) - (7). Substituting expressions (2) - (7) into the dynamical equation (1), describing the structure of the stationary accretion disc, leads to the following general form of this equation:

(8) $\sum[A_{ik}(e, \dot{e}, n)\, \ddot{e} + B_{ik}(e, \dot{e}, n)]\, I_i(e, \dot{e}, n) I_k(e, \dot{e}, n) = 0$, where the sum is over i and k (i, k = 0-, 0+, 0, 1, . . . , 4), and i is less or equal to k.

Functions A_{ik} and B_{ik} are polynomials in e, $\dot{e}$ and n. In the present paper we show that the integrals (5) - (7) can also be expressed as polynomials and exponential functions of e, $\dot{e}$ and n, avoiding in such a way the numerical integrations during the procedure of numerical solution of (8).

Using the identities $1 = \cos^2\varphi + \sin^2\varphi$, $1 = (1 + e\cos\varphi) - e\cos\varphi$, $1 = [1 + (e - \dot{e})\cos\varphi] - (e - \dot{e})\cos\varphi$ and integrating by parts, we can find relations which enable us to eliminate (in principle) the integrals I_4, I_2, I_1 and I_0. For example, for the first two integrals we have:

(9) $$(e - \dot{e})eI_4 = (n - 2)\dot{e}(e^2 - 1)e^{-3} I_{0-} - (n - 2)\dot{e}(e^2 - 1)e^{-3} I_0 + [2e + (n - 2)\dot{e}(e^2 - 1)e^{-2}]\, I_1 + (n - 2)\dot{e}e^{-1} I_2 - [3e + (n - 2)\dot{e}]\, I_3 ,$$

(10) $$(e - \dot{e})eI_2 = [3e + (n - 2)\dot{e}\,]I_1 + [2e^4 - 3e^2 + (-2n + 4)e\dot{e} - 4e^3\dot{e} + (n - 2)\dot{e}^2 + 2e^2\dot{e}^2] \times [(e - \dot{e})e]^{-1} I_0 + (n - 2)(e - \dot{e})(e^2 - 1)e^{-1} I_{0-} + (n + 1)e(1 - e^2 + 2e\dot{e} - \dot{e}^2)(e - \dot{e})^{-1} I_{0+} .$$

Further this approach *is not* appropriate to obtain solutions for $I_{0-}(e, \dot{e}, n)$ and $I_{0+}(e, \dot{e}, n)$, because another integrals (different from the system of the 7 integrals (5) - (7) must be involved; i.e., eliminating I_{0-} and I_{0+} , we would introduce new unknown integrals. It is reasonable then to use the derivatives of these integrals with respect to e and $\dot{e}$. Here we consider e, $\dot{e}$ and n as independent variables, because the analytical solutions $e = e(u)$ and $\dot{e} = \dot{e}(u)$ are so far unknown for us. We shall write the expressions for some of these derivatives:

(11) $\partial I_0/\partial e = (n - 2)e^{-1}I_0 - (n - 2)e^{-1}I_{0-} + (n + 1)(e - \dot{e})^{-1}I_{0+} - (n + 1)(e - \dot{e})^{-1}{}_0$

(12) $\partial I_0/\partial \dot{e} = (n + 1)(e - \dot{e})^{-1}I_0 - (n + 1)(e - \dot{e})^{-1}I_{0+}$,

(13) $\partial I_1/\partial e = (n - 2)e^{-1}I_1 - (n - 2)e^{-2}I_0 + (n - 2)e^{-2}I_{0-} - (n + 1)(e - \dot{e})^{-1}I_1$
$+ (n + 1)(e - \dot{e})^{-2}I_0 - (n + 1)(e - \dot{e})^{-2}I_{0+}$,

(14) $\partial I_1/\partial \dot{e} = (n + 1)(e - \dot{e})^{-1}I_1 - (n + 1)(e - \dot{e})^{-2}I_0 + (n + 1)(e - \dot{e})^{-2}I_{0+}$,
etc.

The recurrence dependence for the derivatives of I_2, I_3 and I_4 is obvious.

(15) $\partial I_{0-}/\partial e = [e(1 - e^2)]^{-1}\{[3 - 2(n - 1)e^2]I_{0-} + (n + 1)(2e^2 - e\dot{e})I_{0+} - 3I_0\}$,

(16) $\partial I_{0-}/\partial \dot{e} = (n + 1)\dot{e}^{-1}(I_{0+} - I_{0-})$.

For $\partial I_{0+}/\partial e$ and $\partial I_{0+}/\partial \dot{e}$ we also have a linear dependence on I_0 , I_{0-} and I_{0+}; for brevity we shall not write it here in an explicit form. For example, differentiating with respect to e and $\dot{e}$ the linear relation between $I_0(e, \dot{e}, n)$, $I_{0-}(e, \dot{e}, n)$ and $I_{0+}(e, \dot{e}, n)$, replacing the derivatives and also the integrals which differ from I_{0-} and I_{0+} , we shall obtain a linear homogeneous system for the later two integrals $I_{0-}(e, \dot{e}, n)$ and $I_{0+}(e, \dot{e}, n)$. For our purposes, it is enough to use not the full solution, but only the proportionality relation between I_{0-} and I_{0+} :

(17) $I_{0-}(e, \dot{e}, n) = D_{0-}(e, \dot{e}, n)I_{0+}(e, \dot{e}, n)$,

where $D_{0-}(e, \dot{e}, n)$ is a polynomial in e, $\dot{e}$ and n. It should be stressed that in the above linear relation there is not a free term, which follows from the homogeneity of the above mentioned system. Returning to the expressions I_0 , I_1 , I_2 and I_4 , which also do not include free terms (in the sense, terms in which absent integrals of the type (5) - (7)), and replacing consecutively the results for I_{0-} , I_0 , I_1 , I_2 , we shall obtain proportionality relations of the same type as (17). There is, however, a gap in our solution for the system of integrals (5) - (7), because we have not found yet any expression for the integral I_3 . We can differentiate $I_3(e, \dot{e}, n)$ with respect to e or $\dot{e}$. In the later case the result is a differential equation for I_3 which takes a simple form :

$$(18) \qquad \partial[I_3 + (e - \dot{e})^{-1} I_2]/\partial\dot{e} = (n + 1)(e - \dot{e})^{-1} [I_3 + (e - \dot{e})^{-1} I_2] - n(e - \dot{e})^{-2} I_2$$

This equation enables us to find $I_3(e, \dot{e}, n)$ if the expression for $I_2(e, \dot{e}, n)$ is already known. It may be checked that a proportionality relation $I_3(e, \dot{e}, n) = D_3(e, \dot{e}, n)I_{0+}(e, \dot{e}, n)$, where D_3 contains a polynomial part in e, $\dot{e}$, n, and, additionally, exponential function of e, $\dot{e}$ and n, may serve as a general solution of the equation (18). Summarising all the results, we see that 6 of the integrals (5) - (7) are expressible through the seventh one:

$$(19) \qquad I_k(e, \dot{e}, n) = D_k(e, \dot{e}, n)I_{0+} (e, \dot{e}, n) , \qquad k = 0-, 0, 1, . . . , 4 .$$

$D_k(e, \dot{e}, n)$ are already known functions, containing polynomials in e, $\dot{e}$, n and exponential functions depending also on e, $\dot{e}$ and n. The dynamical equation (8) then becomes into the form:

$$(20) \qquad \{ \sum[A_{ik} (e, \dot{e}, n)\ddot{e} + B_{ik} (e, \dot{e}, n)]D_i (e, \dot{e}, n)D_k(e, \dot{e}, n) \} (I_{0+} (e, \dot{e}, n))^2 = 0 ,$$

where the sum is over i and k (i, k = 0-, 0+, 0, 1, . . . , 4), and i is less or equal to k. Taking into account that the integral $I_{0+}(e, \dot{e}, n)|_{|e-\dot{e}|<1}$ is always strictly positive, it is possible to cancel out ($I_{0+})^2$ and to rewrite (20) as:

$$(21) \qquad [\sum\underline{A}_{ik} (e, \dot{e}, n)]\ddot{e} + \sum\underline{B}_{ik} (e, \dot{e}, n) = 0 , \qquad i, k = 0-, 0+, 0, 1, . . . , 4 ,$$

where the both sums are again over i and k, and also i is less or equal to k. Here $\underline{A}_{ik}$ and $\underline{B}_{ik}$ are polynomials or exponential functions in e, $\dot{e}$ and n. Numerical integration of the equation (21) does not already require any computation of integrals (which include also the unknown solution $e(u)$ and its derivative $\dot{e}(u)$). So, the situation concerning solution of equation (1) is improved at least in order to simplify the computational procedure. Possibly, equation (21) admits applicability of more stable algorithms in order to find more accurate solution of the problem. Is it possible to obtain an analytical solution to the simplified equation (21) is still an open question, which is under investigation.

References

1. Lyubarkij, Yu. E., K. A. Postnov, M. E. Prokhorov. Eccentric accretion discs, Monthly Not. Royal Astron. Society, 266, 1994, 583 – 596.

2. Dimitrov, D. V. Elliptical accretion discs with constant eccentricity. II. Standard α-disc model, Aerospace Research in Bulgaria, 1999, No.15, 11–21.

ЕДНО ВЪЗМОЖНО ОПРОСТЯВАНЕ НА ДИНАМИЧНОТО УРАВНЕНИЕ, ЗАДАВАЩО ЕВОЛЮЦИЯТА НА ЕЛИПТИЧНИТЕ АКРЕЦИОННИ ДИСКОВЕ

Димитър Димитров

Резюме

Показано е, че при допускането на закон за вискозитета от вида $\eta = \beta\Sigma^{n}$, интегралите, включени в уравнението което описва динамиката на диска, могат да бъдат заместени с полиноми и експоненциални функции от ексцентрицитета e, неговата производна $\acute{e} = \partial e/\partial(ln\ p)$ спрямо фокалния параметър p и от степенния показател n. Тази трансформация е полезна при численото решаване на динамичното диференциално уравнение от втори ред, защото тя допуска да се избегне численото оценяване на интегралите и евентуално обуславя по-стабилна изчислителна процедура. Нашето разглеждане на задачата е ограничено до случая, когато стойностите на параметъра n не са цели числа.

Bulgarian Academy of Sciences. Space Research Institute
Aerospace Research in Bulgaria. 17. 2003. Sofia

SOME FEATURES OF α DISC AND ADVECTIVE-DOMINATED ACCRETION DISC. SELF-SIMILAR SOLUTIONS AND THEIR COMPARISON

Lachezar Filipov, Krasimira Yankova, Daniela Andreeva

Space Research Institute - Bulgarian Academy of Sciences

Abstract

A brief review of the features of Standard Shakura - Sunyaev Disc (SSD) and Advection - dominated Accretion Disc (ADAD) is discussed. In this paper, it is presented the physical bases, which we use to obtain the parameters, describing two models. The built theoretical systems are transformed in a suitably for operation view.

1. Introduction

The new, more functional theory about disc accretion - the advection theory [10], has appeared in the last years.

It has arisen because of that the standard theory gives common view on accretion flows, but couldn't explain any observant phenomena as: very high effective temperature (in standard theory disc is unstable - transforms to tore); non - thermal spectrum with power dependence of luminosity L from accretion rate $\dot{M}$ ($\sim M^2$ in two - temperature model); jets and s.o.

Other priority is that the advection - dominated flows may occur in both cases of optical depth - very large or very small it's value [10], which extend the volume of studying objects: active galactic nuclei, elliptical galactics, X-ray binaries and cataclysmic variables.

The conditions of transition between standard Shakura - Sunyaev disc and Advection - dominated disc are discussed by Abramowicz and Igumenchev [1]. They used a simple two - dimensional hydrodynamical model, assuming an instant destruction of SSD by some unknown physical process at radius r_{tms}. The result of their investigation shows that flux of matter from the destroyed SSD expands and forms thick disc (ADAF). The energy, which is necessary for expansion, is supplied locally by viscous heating. So expanded matter flows in all direction from source of matter and forms a geometrically thick disc.

Yamasaki [13] investigates the stability of two - dimensional ADAD against local thermal perturbations - for optically thin discs. In result he obtains that weakly unstable modes exist due to radiation effects, but the mode is stable when the thermal conduction is efficient. Because of turbulent heat diffusion, in two - temperature ADAF thermal perturbations damp.

Wu [12] proved, that in the case of very small advection, thermal instability exist when the disc is geometrically thin. If consider thermal diffusion, however it disappears. More than if the disc is advective - dominated thermal instability doesn't exist. There are enough dates that advection and thermal diffusion have significant effect on the stability of hot optically thin disc. The detail stability analysis of Wu shows that only two stable thermal equilibria of accretion disc exist. One of them is optically thin advection - dominated and the other is optically thick gas - dominated.

The family of self - similar solutions [10], where the temperature of accreting gas is almost virial and flow is quasi - spherical, define some of properties of the ADAF, as:

- the angular velocity of the flow Ω is less then Keplerian angular velocity Ω_k.
- ADAF is convective instable, because convection transfers energy from small to large radius.
- Bernoulli parameter b (scale changed) is positive in self - similar ADAF for wide range of parameters, e.g. gas may spontaneously expands to infinity.

Nakamura [9] elaborates global steady models of two - temperatures, advection - dominated accretion flows around black holes, as he pays attention to transonic region near black hole.

Chen and Abramowicz [4] present optically thin ADAD, described by full system of differential equations. They obtain global transonic solutions. As a result from this follows that far from sonic point, self - similar solutions is a good approximation to global structure of the flow. That is true if accretion rate is close to maximum value, above, which the solutions for optically thin disc don't exist. The simple self-similar solutions nowhere approach to complete solution [11].

In recent work we consider optically thick advection - dominated flows. The mainly aim of the paper is to show that the optically thin disc remains geometrically thin because of the advection [3]. It is known that when α increases the sonic point removes outward [4]. That is why such advective flow is supersonic, when viscosity parameter α is large for optically thick disc.

This letter is built as follows: It consists of two parts.

Part I: In § 2 we present the main physically characteristics of two flows. In § 3 is present the vertical structure. Comments of part I.

Part II: Paragraph 4 describes the equations of evolution of both discs. In § 5 we have obtained the self-similar solutions. Discussion of part II.

2. Basic equations

Accounting for the form of accretion flows we can use cylindrical coordinate system. The acceleration created by the potential in φ has the form:

$$\frac{V_\varphi}{r} = \frac{d\Phi}{dr} \tag{2.1}$$

where V_φ is the linear velocity in φ.

$$V_\varphi = \omega r \tag{2.2}$$

We shall use the Newtonian gravitational potential for standard discs:

$$\Phi = \frac{GM}{r} \tag{2.3}$$

and pseudo- Newtonian $\Phi = \dfrac{GM}{r - r_g}$ (2.4) for advective discs,

where

(2.5) $r_g = \dfrac{2GM}{c^2}$ is the gravitational radius of the black hole.

G – the gravitational constant, M – the mass of the central object, c -light velocity.

The angular velocities for both discs are:

(2.6) $$\omega_k = \sqrt{\frac{GM}{r^3}}$$

(2.7) $$\omega = \sqrt{\frac{GM}{r(r-r_g)^2}}$$

Geometrically thin discs are described by yet another parameter - surface density of the disc:

(2.8) $$\Sigma = \int_{-H}^{H} \rho dz \cong 2H\rho$$

Now we can form the basic equations of non-stationary accretion:

The mass conservation law:

(2.9) $$r\frac{\partial\Sigma}{\partial t} + \frac{\partial}{\partial r}(r\Sigma V_r) = 0$$

There is no difference in the equation for two discs, but V_r is much larger for the advective one.

The momentum conservation law:

(2.10) $$r\frac{\partial}{\partial t}(\Sigma r^2\omega) + \frac{\partial}{\partial r}(r\Sigma V_r r^2\omega) = \frac{1}{2\pi}\frac{\partial\theta}{\partial r}$$

θ is the momentum by viscosity forces:

(2.11) $\theta = 2\pi W_{r\varphi} r^2$

$W_{r\varphi}$ - vertically integrated viscosity per unit length of circumference.

(2.12) $W_{r\varphi} = \int_{-H}^{H} \omega_{r\varphi} dz = \nu \Sigma r \frac{\partial \omega}{\partial r}$

ν - kinetic viscosity;

(2.13) $\nu = \alpha V_s H$

V_s is sound velocity,

$r\frac{\partial \omega}{\partial r}$ is the displacement between two layers at differential rotation of the disc.

Thermal balance equation

The discs are optically thick. Therefore, Local Thermodynamical Equilibrium exists.

(2.14) $Q^+ \sim Q^-$

where Q^+ is the heating produced by viscosity:

(2.15) $Q^+ = \frac{1}{2} W_{r\varphi} \left(r \frac{\partial \omega}{\partial r} \right)$ and

(2.16) $Q^- = \frac{acT^4}{\tau}$ is radiated cooling

a - radiation constant.
T - effective temperature
τ - optical depth of the disc

(2.17) $d\tau = \rho \chi dz$

χ - opacity coefficient.

However, if for some reason, disc accretion rate increases and inflow time becomes shorter than photon emission time, the disc cannot reradiate generated energy. Part of radiation is caught by the flow, being thus generated, which reduces entropy gradient and the flow is directed to the center. Thereby, advection appears and the thermal balance takes the form:

$$(2.18)\quad Q_{adv} + Q^{+} = Q^{-}$$

where

$$(2.19)\quad Q_{adv} = \Sigma V_r T \frac{dS}{dr}$$

and $\frac{dS}{dr}$ radial gradient of the entropy.

Radial motion equations

$$(2.20)\quad \Sigma \frac{\partial V_r}{\partial t} + \Sigma V_r \frac{\partial V_r}{\partial r} - \Sigma \omega_k^2 r = W_{r\varphi} + G$$

$$(2.21)\quad \Sigma \frac{\partial V_r}{\partial t} + \Sigma V_r \frac{\partial V_r}{\partial r} - \Sigma\left(\omega^2 - \omega_k^2\right) r = -2\frac{\partial Hp}{\partial r} + W_{r\varphi} + G$$

$$(2.22)\quad P = \int_{-H}^{H} P dz$$

$(\omega^2 - \omega^2_K)$ – as a result of advection, disc equilibrium changes. An inertial spring is needed to keep the structure stable.

Using a similar system (2.9, 2.10, 2.18, 2.21), Narayan and Yi [10] have obtained that in advective discs:

$$(2.23)\quad \begin{aligned} V_r &= -c_1' \omega_k r \\ \omega &= \omega_k c_2 \\ V_s &= c_3 \omega_k^2 r^2 \end{aligned}$$

where c'_1 c_2 c_3 are dimensionless constants.

3. Vertical structure [8].

Equations of hydrostatical equilibrium:

$$(3.1)\quad \frac{1}{\rho}\frac{\partial P}{\partial z} = -\omega_k^2 z$$

$$(3.2)\quad \frac{1}{\rho}\frac{\partial P}{\partial z} = -\omega^2 z$$

Equation of continuity:

$$(3.3)\quad \frac{\partial \Sigma}{\partial z} = \rho$$

$$\Sigma = 2H\rho$$

Equation of radiation transfer:

$$(3.4)\quad \frac{c}{3\chi\rho}\frac{\partial\left(aT^4\right)}{\partial z} = -Q^+$$

$$(3.5)\quad -\Sigma V_r T\frac{\partial S}{\partial z} + \frac{c}{3\chi\rho}\frac{\partial\left(aT^4\right)}{\partial z} = -Q^+$$

and we take into account (2.23):

$$(3.6)\quad \frac{c_1^{\cdot}}{\sqrt{c_3}}V_s\Sigma T\frac{dS}{dz} + \frac{c}{3\chi\rho}\frac{\partial\left(aT^4\right)}{\partial z} = -Q^+$$

where

$$(3.7)\quad S = c_p \ln T - R\ln P$$

is the entropy of ideal gas, R is the gas constant.

The vertical gradient of radiating fluctuation is equal to energy released in disc:

$$(3.8)\quad \frac{\partial Q}{\partial z} = \varepsilon$$

Equation of ideal gas:

$$(3.9)\quad P = \rho \frac{RT}{\mu}$$

$$\frac{P}{\rho} = V_s^2$$

χ is opacity coefficient:

$$(3.10)\quad \chi = \frac{\chi_0 \rho^a}{T^b}$$

χ_0 Thompson's opacity coefficient:

a, b are constants.

The obtained differential system will be transformed by an appropriate group, corresponding to the approximation for a slim disc:

(3.11) $\Delta P \sim -P$; $\Delta Q \sim Q$; $\Delta T \sim T$; $\Delta Z \sim H$

This allows us to receive the solution in power dependences of independent variables or their dimensionless combinations – that is the self-similar solution [2].

To obtain a complete algebraic system we must also include the specific moments in the discs:

$$(3.12)\quad h_* = \omega r^2$$

as well as the average momentums of viscosity power between the disc's adjacent payers.

The following system of equations is obtained for both discs:

Standard disc	Equations holding for both discs	Advection-dominated disc
$h=\sqrt{GMr}$ (3.13)		$h_*=\frac{\sqrt{GMr^3}}{r-r_g}$ (3.14)
$\omega_k=\sqrt{\frac{GM}{r^3}}$ (3.15)		$\omega=\sqrt{\frac{GM}{r\left(r-r_g\right)}}$ (3.16)
$V_s=\omega_k H$ (3.17)	$P=\frac{\Sigma}{2H}V_s^2$ (3.18)	$V_s=\omega H$ (3.19)
$W_{r\varphi}=k\Sigma T$ (3.20) $k=-\frac{3}{2}\alpha\frac{R}{\mu}$	$F=W_{r\varphi}r^2$ (3.21)	$W_{r\varphi}=k'\Sigma T$ (3.22) $k'=-\left(\frac{1}{2}+c_2\right)\alpha\frac{R}{\mu}$
$Q^+=-\frac{3}{4}W_{r\varphi}\omega_k$ (3.23)		$Q^+=-\frac{1}{2}\left(\frac{1}{2}+c_2\right)W_{r\varphi}\omega$ (3.24)
$\varepsilon=aT^4=-\frac{3\chi\Sigma}{2c}Q^+$ (3.25)		$\frac{c_1'}{\sqrt{c_3}}\frac{V_s\Sigma T}{H}\left(c_p-R\right)+$ $+\frac{2acT^4}{3\chi\Sigma}=-Q^+$ (3.26)
$\chi=k_1\Sigma^{a_1}T^{b_1}H^{c_1}$ (3.27) $k_1=\frac{\chi_0}{2^{a_1}}$		$\chi=k_{1a}\Sigma^{a_{10}}T^{b_{10}}H^{c_{10}}$ (3.28) $k_{1a}=\frac{\chi_0}{2^{a_{10}}}$

This algebraic system can be solved if in (2.12) we take $\bar{\nu}$ in the advective case and use (2.7) и (3.12). We will obtain the explicit dependence of the parameters of both discs on their Σ and ω_k as well as the dependence of the average viscosity moments on Σ and h [6].

A solution system for both discs is obtained, different for both discs:

Standard α disc	Advection-dominated disc
$T = T_0 \Sigma^{2N_1} \omega_k^{2N_2}$ (3.29) $T_0 = \left\{ \frac{-27\alpha\chi_0}{2^{a_1+4} ac} \left(\frac{R}{\mu} \right)^{\frac{c_1+2}{2}} \right\}^{\frac{2}{6-2b_1-c_1}}$ $N_1 = \frac{a_1+2}{6-2b_1-c_1}$ $N_2 = \frac{1-c_1}{6-2b_1-c_1}$	$T = T_0^{\ a} \omega_k^{\ 2} r^2$ (3.34) $T_0^{\ a} = \frac{W_{r\varphi 0}^{a}}{k}$
$V_s = V_{s0} \Sigma^{N_1} \omega_k^{\ N_2}$ (3.30) $V_{s0} = \left(\frac{RT_0}{\mu} \right)^{\frac{1}{2}}$	$V_s = V_{s0}^{a} \omega_k r$ (3.35) $V_{s0}^{a} = \left(\frac{RT_0^{\ a}}{\mu} \right)^{\frac{1}{2}}$
$W_{r\varphi} = W_{r\varphi 0} \Sigma^{2N_1+1} \omega_k^{2N_2}$ (3.31) $W_{r\varphi 0} = \frac{-3\alpha RT_0}{2\mu}$	$W_{r\varphi} = W_{r\varphi 0}^{a} \Sigma \omega_k^{\ 2} r^2$ (3.36) $W_{r\varphi 0}^{a} = \alpha c_3$
$P = P_0 \Sigma^{N_1+1} \omega_k^{\ N_2+1}$ (3.32) $P_0 = \left(\frac{RT_0}{4\mu} \right)^{\frac{1}{2}}$	$P = P_0^{\ a} \Sigma \omega_k^{\ 2} r$ (3.37) $P_0^{\ a} = \left(\frac{V_{s0}^{a} c_2}{2} \right)$
$F = F_0 \Sigma^A h^B$ (3.33) $F_0 = W_{r\varphi 0} (GM)^{-\frac{-8+4b_1-2c_1}{6-2b_1-c_1}}$ $A = \frac{10+2a_1-2b_1-c_1}{6-2b_1-c_1}$ $B = \frac{18-8b_1+2c_1}{6-2b_1-c_1}$	$F = \left(2\frac{h_*}{h} - \frac{1}{2}\frac{\partial h_*}{\partial h} \right) h \Sigma \bar{\nu}$ (3.38)

4. Discussion

In the paper are shown the main theoretical principles when there is a development of the accretion in a standart and advection regimes. It's formed the horizontal and vertical structures of the accretion discs in two regimes, when the geometrically thin disc approximation is conserved.

We have emphasized on the processes, which determine the behaviour of the disc plasma in two considered cases.

References

1. Abramowicz M. A., IgumenshchevI. V., Lasota J. P., MNRAS, 293, 1998, 443-446.
2. Barenblatt G. I., Подобие, автомоделност, промежуточная асимптотика, Leningradp 1978.
3. Beloborodov A. M., 1999, arxiv: astro-ph/ 9901108
4. ChenX., Abramowicz M. A., Lasota J. P., ApJ, 476, 1997, 6169
5. Dibai E. A., Kaplan S. A., Размерности и подобие астрофизических величин, Москва, Наука, 1976.
6. Filipov L. G., Non-stationary disc accretion (in Russian), Moscow, 1993.
7. Filipov L. G., Space Research in Bulgaria, 6, 1990, 21-28.
8. Lipunova G. V., Shakura N. I., 2000, A&A, 356, 363-372.
9. Nakamura K.E., MatsumotoR., Kusunose M., Kato S., PASJ, 48, 1996, 761-769.
10. Narayan R., Yi. I., ApJ, 428, 1994, L13-L16.
11. Samarskii A. A., Galaktionov V. A., Режимы с обострением в задачах для квазилинейных параболических уравнений, Москва, Наука, 1987.
12. Wu X. B., MNRAS, 292, 1997, 113-119.
13. Yamasaki T., PASJ, 49, 1997, 227-223.

НЯКОИ ОСОБЕНОСТИ НА α ДИСК И АДВЕКТИВНО-ДОМИНИРАН АКРЕЦИОНЕН ДИСК. АВТОМОДЕБНИ РЕШЕНИЯ И ТЯХНОТО СРАВНЕНИЕ

Лъчезар Филипов, Красимира Янкова, Даниела Андреева

Резюме

Направен е кратък обзор на особеностите на Стандартния диск на Шакура-Сюняев и Адвективно-доминиращия акреционен диск. Представена е физичната основа, която ние използваме за да получим параметрите, описващи двата модела. Построените теоретични системи са трансформирани в подходящ за изследване вид.

Bulgarian Academy of Sciences. Space Research Institute
Aerospace Research in Bulgaria. 17. 2003. Sofia

MATHEMATICAL MODEL FOR COORDINATE ATTACHMENT AND RECTIFICATION OF SPACE IMAGES WITH HIGH RESOLUTION

Nikola Georgiev, Svetlin Fotev

Space Research Institute - Bulgarian Academy of Sciences

Abstract

In the paper, a strict method for georeference of high-resolution (1 - 3 m) space images is suggested, through determination of the coordinates of GCPs of the earth cover using GPS measurements. As a projection plane a reference (earth) ellipsoid is assumed and the ellipsoid heights of the identifies GCPs of the cover are accounted for. Determining the scale between the identified points provides for precise rectification of the space images.

1. Introduction

In the last decade, high-resolution space images became quite topical in the communities dealing with large scale mapping and remote sensing of the Earth. Research in this specific area gained a tremendous impetus after the first satellite images of the Earth with resolution from 1.0 to 3.0 m were received. The process of rapid improvement of space cameras and scanner systems [1,5], as well as of their carriers - Space Flying Apparata (SFA) was triggered. Nowadays, cameras of the type *KVR-1000* with focal distance $f = 10\ m$, flying at height $h = 220\ km$ (Fig.1) are used. They provide resolution of $2.0\ m$. Camera *KFA-3000* (f = 3.0 m; H = 270 km) provides resolution of $2-3\ m$. The results provided by the scanner systems *QuickBird, EROS-B, IKONOS1*, orbiting at heights of 600 *km* to 680 *km* and featuring an image resolution of 1 m. are similar. When the scanner systems are launched to higher orbits, lenses are used to insure long focal distances f = 10 m as is the case with *IKONOS*.

The current state-of-the-art with satellite images provides real opportunities for large scale mapping, upgrading of available maps, monitoring of the Earth scene and other practical and research tasks necessitating great precision in determining the mutual position of individual discrete points or contours in some particular region.

To accomplish these tasks it is necessary to refer the image coordinates to some identified ground control points (GCP) of the scene [2,3,4,5].

The various companies and corporations make efforts to supply the users with adequate software to solve this problem. It is of great importance to know the geometrical characteristics of the various types of satellite images (scenes). Users have to take them into consideration when choosing the program packages for processing of these images.

Prof. Gordon Petrie from the Glasgow University pays special attention to this problem [1]. He makes the conclusion that most of the users are aware that the greater part of the program packages for satellite image processing are unable to handle geometrical configurations.

This was confirmed by the distributor of the American-Israeli group IAI/Core of the *EROS* satellite on a conference organized by the Ministry of Defence of the Republic of Bulgaria in October, 2001. He stated that, with immediate determining of the GCP coordinates of the scene by GPS measurements, precision increases 3 to 4 times. Actually, this corresponds to the resolution of the satellite image.

As for remote sensing software, a lot of packages can only provide a very simple geometrical model of the images. Often, satellite images are treated in a 2D-coordinate system (the case with aerial photography), making no lieu with their real geometry, possible relief shift or image slope. In the last case, rectification is made using the method of the "rubber sheet". It is based on calculation of polynomials, aiming to make the image generally coincide with the referent coordinate system of the map, not removing the scene's geometrical deformations.

To fulfill its modern functions: small scale topographic mapping, revision of maps, monitoring of the environment, keeping a precise track of land scene changes etc., satellite images with high resolution have to undergo some preliminary processing [2,3,5,6]:

- high-precision coordinate reference of GCPs by GPS measurements;
- image rectification, accounting for changes in scale coefficients and relief pattern;
- using the Earth (referent) ellipsoid as a projection plane;
- taking into consideration ellipsoid heights;

- using strict methods for processing and evaluation of the results.

Under these condition we will have results precise enough to correspond to the aims of objectives of these modern satellite images.

2. New mathematical model for coordinate connection of the ground control points from the satellite image

The information which is received and used at satellite images is versatile with respect to both the determined elements and their location in time and space. For this reason, the coordinates of the determined values refer to different orthogonal coordinate systems, as follows:

- The coordinates of GCP X_j, Y_j, Z_j, ($j = 1,2,...,n$) from the real earth scene refer to the **Greenwich equatorial geocentric coordinate system** X, Y, Z, having its origin O in the Earth's mass center, axis Z pointing to the central pole, and axis X pointing to the cross point of the Equator and the Greenwich meridian (Fig. 1).

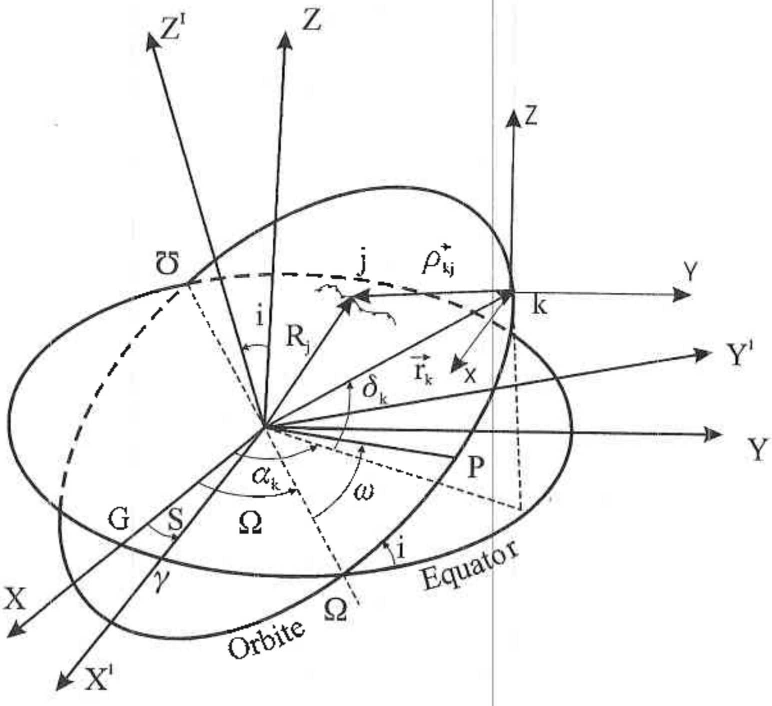

Fig. 1

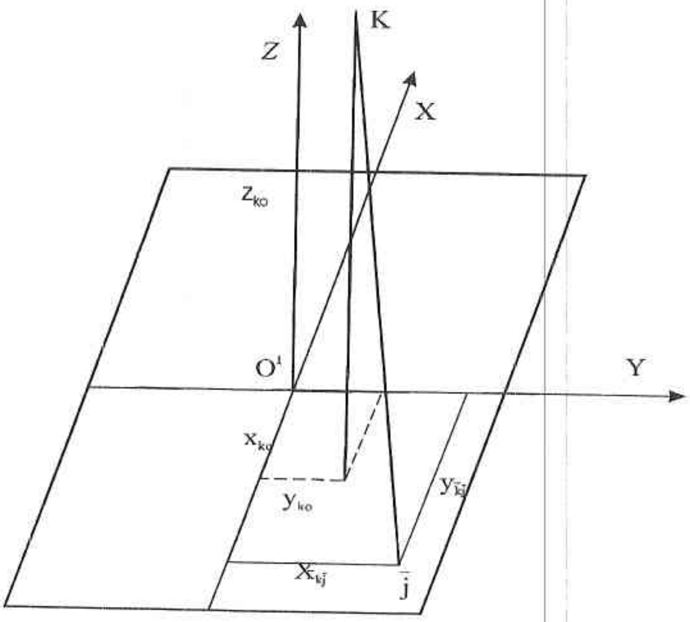

Fig. 2

- The coordinates of the satellite - $X_k^{'}, Y_k^{'}, Z_k^{'}$, *(k=*1, 2,..., *m)* are determined in the ***inertial equatorial geocentric coordinate system*** X', Y', Z' (Fig. 1).

- The coordinates of the images $\bar{j}$ $(x, y, z)_{k\bar{j}}$ of the GCPs are in the ***centric- satellite inertial coordinate system*** x, y, z (Fig. 2).

Quite often, in mathematical processing and evaluation of the precision of coordinate reference and rectification of the scenes, formulae are used where only the x_j and y_j coordinates of the GCPs images are determined, thereby actually handling the image in a 2D coordinate system. As stated and substantiated above, these equations, deprived of scale coefficients, do not provide a clear and accurate idea of the geometrical configuration of the image.

According to Fig. 1, we can draw the following coordinate relation between the centric-satellite vector-radius $\vec{\rho}_{kj}$, geocentric vector-radius $\vec{r}_k$ and topocentric vector-radius $\vec{R}_{kj}$, referred to the inertial geocentric systems, namely:

(1) $$\vec{\rho}_{kj} = (\vec{R}_j - \vec{r}_k) = \begin{vmatrix} X'_j - X'_k \\ Y'_j - Y'_k \\ Z'_j - Z'_k \end{vmatrix} = \rho_{kj} \begin{vmatrix} \cos\alpha_k \cos\delta_k \\ \sin\alpha_k \cos\delta_k \\ \sin\delta_k \end{vmatrix} = \rho_{kj} \begin{vmatrix} \xi_{kj} \\ \eta_{kj} \\ \zeta_{kj} \end{vmatrix},$$

where:

$\xi_{kj}{}^2 + \eta^2{}_{kj} + \zeta^2{}_{kj} = 1$

α_{kj} and δ_{kj} are the satellite's rectascensia and declination, accordingly.

$\vec{R}_j = (X', Y', Z')_j^T$ - coordinates of GCP - j in inertial coordinate system

$\vec{r}_k = (X', Y', Z')_k^T$ - coordinates of satellite in inertial coordinate system

Let us assume that vector $\vec{D}_{k\bar{j}}$ of the image $\bar{j}$ on the space image (Fig.2) of ground point j in a *centric-satellite inertial coordinate system* is as follows:

(2) $$\vec{D}_{kj} = \begin{vmatrix} x_{k\bar{j}} - x_{ko} \\ y_{k\bar{j}} - y_{ko} \\ z_{k\bar{j}} - z_{kj} \end{vmatrix} = D_{k\bar{j}} \begin{vmatrix} \xi_{kj} \\ \eta_{kj} \\ \zeta_{kj} \end{vmatrix},$$

where:

(3) $$D_{k\bar{j}} = \sqrt{(x_{k\bar{j}} - x_{ko})^2 + (y_{k\bar{j}} - y_{ko})^2 + (z_{k\bar{j}} - z_{ko})^2}$$

$(x, y, z)_{kj}$ - coordinates of the image of GCP - j on the satellite image;

$(x, y, z)_{ko}$ - coordinates of the main point of the scene O, obtained from the perpendicular drawn from the hind point of the lens's focal plane.

In reality, the main point does not coincide with the origin of the coordinate system O on the satellite image (Fig. 2). From (2), we receive the unit vector $\vec{D}^o{}_{k\bar{j}}$, whereas equation (3) will be uses as a norm factor:

$$(4) \qquad \vec{D}^{o}{}_{kj} = \frac{1}{D_{kj}} \begin{vmatrix} x_{kj} - x_{ko} \\ y_{kj} - y_{ko} \\ z_{kj} - z_{ko} \end{vmatrix} = \begin{vmatrix} \xi_{kj} \\ \eta_{kj} \\ \zeta_{kj} \end{vmatrix}$$

Formulae (1)-(4) provide the opportunity to define the point from the satellite image in a *centric-satellite inertial coordinate system.* But the coordinate reference of the images suggests that this be done in the *Greenwich system* defined above, in which the centric-satellite vector-radius is as follows:

$$(5) \qquad \vec{\rho}_{kj} = \rho_{kj} \begin{vmatrix} \cos(\alpha_{kj} - S_k)\cos\delta_{kj} \\ \sin(\alpha_{kj} - S_k)\cos\delta_{kj} \\ \sin\delta_{kj} \end{vmatrix} = \rho_{kj} \begin{vmatrix} \xi_{kj} \\ \eta_{kj} \\ \zeta_{kj} \end{vmatrix} = - \begin{vmatrix} X_k - X_j \\ Y_k - Y_j \\ Z_k - Z_j \end{vmatrix},$$

where:

$$(6) \qquad \rho_{kj} = \sqrt{(X_j - X_k)^2 + (Y_j - Y_k)^2 + (Z_j - Z_k)^2},$$

- S_k is the star time at Greenwich, corresponding to the moment t_k of receiving of the satellite image. The coordinates of *KJIA*- $(X,Y,Z)_k$ and of the GCP - $(X,Y,Z)_j$ are in *the Greenwich coordinate system.*

Using the operator $\vec{P}_o$, we can obtain the unit vector $\vec{D}_{kj}{}^{o}$, which points to *GCP- j from the scene* in the *Greenwich geocentric system,* namely:

$$(7) \qquad \vec{D}_{kj}{}^{o} = \vec{P}_o \begin{bmatrix} \xi_{kj} \\ \eta_{kj} \\ \zeta_{kj} \end{bmatrix} = \frac{1}{D_{kj}} \vec{P}_o \begin{bmatrix} x_{kj} - x_{ko} \\ y_{kj} - y_{ko} \\ z_{kj} - z_{ko} \end{bmatrix}$$

From formulate (5) and (7) we obtain the following equation:

$$(8) \qquad \vec{\rho}_{kj} = \rho_{kj} \begin{bmatrix} \xi_{kj} \\ \eta_{kj} \\ \zeta_{kj} \end{bmatrix} = \frac{1}{D_{kj}} \rho_{kj} \vec{P}_o \begin{bmatrix} x_{kj} - x_{ko} \\ y_{kj} - y_{ko} \\ z_{kj} - z_{ko} \end{bmatrix} = \begin{bmatrix} X_j - X_k \\ Y_j - Y_k \\ Z_j - Z_k \end{bmatrix}$$

or we can draw the following relation:

$$(9)\qquad \begin{bmatrix} x_{kj}-x_{ko} \\ y_{kj}-y_{ko} \\ z_{kj}-z_{ko} \end{bmatrix} = \frac{D_{kj}}{\rho_{kj}} \vec{P}_o^{\,T} \begin{bmatrix} X_j-X_k \\ Y_j-Y_k \\ Z_j-Z_k \end{bmatrix} = m\vec{P}_k \begin{bmatrix} X_j-X_k \\ Y_j-Y_k \\ Z_j-Z_k \end{bmatrix},$$

where:

$$(10)\qquad m_{kj} = \frac{D_{kj}}{\rho_{kj}} \text{ - scale coefficient}$$

$$(11)\qquad \vec{P}_k = \vec{P}_o^{\,T} = \begin{bmatrix} a_1 & a_2 & a_3 \\ b_1 & b_2 & b_3 \\ c_1 & c_2 & c_3 \end{bmatrix}$$

The operator $\vec{P}_k = \vec{P}_o^{\,T}$ is an orthogonal matrix accomplishing the transition from *the Greenwich coordinate system* to the *satellite-centric coordinate system.*

a_i, b_i and c_i, $i = 1,2,3$ are elements of the matrix $\vec{P}_k$, which are function of the Euler angles (Fig.1): Ω - length of the ascending knot; w - argument of the pericenter; i - orbit slope have the following form:

$$(12)\begin{cases} a_1 = \cos w\cos\Omega - \sin w\sin\Omega\cos i, & b_1 = -\sin w\cos\Omega - \cos w\sin\Omega\cos i, \\ a_2 = \cos w\sin\Omega + \sin w\cos\Omega\cos i, & b_2 = \sin w\sin\Omega + \cos w\cos\Omega\cos i, \\ a_3 = \sin w\sin i, & b_3 = \cos w\sin i, \\ c_1 = \sin\Omega\sin i, \qquad c_2 = \cos\Omega\sin i, & c_3 = \cos i \end{cases}$$

From formulae (9), substituting (10) and (11), we can obtain:

$$(13)\qquad \begin{bmatrix} x_{kj}-x_{ko} \\ y_{kj}-y_{ko} \\ z_{kj}-z_{ko} \end{bmatrix} = m_{kj} \begin{bmatrix} a_1 & a_2 & a_3 \\ b_1 & b_2 & b_3 \\ c_1 & c_2 & c_3 \end{bmatrix} \begin{bmatrix} X_j-X_k \\ Y_j-Y_k \\ Z_j-Z_k \end{bmatrix}$$

From equations (13) we obtain a system of linear equations to determine the coordinates of the GCPs of the image.

From equation (13) we obtain the linear equations:

$$(14)\qquad \begin{cases} x_{k\bar{j}} - x_{ko} = m_{kj}[a_1(X_j - X_k) + a_2(Y_j - Y_k) + a_3(Z_j - Z_k)] \\ y_{k\bar{j}} - y_{ko} = m_{kj}[b_1(X_j - X_k) + b_2(Y_j - Y_k) + b_3(Z_j - Z_k)] \\ z_{k\bar{j}} - z_{ko} = m_{kj}[c_1(X_j - X_k) + c_2(Y_j - Y_k) + c_3(Z_j - Z_k)] \end{cases}$$

Equation (14) can be also presented in the form:

$$(15)\qquad \begin{cases} x_{k\bar{j}} = m_{kj}[a_1\Delta X_{kj} + a_2\Delta Y_{kj} + a_3\Delta Z_{kj}] + x_{ko} = m_{kj}\overline{N}_{kj} + x_{ko} \\ y_{k\bar{j}} = m_{kj}[b_1\Delta X_{kj} + b_2\Delta Y_{kj} + b_3\Delta Z_{kj}] + y_{ko} = m_{kj}\overline{P}_{kj} + y_{ko} \\ z_{k\bar{j}} = m_{kj}[c_1\Delta X_{kj} + c_2\Delta Y_{kj} + c_3\Delta Z_{kj}] + z_{ko} = m_{kj}\overline{Q}_{kj} + z_{ko} \end{cases},$$

where, according to (14), we have:

$$(16)\qquad \Delta X_{kj} = X_j - X_k, \quad \Delta Y_{kj} = Y_j - Y_k \quad \text{и} \quad \Delta Z_{kj} = Z_j - Z_k$$

x_{kj}, y_{kj}, z_{kj} - the definable coordinates of the images of the GCPs on the satellite image;

x_{ko}, y_{ko}, z_{ko} - the coordinates of the main point of the satellite image;

X_j, Y_j, Z_j - geocentric Greenwich coordinates of a GCP from the earth cover;

X_k, Y_k, Z_k - geocentric Greenwich coordinates of the "hind" lens point;

a_i, b_i, c_i, $i = 1,2,3$ - elements of the orthogonal matrix

$\vec{P}_k$ - function of the Euler angles Ω, w, i.

3. Determination of the correction equations

For every point $\bar{j}$ from the satellite image, which turns to be image of GCP-j from the earth scene, we have twelve unknown quantities according to equations (14), accordingly (15).

$$(17)\qquad X_j,\ Y_j,\ Z_j,\ X_k,\ Y_k,\ Z_k,\ \Omega_k,\ w_k,\ i_k,\ x_{ko},\ y_{ko},\ z_{ko}$$

whereas their approximately values will be denoted by:

$$X_j^{\,o}, Y_j^{\,o}, Z_j^{\,o}, X_k^{\,o}, Y_k^{\,o}, Z_k^{\,o}, \Omega_k^{\,o}, w_k^{\,o}, i_k^{\,o}, x_{ko}^{\,o}, y_{ko}^{\,o}, z_{ko}^{\,o} \tag{18}$$

Linearizing equations (14), accordingly (15), for each support point j from the scene of the space image with coordinates $\bar{j} = (x \quad y \quad z)^T{}_{kj}$, yields correction equation:

$$\vec{V}_{U_{kj}} = \begin{pmatrix}\vec{A}_k & \vec{B}_k & \vec{C}_j & \vec{D}_{ko}\end{pmatrix} \begin{pmatrix} d_k\vec{S}_k \\ d\vec{r}_k \\ d\vec{R}_j \\ d\vec{n}_{ko} \end{pmatrix} + \vec{L}_{kj}\,; \qquad P_{kj} \tag{19}$$

P_{kj} - weight coefficient

The values $\vec{A}_k, \vec{B}_k, \vec{C}_j, \vec{D}_{ko}$ in correction equation (19) should be considered as partial derivatives of the coordinates x_{kj}, y_{kj}, z_{kj}, namely

$$\vec{A}_k = \frac{\partial(x, y, z)_{kj}}{\partial(\Omega, w, i)_{kj}} \tag{20}$$

$$\vec{B}_k = \frac{\partial(x, y, z)_{kj}}{\partial(X, Y, Z)_{k(j)}}, \tag{21}$$

whereas $\vec{B}_k = -\vec{C}_j$, the index "k" is differentiation along the coordinates of satellite, and the index "j" - differentiation along the coordinates of the GCPs of the scene.

$$\vec{D}_{ko} = \frac{\partial(x, y, z)_{kj}}{\partial(x, y, z)_{ko}} \tag{22}$$

The correction vectors $d\vec{S}_k, d\vec{r}_k, d\vec{R}_j, d\vec{n}_{ko}$ of the unknown values (17) for the approximate values of (18) have the form:

$$(23)\qquad \begin{cases} \vec{V}_{U_{kj}} = \begin{pmatrix} v_x & v_y & v_z \end{pmatrix}_{kj}^T \\ d\vec{S}_k = \begin{pmatrix} d\Omega & dw & di \end{pmatrix}_k^T \\ d\vec{r}_j = \begin{pmatrix} dX & dY & dZ \end{pmatrix}_k^T \\ d\vec{R}_j = \begin{pmatrix} dX & dY & dZ \end{pmatrix}_j^T \\ d\vec{n}_{ko} = \begin{pmatrix} dx & dy & dz \end{pmatrix}_{ko}^T \end{cases}$$

For the vector of the free term $\vec{L}_{kj}$ we have:

$$(24)\qquad \vec{L}_{kj} = \vec{U}_{kj} - \vec{U}'_{kj} = \begin{vmatrix} x_{kj} - x'_{kj} \\ y_{kj} - y'_{kj} \\ z_{kj} - z'_{kj} \end{vmatrix},$$

where:

$\vec{U}_{kj} = \begin{pmatrix} x & y & z \end{pmatrix}_{kj}^T$ - the defined values of the coordinates x_{kj}, y_{kj}, z_{kj} along (14), accordingly (15);

$\vec{U}'_{kj} = \begin{pmatrix} x' & y' & z' \end{pmatrix}_{kj}^T$ - the measured coordinates of the space image

4. Obtaining equations to determine the values $\vec{A}_k, \vec{B}_k, \vec{C}_j$

To obtain the partial derivatives, constituting elements of the matrix (20), (21) and (22), it is necessary to successively differentiate the coordinates $x_{k\bar{j}}$, $y_{k\bar{j}}$, $z_{k\bar{j}}$ in relation to the Euler angles (Ω, w, i), the space coordinates of the ground points GCP - j $\begin{pmatrix} X & Y & Z \end{pmatrix}_j$, the Greenwich coordinates of *КЛА*-$\begin{pmatrix} X & Y & Z \end{pmatrix}_k$ and to coordinates $\begin{pmatrix} x & y & z \end{pmatrix}_{ko}$.

4.1. Partial derivatives of the value $\vec{A}_k$

According to equation (22), it is necessary to differentiate the image coordinates from (14), accordingly (12), in relation to (Ω, w, i). But since only values $a_i, b_i, c_i, (i = 1,2,3)$ are function of the Euler angles, it is necessary to differentiate $\overline{N}_{kj}$, $\overline{P}_{kj}$, $\overline{Q}_{kj}$, according to the equations:

$$(26)\qquad \begin{cases} \dfrac{\partial x_{kj}}{\partial(\Omega,w,i)_k} = \dfrac{\partial(m_{kj}\overline{N}_{kj})}{\partial(\Omega,w,i)_k} = m_{kj}\dfrac{\partial(\overline{N}_{kj})}{\partial(\Omega,w,i)_k} \\ \dfrac{\partial y_{kj}}{\partial(\Omega,w,i)_k} = \dfrac{\partial(m_{kj}\overline{P}_{kj})}{\partial(\Omega,w,i)_k} = m_{kj}\dfrac{\partial(\overline{P}_{kj})}{\partial(\Omega,w,i)_k} \\ \dfrac{\partial z_{kj}}{\partial(\Omega,w,i)_k} = \dfrac{\partial(m_{kj}\overline{Q}_{kj})}{\partial(\Omega,w,i)_k} = m_{kj}\dfrac{\partial(\overline{Q}_{kj})}{\partial(\Omega,w,i)_k} \end{cases}$$

4.2. Partial derivatives of the values $\vec{B}_k = -\vec{C}_j$

As stated above, to obtain the derivatives of the reflectance coordinates from $(x,y,z)_{kj}$ in relation to $(X\quad Y\quad Z)_k^T$ and $(X\quad Y\quad Z)_j^T$, equations (14), accordingly (15), should be used, which means both the scale $m_{kj} = \dfrac{D_{kj}}{\rho_{kj}}$, following formula (10), and $\overline{N}_{nj}, \overline{P}_{kj}, \overline{Q}_{kj}$ are function of the Greenwich coordinates. Having in mind this fact, we will differentiate, using equations:

$$(27)\begin{cases} \dfrac{\partial x_{kj}}{\partial(X,Y,Z)_{k(j)}} = \dfrac{\partial(m_{kj}\overline{N}_{kj})}{\partial(X,Y,Z)_{k(j)}} = \dfrac{\partial(m_{kj})}{\partial(X,Y,Z)_{k(j)}}\overline{N}_{kj} + m_{kj}\dfrac{\partial(\overline{N}_{kj})}{\partial(X,Y,Z)_{k(j)}} \\ \dfrac{\partial y_{kj}}{\partial(X,Y,Z)_{k(j)}} = \dfrac{\partial(m_{kj}\overline{P}_{kj})}{\partial(X,Y,Z)_{k(j)}} = \dfrac{\partial(m_{kj})}{\partial(X,Y,Z)_{k(j)}}\overline{P}_{kj} + m_{kj}\dfrac{\partial(\overline{P}_{kj})}{\partial(X,Y,Z)_{k(j)}} \\ \dfrac{\partial z_{kj}}{\partial(X,Y,Z)_{k(j)}} = \dfrac{\partial(m_{kj}\overline{Q}_{kj})}{\partial(X,Y,Z)_{k(j)}} = \dfrac{\partial(m_{kj})}{\partial(X,Y,Z)_{k(j)}}\overline{Q}_{kj} + m_{kj}\dfrac{\partial(\overline{Q}_{kj})}{\partial(X,Y,Z)_{k(j)}} \end{cases}$$

The essential thing here is that the scale coefficient m_{kj} is calculated for each available *GCP* from the cover, with the obtained deformations of the image between each determined reflectance point and the origin of the coordinate system.

4.3. Equation to determine the derivatives $(x,y,z)_{kj}$ in relation to $(x,y,z)_{ko}$

Following equation (22) and the system of linear equations (14), accordingly (15), and having in mind that, according to equation (10), in determining m_{kj}, the distance D_{kj} of the image is used, formula (3), which is a function of the coordinates of the main point x_{ko}, y_{ko}, z_{ko} on picture O. Based on this, we have the following meanings for the matrix D_{ko}:

$$(28) \qquad \vec{D}_{ko} = \begin{vmatrix} \frac{(x_{kj} - x_{ko})^2}{D^2{}_{ko}} & 0 & 0 \\ 0 & \frac{(y_{kj} - y_{ko})^2}{D^2{}_{ko}} & 0 \\ 0 & 0 & \frac{(z_{kj} - z_{ko})^2}{D^2{}_{ko}} \end{vmatrix}$$

The essential thing here is that the scale coefficient m_{kj} is calculated for each available *GCP* from the cover, with the obtained deformations of the image between each determined reflectance point and the origin of the coordinate system.

Correction equation (19) has the form:

$$(29) \qquad \vec{V}_{U_{kj}} = \vec{A}_k d\vec{S}_k + \vec{B}_k d\vec{r}_k + \vec{C}_j d\vec{R}_j + \vec{D}_{ko} d\vec{n}_{ko} + \vec{L}_{kj}; \qquad P_{kj}$$

6.Conclusion

As a conclusion we will note that the developed mathematical model provides the opportunity for georectification of the images of GCPs from the cover in a 3D satellite-centric coordinate system $(x, y, z)_{kj}$ having its origin O in the lens's hind point, thereby obtaining a 3D model of the image. Usually, in the program packages used in remote sensing of the Earth, the images of the GCPs are rectified in a ground coordinate system $(x, y)_{kj}$. The essential point here is that we obtain the real geometry of the image and it is possible to determine the shift of the projected GCP as a result of the cover pattern and slope.

In the obtained equations, the scale coefficient $m = \frac{D_{kj}}{\rho_{kj}}$ is also included,which provides the opportunity to determine the geometric deformation of the scenes and to perform a precise rectification of the space images, accordingly.

References

1. Георгиев, Н., Р. Недков. Ректификация на геометричeските деформации при космическите сканерни изображения чрез апроксимиращи функции, "Аерокосмически изследвания в България", София, 15, 1998.

2. Георгиев, Н., Р. Недков, А. Христов. Високоточен метод за привързване и ректификация на космическите фотографски изображения, сб. "30 год. организирани космически изследвания в България", ИКИ – БАН, 2000, 124-131.

3. ГеоргиеН., Р.Недков, Д. Неделчева, Използване на метод и GPS измервания на опорни точки от терена при координатното привързване на космически фотографски изображения . сб.докл. "Международна научна сесия 50 години Г И - БАН, 2000, с. 179-189.

4.Георгиев, Н.И., Спиридонов, Х.Н, Методи за координатно привързване, ректификация и интерпретация на космически изображения . сбор. от доклади на Юбилейна научна сесия "40 години от първия полет на човек в Космоса" Д. Митрополия, 2001, ст. 150-161.

5. Prof. Gordon Petric. Mapping Awareness, Nov.1999, Depart. of Topographic Science, University of Glasgow.

6. N. Georgiev, R.Nedkov . D.Nedelcheva . Using an Orbital Method and GPS Measurements of the Ground Control Point in Georeference of Space Images, Aerospace Research in Bulgaria, 16, pp. 70-80, Sofia.

7. Урмаев, М.С., Орбитальные методы космического геодезии, М., "Недра", 1981.

8. Даскалова М. Върху обработката на сканерни изображения в приета картографска проекция., Год. на ВИАС, С., 1987 - 88, т. XXXIII.

МАТЕМАТИЧЕСКИ МОДЕЛ ЗА ПРИВЪРЗВАНЕ НА КОСМИЧЕСКИ ИЗОБРАЖЕНИЯ С ВИСОКА РАЗДЕЛИТЕЛНА СПОСОБНОСТ ЧРЕЗ ОПРЕДЕЛЯНЕ НА КООРДИНАТИТЕ НА ОПОРНИ ТОЧКИ С GPS ИЗМЕРВАНИЯ

Никола Георгиев, Светлин Фотев

Резюме

В статията се предлага строг метод за привързване на космически изображения с голяма разделителна способност от 1 - 3 м, чрез определяне координатите на опорните точки (ОТ) от физическата земна повърхност с помощта на GPS измервания.За проекционна повърхнина се приема референтен (земен) елипсоид и съответно се отчитат елипсоидните височини на идентифицираните от терена. Определянето на мащабите между идентифицираните точки дава възможност за прецизна ректификация на космическото изображения.

Bulgarian Academy of Sciences. Space Research Institute
Aerospace Research in Bulgaria. 17. 2003. Sofia

MEASUREMENTS OF ELECTROMAGNETIC ULF FIELD ONBOARD THE MAGION-4 SATELLITE: THE ULF EXPERIMENT

P.Triska[1], J.Vojta[1], A.Czapek[1], J. Chum[1], D.Teodosiev[2], G.Galev[2], I.Shibaev[3]

[1] Institute of Atmospheric Physics-Academy of Sciences of the Czech Republic
[2] Space Research Institute-Bulgarian Academy of Sciences, Bulgaria
[3] IZMIRAN-Russian Academy of Sciences, Russia

Abstract

The ULF instrument is a part of the research complex of the Magion-4 satellite. This experiment is designed for measuring 4 electromagnetic field components (3 magnetic and 1 electric) in a frequency range from 0.1 to 30 Hz. Preliminary results on ULF emissions and associated phenomena are presented. Peculiarities of ULF emissions in the magnetosphere are discussed.

Introduction

The ULF instrument provides the ability to solve independent tasks jointly with the KEM-3 and SAS instruments on board of the satellite Magion-4 (Agafonov et al., 1996, Galeev et al., 1996, and Perraut et al., 1998), as well as complex tasks jointly with the instrument IESP-2M, which is placed on board of the main satellite INTERBALL-2. The orbital parameters of the satellite Magion-4, launched on August 3, 1995, are apogee 192,000 km, perigee 750 km and inclination 63°.

The complex of instruments ULF-IESP represents a very convenient apparatus for the solutions of the following tasks:

- Research of global processes taking place within the magnetosphere and ionosphere of the Earth,

- Local processes during mutual influence of waves and particles within the active magnetosphere regions,
- Fine structures of electric currents and particle flows within the aurora zone and within the tail of magnetosphere,
- Evolution and dynamics of nonlinear electromagnetic and electrostatic structures like the spirals of the Alfvenic type, impact waves, double layers etc.
- Various mechanisms of particle acceleration by non-linear wave structures within the ionosphere and magnetosphere plasma,
- Mechanisms of generation and propagation of different types of geomagnetic micro-pulsations.

Technical description

The ULF instrument is designed for acquisition of three magnetic field components and one electric field component in the range of 0.1 to 30 Hz. This instrument performs filtration of analog signals and their conversion into digital form, convenient for the on-board block of data acquisition STS (Small Telemetry System)

The ULF-DIGITAL unit provides an interface between the ULF-ANALOG unit and the STS. It accepts four channels (Bx, By, Bz, E) of ULF signals in the range of +/-5V relative to the analog ground. The ULF experiment is supported only in the following TM speed - TM structure combinations:

- Telemetry rate of 40 and 20 Kbits/sec - all four measured components are transmitted, sampling speed is about 280 samples per sec.
- Telemetry rate of 5 Kbits/sec - one component is transmitted at sampling rate ~70 samples/sec.
- Telemetry rate of 1.2 Kbits/sec - one component (f_{max} = 10 Hz) is transmitted at sampling rate ~ 25 samples/sec.

The electric antenna comprises a dipole consisting of two spherical graphite sensors with diameter of 8 cm. Inside the balls, there is a low-noise preamplifier, with +1 amplification, which transforms the high impedance of the spherical sensor into the low impedance of the satellite's cable wiring. The spherical sensors, designated EDA and EDB are placed on the 1.7 m long satellite deployable booms (see Fig.1).

The sensors MSUX, MSUY and MSUZ of the "search coil" type for the three-component measurement within the ULF range are attached to the deployable booms (Fig.1) together with the low-noise preamplifiers. The sensors are operated by the feedback by means of magnetic field, which rejects the own resonance of the working circuit, thus compensating the frequency characteristics of the sensor.

Sensitivity: component E 5.10^{-8} V Hz^{-1}
component B 1.10^{-4}nT Hz^{-1}

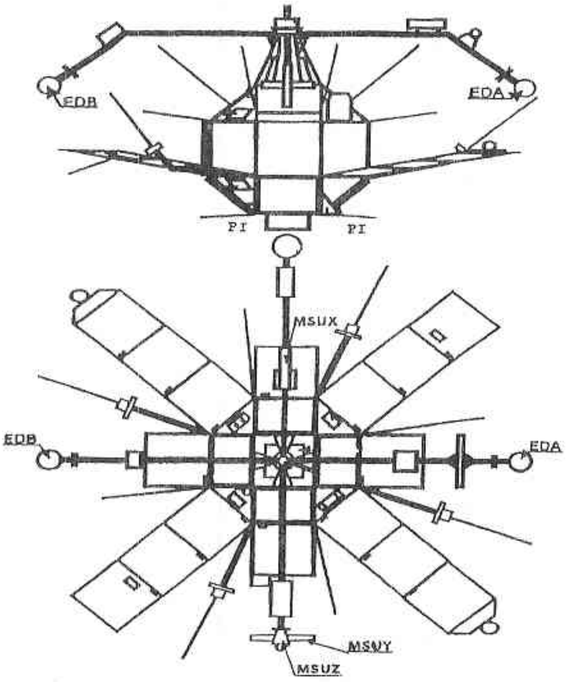

Fig. 1. General overview of the subsatellite Magion-4 in the flight configuration.

To the inputs of all the sensors (electric and magnetic), a calibration signal may be fed through the preamplifier relay contact. Thus, the test calibration cycle is effected with each switching on of the instrument, or by a command from the ground station.

Upon amplification, the signals from the electric and magnetic sensors are tied to the high-pass filter (0.1Hz). Then, they are digitized.

Upon being added in the differential amplifier, the output signals of the electric preamplifiers, the dipole EDA and EDB, are then processed in the instruments KEM, KEMVLS and SAS.

Measurement results

A lot of experimental data is collected using the ULF instrument. We have got data from 160 orbits and at this moment their analyses and interpretation is still going on. To analyze the data from the multi-component measurements of the electromagnetic field in the ULF band we have developed an universal software in DOS environment. It is user-friendly and provides for quick and flexible data analysis, applying numerous standard data processing algorithms and dedicated programs for wave process analyses.

Below, the results obtained from measurements on two orbits are presented in order to illustrate the applications of both the instrument and the software. Although the instrument has three different operation modes, due to the lack of space only two examples are shown. Records from various orbits are also discussed.

Orbit 58/27.02.1996

The first and the second panels in Fig.2 present data characterizing the magnetosphere region, which is crossed by the satellite. The results were obtained by two instruments:

- MPS (electrostatic analyzer for measurements of electrons and ions from 200 eV-20 keV along the axis ± Z in 16 different energetic levels) and
- VDP (Faraday Cup 120°, for electrons and ions with energy >170eV).

The third panel presents the By component in frequency-time space, i.e. in the form of a spectrogram.

At 23:34UT, the ULF experiment recorded a monochromatic wave packet with frequency of 1.5Hz.

At 00:14UT, the ULF experiment recorded an increase of broad band noise plus an intensification of ion flux, which corresponded to the crossing of the magnetopause and the time of its leaving. The ULF data is in accordance with the data registered by MPS on the M-4 satellite.

The increase of fluctuation corresponds to the zone of magnetosheath. It should be emphasized that, at that moment, the ULF instrument measured only the By component. The ULF measurements were compared to the By component recorded by the ASPI/MIF-M instrument launched on INTERBALL-1 satellite. The comparison revealed:

- ❖ Coincidence of the enhanced intensity at magnetopause and magneto-sheath crossing recorded by several instruments.
- ❖ Crossing of the magnetopause at 00:14 UT.

Of course we render an account of the fact that Magion-4 and INTERBALL-1 crossed the magnetopause at different moments of one and the same orbit. Magion-4 was outdistanced to INTERBALL-1 by almost 40 minutes. In other words, such simultaneous measurements by two different satellites provides the possibility to study the dynamics and movement of the magnetopause. The required condition is to know the satellite's ballistics (Rezeau et al., 1989, Styazhkin et al., 1999).

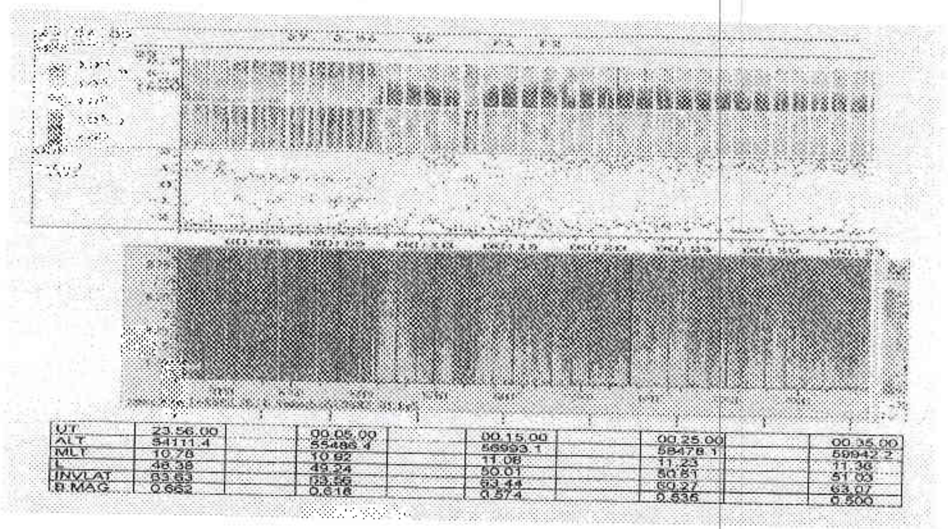

Fig. 2. Frequency-time spectrograms of the By magnetic component and spectrograms of electrons and ions measured by the MPS and VDP instruments on Magion-4, orbit 58 from February 27, 1996. By component is perpendicular to the spin axis.

Orbit 38/7.02.1997

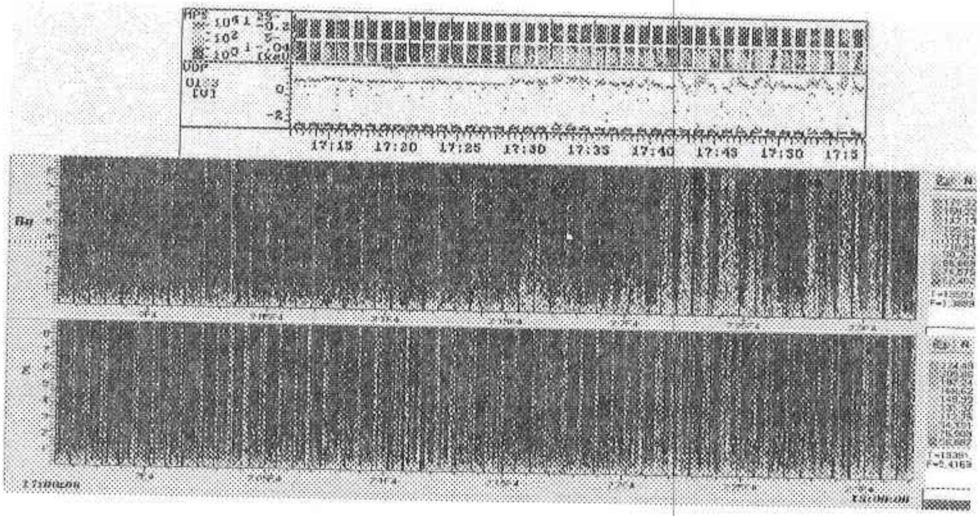

Fig. 3. Frequency-time spectrograms of the magnetic component By, electric component E, and spectrograms of electrons and ions measured by the MPS and VDP instruments on Magion-4, orbit 38 from February 7, 1997 at 17:00 UT to 18:00 UT. By end E are perpendicular to the spin axis.

The data shown in Fig. 3 illustrates the strong correlation between ion and electron fluxes and ULF noises in the frequency range from 0,1 Hz to 9 Hz. The magnetic component has a maximum at 1,5 Hz and the electric component at 0,5 Hz. This example corresponds again to the Magion-4 satellite movement from the magnetopause into the magneto-sheath.

Conclusion

The ULF instrument is a part of a larger scientific instrument KEM-3 dedicated to the VLF range. Identical magnetic and electrical detectors are used for recording of both the ULF and the VLF bands.

The presented results show that the instrument operated well and with sufficient sensitivity. The technical arrangement and especially the overlapping of the frequencies up to 30 Hz allows us to:

- Compare the recorded data,
- Complement the data sets for calculation of the E/B ratio. This ratio allows to judge the wave type and to interpret the mechanisms and the place of their origin.

The knowledge of wave processes in the boundary layers of the magnetosphere is of enormous importance for estimation of the transmission mechanism of solar wind energy into the magnetosphere (De Keyzer et al., 1999, and Tsurutani et al., 1989 and 1998).

References

1. Agafonov, Yu. N., P. Triska, J. Volta, and V. V. Khrapchenkov, Subsatellites of the Project INTERBALL, Space Research, 34, 1996, 371-380.
2. De Keyzer, J., M. Roth, F. Rezeau, and G. Belmont, Resonant amplification of MHD waves in realistic subsolar magnetopause configurations, J. Geophys. Res., 104, 1999, 2399-2410.
3. Galeev A. A., Yu. I. Galperin, and L. M. Zelenyi, The INTERBALL Project to Study Solar-Terrestrial Physics, Space Research, 34, 1996, 339-362.
4. Perraut, S., A. Roux, F. Darrouzet, C. De Villedary, M. Mogilevsky, and F. Lefeuvre, ULF wave measurements onboard the Interball auroral probe, Ann. Geophysicae, 16, 1998, 1105-1116.
5. Rezeau, L., A. Morane, S. Perraut, and A. Roux, Characterization of Alfvenic Fluctuations in the Magnetopause Boundary Layer, J. Geophys. Res., 94, 1989, 101-110.
6. Styazhkin, V. A., G. A. Zastenker, V. G. Petrov, M. N. Nozdrachev, A. J. Lazarus, and R. P. Lepping, Strong and Quick Variations of Parameters in the Magnetosheath. 2. Magnetic Field Variations and a Comparison of Them with Ion Flux Variations, Space Research, 37, 1999, 616-624.
7. Tsurutani, B., A. L. Brinca, E. J. Smith, and R.T. Okida, A Statistical Study of ELF-VLF Plasma Waves at the Magnetopause, J. Geophys. Res., 94, 1989, 1270-1280.
8. Tsurutani, B., J. K. Arballo, G. S. Lakhina, C. M. Ho, B. Buti, J. S. Pickett and D. A. Gurnett, Plasma waves in the dayside polar cap boundary layer: Bipolar and monopolar electric pulses and whistler mode waves, Geophys. Res. Lett., 25, 1998, 4117-4120.

ИЗМЕРВАНЕ НА ЕЛЕКТРОМАГНИТНОТО СНЧ ПОЛЕ НА БОРДА НА СПЪТНИКА МАГИОН-4: СНЧ ЕКСПЕРИМЕНТ

П.Тришка, Дж.Войта, А.Чапек, Дж.Чум, Д.Теодосиев, Г.Галев и И.Шибаев

Резюме

СНЧ уредът е част от научния комплекс на спътника Магион-4. Експериментът има за цел да измери 4 компоненти на електромагнитното поле (3 магнитни и 1 електрическа) в честотния диапазон от 0.1 до 30 Hz. Показани са предварителни резултат за СНЧ емисиите и свързаните с тях явления. Обсъдени са особеностите на СНЧ емисиите в магнитосферата.

Bulgarian Academy of Sciences. Space Research Institute
Aerospace Research in Bulgaria. 17. 2003. Sofia

ON THE SEISMIC SOURCE MECHANISM OF ELECTRIC SIGNALS

*Petko Nenovski, Boytcho Boytchev**

Geophysical Institute-Bulgarian Academy of Sciences
**Space Research Institute-Bulgarian Academy of Sciences*

Abstract

We propose a seismic electric signals (SES) model related to the charge and current production associated with a discharge process occurring in the microcrack void. The electric field is intensified until a discharge process is initiated. A current j is spread in the microcrack surroundings which follows the electric field build-up process and its cancellation. The spatial and temporal distribution of the electric field related to the current j in the microcrack void. The field is controlled by the aggregation mechanism, the discharge, and the geophysical properties of the void.

1. Introduction

The bursts of ULF and concomitant electromagnetic emissions registered before and after great earthquakes are a form of electromagnetic events connected with seismic processes. [1, 2, 3, 4] have tried to explain these electromagnetic emissions by oscillating electric dipoles. The seismic electric signals (SES) [5] are another form of electromagnetic events associated with lithospheric processes. The SES are aperiodic and their duration is from several minutes to several hours [6]. The registered SES [7,8] usually have characteristic bay-like, or bell-shaped curves of variable width and duration. Experimental data on repetitive SES signals of pulse form with nearly 24 h periodicity occurring a couple of days before the earthquake has been reported, as well as [9, 10, 2, 8] have proposed the micro-crack model of charge production and associated current connected with the micro-crack growth. They succeeded to derive the long-term evolution of the magnitude of the ULF emission prior to the earthquake. This model provides a qualitative estimate of the experimental evidence for consecutive increases and decreases of the intensity of ULF emission before the Loma-Prieta eathquake [1]. The currents connected with an ensemble of micro-cracks and the relation between the growth of their size and the current density seem to be promising mechanism of ULF emission. Molchanov and Hayakawa's model does not treat seismic electric signals (SES), although they appear to be also ULF emission. The SES duration lasts from several minutes to several hours [6]. The SES mechanism is believed to be connected with electrokinetic effects [11, 12]. The latter are highly damped while the SES signals are recorded at large distances. There are several mechanisms of charge production. The piezoelectric mechanism of charge production proposed by [13] yields polarization electric field E_c of 2×10^8 V/m for stress changes δS of 200 Bar under crystal conditions [3]. Here, the electric field E_c emerges in the void space of the micro-cracks. The process of an increase of the electric filed will however be limited because of the enormous electric fields produced within the void space formed between separated charges. In the presence of enormous electric fields, a process like the anomalous glow discharges is possible. The magnitude of the initial electric field for the discharge process depends on the crust material conditions. The discharge process could be initiated by a gas release in the void regions provoking an ionization that produces free charges. In such discharges, the produced cathode currents reach $10 \div 10^2$ A/m^2. The discharge will stop when the dipole-like electric field within the separated charges is cancelled and the ionization process becomes impossible. A widely assumed model is that the source of these SES are charges that emerge during microcrack generation. Czechovski [14] used a kinetic point of view and obtained a kinetic equation of the microphysics of cracks. By exploiting kinetic and qualitative models of crack interaction and propagation, Tzanis et al. [15] pointed out theoretically that the seismic electric signals (SES) may have a limited class of permissible waveforms of arbitrary width, or duration. On the other hand, laboratory experiments of electrification processes caused by microcracks have revealed not only charge production, but also current spikes. With crack opening times of the order of 10^{-6} s every individual microcrack yields current spikes of the order of 10-3 A/m^2. Transient and electromagnetic emissions associated with the microcracks have also been observed [16, 13]. Since the current spikes are presumably due to microcracks, various important physical characteristics of the microcrack processes are to be sought, the major ones being crack population production rate and their growth with time. We assume that the random aggregation process with an injection is a source of charges and/or currents and could be applied for both the accumulation of pressure and strain at some place and time. The currents connected with an ensemble of microcracks and the relation between the growth of their size and the current density seem to be a promising mechanism of ULF emission. In our paper, we assume current production (associated with a random aggregation mechanism of the microcracks) as a primary source of the observed SES signal and probably of some ULF electromagnetic emissions. These signals would be controlled by the electrodynamical conditions of the crust material away from the current source.

2. Random aaggregation model of charge production

First, let us mention that there are experimental evidences for micro-cracks behavior under stress conditions. A lot of laboratory experiments show that micro-cracks pass through several stages: i) at some pressure level, an initial stage of micro-cracks emerges, under which the micro-cracks are randomly distributed; ii) at the second stage, which appears at some intermediate values of the pressure, the micro-cracks tend to concentrate at a certain point, thus increasing their density, or population; iii) at some critical pressure value, the micro-cracks evolve in a fracture of example [17]. Second, under natural conditions the physics of micro-cracks is unknown, but we tentatively assume that the micro-crack dynamic behavior illustrates the spatial and temporal changes in the tectonic pressure, strain and stress prior to earthquake. Third, the primary sources of charge/current production in both cases are the stress and/or pressure changes. For a simulation of constantly increasing 'tectonic' driving forces, a two-dimensional array of particles, representing segments of the sliding surface has been considered [18]. In our study, the tectonic driving forces as a common source of charge/current production are suggested to be identical to the random aggregation model [19]. Below, we summarize briefly the major steps of this model.

According to the model we assume an ensemble of 'particles' with integer 'mass'. The particles could correspond to micro-cracks with certain length. In order to obtain the micro-cracks distribution we assume all the micro-cracks of identical geometry. The crust is considered to be a one-dimensional 'lattice'. We have discrete time steps for the 'mass' S(n) at a certain nod of this lattice, where n is the number of the step, S could corresponds to the micro-crack density. Assuming a certain random process, the following stochastic equation for S(n) holds [20]:

(1) $$S_i(n+1) = \Sigma W_{ij}(n)S_j(n) + 1,$$

where $S_i(n)$ is the density of the micro-crack on the i-th site at time n; $W_{ij}(n)$ is a random variable given by $W_{ij}(n) = 1$ with probability q(i-j), or 0 with probability 1-q(i-j). As follows $\Sigma W_{ij}(n) = 1$ and $\Sigma q(i) = 1$. We consider the case with q(i-j) of 1/2 for i-j =0, or 1 and q(i-j) =0 otherwise. The initial condition accordingly reads: $S_i(0) = 1$. We need to define the probability p(s,n) and the cumulative distribution P(≥s) given by:

(2) $$p(s,n)ds = N^{-1}\Sigma\int_s^{s+ds} ds'\delta(S_i(n)-s'),$$

where N is the total number of sites and:

(3) $$P(\geq s) \equiv \int_s^{\infty} p(s')ds'.$$

We define a characteristic function

(4) $$Z(\rho,n) \equiv <e^{-ps}> = \Sigma e^{-ps}p(s,n).$$

Here <...> denotes the average taken over the stochastic variables $W_{ij}(m)$, m= 0,1,..., n-1. Functions for the density Z at $i_1,i_2,\dots i_r$ and for r-adjacent sites are determined as follows:

(5) $$Z_r(\rho,n;\ i_1,i_2,\dots i_r) \leq <e^{-\rho(S_{i1}+S_{i2}+\dots+S_{ir})}>,$$

and

(6) $$Z_r(\rho,n) = <e^{-\rho(S_{i1}+S_{i+1}+\dots+S_{i+r-1})}>,$$

This process is named Sheidegger rivers [21]. Qualitatively, it represent a process of production of macroscopic water mark formed along some tilted plane on which initial droplets of rainfall are consecutively accumulated at certain points into greater drops, which suddenly burst into smallerr streamlets breaking trails for the water downwards. The effective interaction forces are gravity and surface tension. We assume that the process of fractures during an earthquake is the final stage of similar processes. The micro-cracks gathered at certain points will break into a macro-crack. The interaction forces under the earthquake process are the pressures and the strength, or solidity of the lithosphere material. From (5) and (6) it follows that the distribution functions of energy release stimulated by the above-mentioned aggregation process have power law form. It is worth noting that, modelling segments of a sliding surface as two-dimensional arrays of particles [18] has yielded a similar power law distribution.

Without quoting all the steps of the aggregate model we shall mention only that the number n corresponds to time t and r (site) - to a one-dimensional spatial coordinate, e.g. x. It is noteworthy to mention that the density of micro-cracks is given by the number of connected lattice sites which constitute a river-like cluster in (1+1) dimensional space-time. In the limit n → ∝, the characteristic function $Z_\tau(\rho,n)$ tends to $Z_\tau(\rho,n)$ with the following relationship:

$$Z_{\tau+1}(\rho)+(2-4e^{\tau\rho})\,Z_\tau(\rho)+Z_{\tau-1}(\rho,n)=0 \tag{7}$$

It corresponds to steady-state condition. In the most important case of time-dependent condition, the following relationship holds:

$$Z_\tau(\rho,\ n+1)=e^{-\rho\tau}\,[Z_{\tau+1}(\rho,n)+2Z_\tau(\rho,n)+Z_{\tau-1}(\rho,n)]/4 \tag{8}$$

In a system with continuous time and spatial coordinates the above equation has its counterpart:

$$\partial Z/\partial t = (D/2)\partial^2 Z/\partial x^2 - \rho x Z, \tag{9}$$

where diffusion rate D and background 'particle' (microcrack) production ρ are determined from the physical characteristics of the crust material and the driving forces. The first term in the right-hand side results from the effect of aggregation due to the short-range interaction, while the second term results from the uniform input of new microcracks. The distribution $Z(x,t)$ is expected to be a source of charges and/or currents.

Several authors have involved discharge mechanisms of free charges to examine processes of electrification of gases trapped in rock pores [22,16]. The magnitudes of the discharge electric fields and currents can be compared with the charge production and the currents magnitudes observed under microcracks conditions. The charge density measured in microcracks amounts to $q = 10^{-3}$ C/m2 [23, 22]. Since any fluctuations of free charges generated in rock specimen should disappear after a time $\tau \approx 10^{-5} \div 10^{-7}$ s, the magnitude of the current spikes j ($j = q/\tau$) is $10^2 \div 10^4$ A/m^2. Such currents of $10^2 \div 10^4$ A/m^2 detected from rock specimen even exceed the currents flowing in glow discharges and are comparable with those of arcs. The orders of current magnitudes are suggestive for some forms of discharges involved in the microcrack physics. Hence, it is quite reasonable to suggest that the electric field build-up will stop at time t_0. Such a characteristic time exists even assuming another mechanism for charge production, e.g. mechanical one connected with the microcrack growth [10]. A process of gas release is expected in the microcrack void. In the presence of electric fields of sufficient magnitude the gas is ionizable. During such a discharge process, the charges accumulated at individual microcrack boundaries are effectively exhausted. Thus, electric field of 10^4 V/m or more is easily reduced to nearly zero magnitudes by, for example, an anomalous low-pressure discharge process [24]. The currents $j_0(x,t)$ that emerge will flow in the surroundings with certain velocity v determined by the state of the crust material around the source. Electric fields depending on the crust conductivity are induced as well. The source for the electric field is then $dj_0(t,x)/dt$. The current production due to the aggregation mechanism of microcracks could however continue irrespectively of any process of electric charge discharge. In general, growth time t_0 depends on the possible rates of gas release and the properties of the aggregation mechanism. We assume that microcrack distribution Z(x,t) is a measure of the current rate source. Therefore, assuming that current density rate is proportional to distribution Z(x,t) we have

(10) $$\partial\rho_0/\partial t \cong a\, Z(x,t),$$

where a is a constant. The electric current density rate $\partial j_0(x,t)/\partial t$ is connected to the particle density distribution rate by the relation $\partial j_0(x,t)/\partial t = v\partial\rho_0/\partial t$, where v is the charge velocity. The latter is considered to be nearly constant for the crust material under the stress action. Therefore, the time evolution of the SES is determined from the competitive action of the charge/current aggregation rate given by (9) and the dissipative effect of the crust material between the source and the measurement point. The electric field generated by the currents produced at some area ($-x_0 < x < x_0$) and time t is determined by

(11) $$(\Delta - \partial^2/\partial t^2 - \mu_0\sigma_{crust}\partial/\partial t)E = \mu_0 \partial j_0(t, x)/\partial t,$$

where Δ is Laplace's operator, z is the propagation direction of the electromagnetic disturbances generated by transient current $j_0(x,t)$ localized in x direction, where

(12) $$\partial j_0(x,t)/\partial t \cong v\partial\rho_0(x,t)/\partial t \propto Z(x,t) = \sqrt{(1/t)}\exp(-x^2/2Dt) + O(\rho),\quad t \le t_0$$

Here, v is the velocity magnitude of the charges that spread through the surrounding in the form of current; O (ρ) is a small term proportional to $\rho(\rho << 1)$. Fig. 1 illustrates the time envelope of microcrack production associated with the random aggregation mechanism of stress, or strain forces. The current density shape with time depends strongly on the magnitude of the diffusion coefficient D. Let us study the propagation characteristics of the electromagnetic disturbances generated by transient current $j_0(t,x)$ localized in time and x direction. For convenience we will study the potential behavior along the z axis. Hence, we examine only solutions around x = 0, where x<<z.

(13) $$(\partial^2/\partial z^2 - \mu_0\varepsilon_0\partial^2/\partial t^2 - \mu_0\sigma_{crust}\partial/\partial t)E = \mu_0\, (va)Z(x,t),$$

Thus, the equation resembles the telegraph equation of transmission line of conductivity σ_{crust}, where inductance L and capacity C stand for permeability μ_0 and the permitivity ε_0 [25]. This equation will account for the SES generation from a microcrack source Z(x,t) and propagation effects in one direction, z. The induced electric field magnitude is determined from the current production magnitude of $j_0(t,x)$, i.e. a. Equation (13) is solved in a straightforward way. The solution reads:

(14) $E(x,t;k) = \mu_0(va)/2[\exp(\gamma t)\int Z(x,t)\exp(-\gamma t)dt + \exp(-\gamma t)\int Z(x,t)\exp(\gamma t)dt]$,

where the characteristic time γ is given by

(15) $\gamma = -\sigma_{crust}/2\varepsilon_0\,(1 - \sqrt{(1 - 4k^2\varepsilon_0/\mu_0\sigma_{crust}{}^2)})$,

and k is the wavenumber of the ULF disturbance spectrum assumed to propagate along z. In the case of sufficiently small wavenumbers, i.e.:

(16) $k << \mu_0\sigma_{crust}/2$,

we obtain:

(17) $\gamma \cong -k^2/\mu_0\sigma_{crust}$

The characteristic time γ has real values for $\mu_0\sigma_{crust} > 2k$ and it is a complex quantity for $\mu_0\sigma_{crust} < 2k$. In the latter case, we have ULF events with frequency ω:

(18) $\omega = \sqrt{(k^2c^2 - \mu_0{}^2\sigma_{crust}{}^2/4)}$

and damping rate:

(19) $\gamma_p = -\mu_0\sigma_{crust}/2$.

Fig. 2 illustrates the behavior of both quantities, γ and the frequency ω. It follows that there are two different regions of ULF disturbances: i) first, a region of only aperiodic ULF disturbances where $2k/\mu_0\sigma_{crust} < 1$; ii) second, a region of damped electromagnetic waves of frequency ω and damping rate γ_p where $2k/\mu_0\sigma_{crust} > 1$. It follows that periodic solutions exist at shorter spatial scales and/or smaller conductivities σ_{crust}. The crucial parameter is the wavenumber k. The main constraints for the spatial scales ($\sim 2\pi/k$) come from the microcrack source size and its depth. The former is to be related to the spatial spectrum of the current source $\mathbf{j}_0(x,t)$. The source depth determines the characteristic size of the electromagnetic field localization. For example, if the source depth is 10 km, the upper frequency of the ULF/ELF/VLF signal is about 10 kHz. The spatial spectrum is limited by the size of the fracture event that follows microcrack growth.

Let us examine the case of aperiodic ULF disturbances. For convenience, we shall neglect the displacement current, it corresponds to the assumption that the velocity of light c goes to infinity. Then, the basic equation yields only aperiodic solutions. Eq. (13) possesses a general solution in the form (provided that $c \to \infty$):

(20) $E(x,t;k) = \mu_0(va)\,(1/\sqrt{t})\exp(-z^2\mu_0\sigma_{crust}/4t)\int\exp(z^2\mu_0\sigma_{crust}/4t - x^2/2Dt)dt$

Using an expression for the integrand we arrive to the following analytical expression for E(x,z;t):

$$E(x,z;t) = \mu_0(va)(pE_1(p/\tau_0) + \tau_0 \exp(-p/\tau_0)t^{-1/2}\exp(-z^2\mu_0\sigma_{crust}/4t)), \quad t > t_0 \quad (21)$$

$$E(x,z;t) = \mu_0(va)(pE_1(p/t)/\sqrt{t} + \sqrt{t}\exp(-p/t))\exp(-z^2\mu_0\sigma_{crust}/4t)), \quad t \leq t_0$$

where $p = x^2/2D - z^2\mu_0\sigma_{crust}/4$, and $E_1(p/t)$ is the elliptical integral [26]. The principal contribution comes from the first term. An examination of (14) shows that the SES forms are determined from the parameters D and $\mu_0\sigma_{crust}$ entering in p. Indeed, the distance $d = \sqrt{(x^2 + z^2)}$ at which the aperiodic signal still has a non-negligible amplitude depends on D and crust conductivity σ_{crust}. Comparing both terms in p we observe that the time envelope of the signal depends crucially on the size of the charge localization x_0 and the distance d between the charge source and the point of electric field measurement. Under low conductivity, reasonable values of charge localization size x_0 and diffusion D conditions, the sign of p is practically positive. The localization size of the aggregation of stresses usually does not exceed 1 km, while for diffusion D we could choose a value of about $1 \div 100$ m^2/s [27, 28]. The latter is taken from the electrokinetic mechanism model. Fig. 3 illustrates the SES shape for different values of parameter p.

Under isotropic conditions, e.g. when the center of aggregation of stresses is not collocated with faults, the time evolution for an isotropic aggregation stress and consequent charge and current production is illustrated in Fig. 4. Positive p values correspond to rock conditions where σ_{crust} lies in the ranges $10^{-6} \div 10^{-4}$ S/m. Inversely, under negative p conditions, no distinctive SES signals of duration of half an hour, or up to several hours are possible. One can see that, under high conductivity conditions, e.g.$\sigma_{crust}>10^2$S/m, and a distance of about 100 km, the sign of p could even become negative. We note that under high conductivity conditions, e.g. under sediment, or soil conditions, the SES envelope will have duration greater than that under rock conditions. It is quite possible for such SES events to be comparable to the diurnal variations of the Earth potentials. In such a case, they could not be substracted from the diurnal variations. Another feature of the SES events is that the electric field is oriented mainly in one direction, probably perpendicular to the fault plane. Fig. 5 illustrates various forms of the SES envelope. Along the z direction, the SES envelope does not depend on distance d, the SES amplitude however decreases. Along the x direction, the SES changes its structure (Fig. 4). Even under isotropic conditions, the SES behaves differently in the x and z directions. The SES envelope usually has a triangle form. In other cases, the SES envelope possesses 'shark fin' profile (Fig. 4). This effect is probably related to the fact that the aggregation mechanism acts also in the x direction. Therefore, the SES form will change according to the course of the aggregation mechanism. Recalling the Ralchovsky and Komarov observations [8], the greatest SES event has a form similar to case b) in Fig. 4. Our model could be applied if there were isotropic conditions in the Earth crust. Under real conditions, the Earth surface acts as a reflection boundary for the SES sources placed at certain depth. We do not consider either the additional effects coming from possible differences in the conductance on both sides of the fault plane ($x = 0$). In reality, the characteristic time t_0 is not constant, as well. In general, we could expect quite complex SES forms depending on distance, orientation, depth, Earth surface and geology conditions at the measurement site, etc.

3. Comments

The microcrack production process is responsible for the charge density rate, $\partial\rho_0/\partial t$. Equation (13) for the electric field built-up (that we suggest) contains on the right hand side the source term that is proportional to the current density rate. The electric field built-up process will break down at time t_0 due to the discharge process. The mechanical stresses and strains will initiate further microcrack production and the seismic electric signal generation process will be resumed. The aperiodic electric field signal related with microcracks at great distances and in a preferable direction is examined in detail. The aperiodic SES has two parameters that have to be known: relaxation (duration) time γ and microcracks 'diffusion' D. The duration is controlled by the spatial scales of the electric field disturbance that could arrive at the Earth surface from the earthquake center located at some depth. The diffusion of microcracks depends on the mechanical properties of the geological materials, the inhomogeneities of various scales and is controlled by the level of pressures and strains related to the active tectonic processes.

An examination of the SES shapes determined from parameters D and γ shows that high conductivity conditions, e.g. $\sigma_{crust} > 10^{-2}$ S/m result in SES signals of duration comparable with the diurnal variations of the Earth potentials. Therefore, clear SES signals with duration of half of hour or up to several hours are to be formed under rock conditions where σ_{crust} lies in the range $10^{-6} \div 10^{-4}$ S/m. Inversely, under higher conductivity conditions, ULF signals are plausible for characteristic spatial scales of hundreds of meters or kilometers. In our model of the SES signal there are other parameters – the distance d to the epicentre of the incoming earthquake and the angle θ between the fault axis and the direction to the measurement point. The relationship between distance d and angle θ and x is given by $x = d \sin(\theta)$.

As follows from the above analysis, a fundamental characteristics of the proposed aggregate model of SES is the anisotropy of the generated signal. The main component of the SES signal could be observed mostly in the direction perpendicular to the fault axis, i.e. the pair of electrodes should be oriented in the direction perpendicular, or normal to the fault axis. This suggestion corresponds to experimental evidences that all the SES signals are one-dimensional. Indeed, the bay-, or bell-shaped signals are clearly visible in one of the two orthogonal tracks of the electric field measuring systems. They have usually been registered either in the E-W direction [7] or in the N-S direction [8]. The other track remained at noise level, i.e. undisturbed.

4. Conclusion

Our model of the SES signal describes electric field production due to the current density generation during microcrack aggregation process. The current associated with this electric field build-up dissipates in the surrounding medium and governs the spatial and temporal distribution of the electric field. The electric field built-up process will break down due to the discharge process. We demonstrate that, in additional to ULF/ELF/VLF wave events, the generated seismic electric signal (SES) possesses pulse-like (aperiodic) behavior. The initial anisotropy of the stresses and associated currents are the cause for an electric field that is oriented perpendicular to the forthcoming fracture events. Thus, electric field responses at great distance from the current sources are possible and our model reveals another mechanism of electric field generation that is not connected to electric field due to charge dipoles.

Acknowledgements. The authors are obliged to Prof I. Kutiev, Prof. L. Christoskov, Dr. B. Rangelov and V. M. Chmyrev for reading the manuscript and their valuable comments. P. Nenovski also thanks Prof. M. Hayakawa for the receipt of the Final 2001 Report of the NASDA's Earthquake Remote Sensing Frontier Project.

References

1. Fraser-Smith, A. C., A. Bernardi, P. R. McGill, M. E. Ladd, R. A. Helliwell, and O. G. Villard, Low frequency magnetic field measurements near the epicenter of the Ms 7.1 Loma Prieta earthquake, Geophys. Res. Lett., 17, 1990, 11465-11468.

2. Molchanov, O.A., M. Hayakawa, Generation of ULF electromagnetic emissions by microfracturing, Geophys. Res. Lett., 22, 1995, 3091-3094.

3. Warwick, J.W., C. Stoker, T. R. Meyer, Radio emission associated with rock fracture: possible application to the great Chilean earthquake of May 22, 1960, J. Geophys. Res. 87, 1982, 2851-2859.

4. Gershenson, N.I., M. B. Gokhberg, A. V. Karakin, N. V. Petviashvili, A. L. Rykunov, Modeling the connection between earthquake preparation process and crustal electromagnetic emission, Phys. Earth Planet. Inter., 57, 1989, 128-138.

5. Uyeda, S., Introduction to the VAN method of earthquake prediction, in The Critical Review of VAN: Earthquake Prediction from Seismic Electric Signals, ed. Sir J. Lighthill, World Scientific Publishing Co., Singapore, 1996, 3-28.

6. Hayakawa, M., O. Molchanov, A. Tronin, Y. Hobara, Y. T. Kodama, Seismo-electromagnetic phenomena in the Lithosphere, Atmosphere and Ionosphere, Earthquake Remote Sensing Frotier Research, Final Report, March 2001, Unioversity of Electro-Communications, Chofu, Tokyo. 2001.

7. Varotsos, P., K. Alexopoulos, Physical properties of the variations of the electric field of the Earth preceding earthquakes, Tectonophysics, 110, 1984, 73-98; 99-125.

8. Ralchovsky, Tz. M., L. N. Komarov, Periodicity of the earth electric precursor before strong earthquakes, Tectonophysics 145, 1988, 325-327.

9. Meyer, K., R. Pirjola, Anomalous electroteluric residuals prior to a large imminent earthquake, Tectonophysics, 125, 1986, 371-376.

10. Molchanov, O. A., M. Hayakawa, On the generation mechanism of ULF seismogenic electromagnetic emissions, Phys. Earth Planet.Inter. 105, 1998, 229-238.

11. Mizutani, H., T. Ishido, T. Yokokura, S. Ohnishi, Electrokineti phenomena associated with earthquakes, Geophys. Res. Lett. 3, 1976, 365-368.

12. Jouniaux, L., J. P. Pozzi, Permeability dependence of streaming potential in rocks for various fluid conductivities, Geophys. Res. Lett., 22, 1995, 485-488.

13. Nitsan, U., Electromagnetic emission accompanying fracture of quartz-bearing rocks, Geophys. Res. Lett. 4, 1977, 333-337.

14. Czechowski, Z., A kinetic model of crack fusion, Geophys. J. Int. 104, 1991, 419-422.

15. Tzanis, A., F. Vallianatos, F., S. Gruszow, Phys. Earth Planet. Int. 105, 2000, 201-210.

16. Cress, G.O., B. T. Brady, G. A. Rowell, Sources of electromagnetic radiation from fracture of rock samples in laboratory, Geophys. Res. Lett. 14, 1987, 331-334.

17. Rikitake, T., Earthquake prediction, Developments in Solid Earth Geophysics, Ser. 9, Elsevier Sci. Publ. Company, Amsterdam. 1976.

18. Troyan, V. N., N. A. Smirnova, Yu. A. Kopitenko, Th. Peterson, M. Hayakawa, Development of complex approach for searching and investigation of electromagnetic precursors of earthquakes: Organization of experiments and analysis procedure, in Atmospheric and Ionospheric Electromagnetic Phenomena Associated with Earthquakes, ed. M. Hayakawa, Terra Scientific Publishing Co., Tokyo, 1999, 147-170.

19. Takayasu, H., I. Nishikawa, H. Tasaki, Power-law mass distribution of aggregation systems with injection, Phys. Rev. A37, 1988, 3110-3117.

20. Ishizaka S., in Proc. Ist. Symp. For Science on Form, ed. S. Ishisaka, KTK Scientific, Tokyo, 1986, 15.

21. Huber G., Scheidegger`s rivers, Takayasu`s aggregates and continued fractions, Physica A, A 170, 1991, 463-470.

22. Enomoto, J., H. Hashimoto, Emission of charged particles from indentation fracture of rocks, Nature 346, 1990, 641-643.

23. Ogawa T., K. Oike, T. Miura, Electromagnetic radiation from rocks, Jour. Geophis Res., 90, 1985, 6245-6249.

24. Granovskiy, V. L., Electric current in gases (in Russian), eds. L.A. Sen and V.E. Golant, Nauka, Moscow, 1971.

25. Landau, L.D., E. M. Lifshits, Electrodynamics of continuous media (in Russian), Theoretical Physics, vol. VIII, second edition, Nauka, Moscow. 1982.

26. Abramovitz, M., I. A. Stegun, Handbook of Mathematical Functions, Nat. Burreau of Standarts, Appl. Math. Series, 55, 1964.

27. Dobrovolsky, I. P., N. I. Gershenzon, M. B. Gokhberg, Theory of electrokinetic effects occuring at the final stage in the preparation of a tectonic earthquake, Phys. Earth Planet. Inter. 57, 1989, 144-156.

28. Fenoglio, M.A., M. S. Johnson, J. D. Byerlee, Magnetic and electric fields associated with changes in high pore pressure in fault zone – application to the Loma Prieta ULF emissions, Proc. Workshop LXII, Menlo Park, CA, 1994, 262-278.

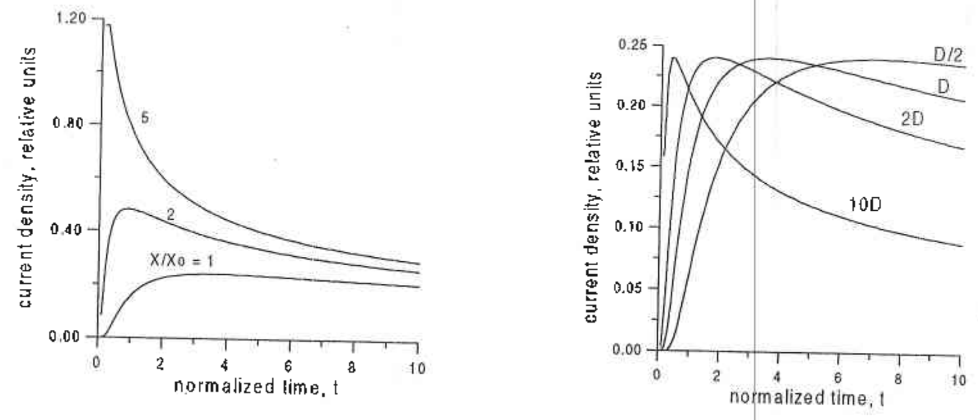

Fig. 1. Microcrack density production Z(x,t) according to random aggregation mechanism. The production depends on the position x and diffusion coefficient D.

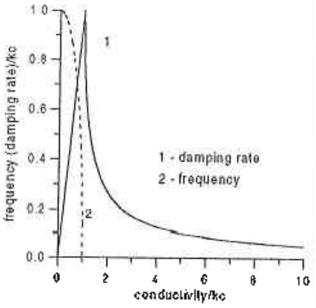

Fig. 2. The frequency and the damping rate of SES and ULF disturbances vs. normalized conductivity: $\sigma_{crust}/(2k/\mu_0 c)$.

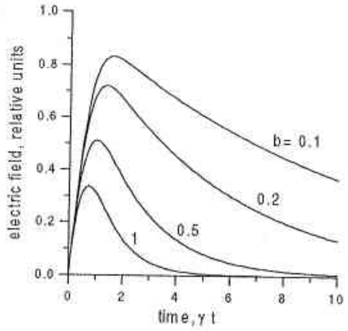

Fig. 3. The SES envelopes for given wavenumber k provided that the discharge moment $t_0 \to \propto$. Time is normalized – $T = \gamma t$. Parameter $b \equiv \surd Ddcotg(\theta)/\gamma$ (see text)

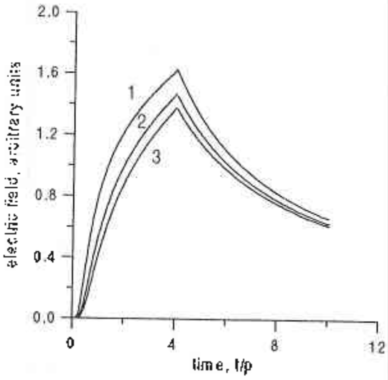

Fig. 4a

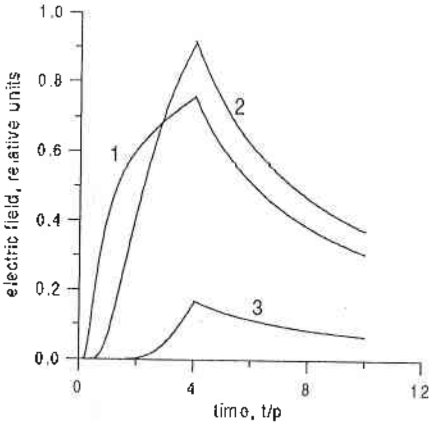

Fig. 4b

The SES envelopes in z (5a)) and x (5b)) directions. Curves 1–3 correspond to different distances: 1) 100/√π km; 2) 200/√π and 3) 400/√π km. Various forms of SES envelope in x direction are indicated. In x direction the SES envelopes feature either triangle form of different amplitudes, or ‘shark fin’ profile.

ВЪРХУ МЕХАНИЗМА НА ГЕНЕРАЦИЯ НА СЕИЗМИЧНИ ЕЛЕКТРИЧЕСКИ СИГНАЛИ

Петко Неновски, Бойчо Бойчев

Резюме

Предложен е модел на генерация на сеизмични електрически сигнали (СЕС), свързан с формирането на заряди и токове при процеса на разряд в пространството на микропукнатини. Електрическото поле в микропукнатината нараства до започването на разряден процес. След формиране на електрическото поле и неговото неутрализиране токът j се разпространява в околността на микропукнатината. Изследват се пространственото и времевото разпределение на електрическото поле, свързано с тока около микропукнатината. Полето зависи от скоростта на агрегация, разряда и геофизичните свойства на средата.

Bulgarian Academy of Sciences. Space Research Institute
Aerospace Research in Bulgaria. 17, 2003. Sofia

NONLINEAR OSCILLATOR UNDER EXTERNAL ASYNCHRONOUS INFLUENCE: COMPARISON OF CANONICAL AND NON-CANONICAL PERTURBATION METHODS OF ANALYSIS [+)]

Vladimir Damgov[*] *and Petar Georgiev*[**]

[*] *Space Research Institute-Bulgarian Academy of Sciences*
[**] *Department of Physics at the Technical University-Varna*

Abstract

A non-canonical (non-Hamiltonian) perturbation method for study of nonlinear oscillator under external asynchronous action in variables "energy-angle" is presented. As new variables, the iteration constants of the original solution are introduced. Consistently applying the method of canonical transformations and producing functions, a canonical approach in "action-angle" variables is developed for analysis of the same system under similar conditions. Both approaches are characterized by the transition, in the very beginning, to functions with constant period and only then the necessary functional matrices are introduced. The same problem is studied by Kuzmak's method, characterized by the opposite approach: first, a functional square matrix is introduced, and only then a transition to functions with a constant period is made. A comparison of the results obtained using the three above-mentioned methods and approaches is made. It is shown that the solutions in the first approximation lead to equal results. In particular, this conclusion is a contribution to the idea that there is no essential difference between non-canonical (non-Hamiltonian) and canonical (Hamiltonian) methods. However, attention is drawn to the fact that the other analytical methods developed in the frame of the Theory of Nonlinear Oscillations could not give, even in the first approximations, a complete coincidence with the solution obtained using the three above-mentioned methods.

The analysis of oscillations and vibrations reduces to the problem of a nonlinear oscillator, subjected to external periodic influence (perturbation). With the development of perturbation methods, two main directions have formed: canonical (Hamiltonian) methods and non-canonical (non-Hamiltonian) methods.

[+)] Research supported by the "Scientific Research" National Council at the Bulgarian Ministry of Education and Sciences under Contract № H3-1106/01

The methods using mainly canonical transformations in action-angle variable developed earlier. This was in response to the needs of celestial mechanics – see [1]. The method of Lindstedt-Poincare as well as other methods were developed. The second direction of development of the perturbation methods are the methods of the averaged Lagrangian and the averaged Hamiltonian [2]. An overview and a modern presentation of the canonical methods are given in [3-5].

In the first half of the twentieth century, mainly the non-canonical (non-Hamiltonian) perturbation methods were developed for the purpose of analysis of nonlinear electric circuits [6-9]. M.Kruskal has developed a non-canonical theory showing that it can be equivalent to the canonical theory [10]. The development of these methods is reflected in [4, 11-13].

In the application of perturbation and in particular of the asymptotic methods a transformation is made to a generating solution with constant period $P_0 = 2\pi$. A number of methods have been developed for this purpose. In the case of non-canonical methods, the integration constants of the generating solution serve as the new variables while in the case of the canonical methods with the aid of a canonical transformation the treatment is done in action-angle variables (these two approaches are used below). A third possible method is the regularized Euler method introducing a new independent variable [14-16]. After the transformation the generating (non-perturbed) equation coincides with the equation of the harmonic oscillator. K.A.Samoylo has suggested the so-called method of non-linear transformation employing the transformation of the dependent (coordinate) as well as the independent (time) variables. In this case the generating equation again coincides with the equation of the harmonic oscillator. Finally, a method has been developed in which the generating solution has a variable period (dependent on the amplitude). In this case the solution of the variation equation contains secular terms which at a later stage are compensated. This method is by G.E. Kuzmak [18] and has been further developed in a number of works, i.e. [19-23].

We should also mention a number of modifications of the perturbation methods used for analysis of non-linear waves as well as a number of perturbation methods based on conservation laws. In the analysis of solution phenomena perturbation methods are used which based on the Inverse Scattering Method (ISM) for equations such as the Korteweg-de-Vries, the Sine-Gordon, the non-linear Schroedinger equation etc. [26,27].

The present work compares the results obtained through different perturbation methods. It is shown that the solutions using energy-angle variables and action-angle variables (via canonical transformations) and by Kuzmak's method to first approximation lead to equivalent results. This confirms the idea that between the canonical and the non-canonical perturbation methods used in particular for the analysis of an asynchronous oscillator there isn't any principal difference.

1. Generating solution

Let us consider a generalized nonlinear oscillator described by the following system of equations:

$$(1)\qquad \left|\begin{aligned} &\frac{dx}{dt} - p = 0 \\ &\frac{dp}{dt} + f(x,T) = \mu F_\nu\left(\frac{dx}{dt}, x, t, T\right) \end{aligned}\right.$$

where $0 \leq \mu \ll 1$ is a small parameter, T is secondary scaling /slow time/, $T = T_o + \mu t$, $T_o = const$, $dT/dt = \mu$. The secondary scaling (slow time) could represent the slow change of the oscillator parameters: i.e. modulation of the oscillator inductance or capacity, a drift in the supplied power etc. We will take $f(0,T) = 0$. We will seek a solution of equation (1) for x belonging to the interval satisfying $xf(x,T) \geq 0$.

The solution of the system of equations (1) for $\mu = 0$ represents the so called **generating solution** which we will represent as:

$$(2)\qquad X = X_a(E, t + t_o, T), \quad p = p_a(E, t + t_o, T),$$

Here E = const and $t_o = const$ are the constants of integration.

We introduce a circular frequency into the generating solution (2), as follows:

$$\omega(E,T) = \frac{2\pi}{\Pi(E,T)}, \quad \text{where} \quad \Pi(E,T) = 2\int_{x_{\min}}^{x_{\max}} \frac{dx}{\sqrt{2E - V(x,T)}}$$

is the period in time t and $V(x,T) = \int_0^x \sqrt{f(x',T)dx'}$ is the potential energy,

$$V(x_{\min}, T) = V(x_{\max}, T) = E(T)$$

An angle variable Ψ and an integration constant $\alpha = const$ are introduced through the expressions: $t = \dfrac{\Psi}{\omega(E,T)}$, $t_o = \dfrac{\alpha}{\omega(E,T)}$.

Let $\theta = \Psi + \alpha$. We introduce the new functions:

$$(3)\qquad \left|\begin{aligned} &x = x_b(E,\theta,T) = x_a\left(E, \frac{\theta}{\omega(E,T)}, T\right) \\ &p = p_b(E,\theta,T) = p_a\left(E, \frac{\theta}{\omega(E,T)}, T\right) \end{aligned}\right.$$

which are periodic in Ψ and θ with period $p_0 = 2\pi$, independent of E. Therefore the derivatives $\partial x_b/\partial\theta$, $\partial p_b/\partial\theta$, $\partial x_b/\partial E$ and $\partial p_b/\partial E$ are periodic, i.e. they do not contain secular terms.

The system of equations (1) takes the form:

(4)
$$\left|\begin{array}{l} \omega(E,T)\dfrac{\partial x_b(E,\theta,T)}{\partial\theta} - p_b(E,\theta,T) = 0, \\ \omega(E,T)\dfrac{\partial p_b(E,\theta,T)}{\partial\theta} + f(x_b,T) = 0, \end{array}\right.$$

or

(5)
$$\mathbf{Y}\begin{bmatrix} 0 \\ \omega \end{bmatrix} + \begin{bmatrix} -p_b \\ f(x_b,T) \end{bmatrix} = 0\,,$$

where

(6)
$$\mathbf{Y}(E,\theta,T) = \begin{bmatrix} \dfrac{\partial x_b(E,\theta,T)}{\partial E} & \dfrac{\partial x_b(E,\theta,T)}{\partial\theta} \\ \dfrac{\partial p_b(E,\theta,T)}{\partial E} & \dfrac{\partial p_b(E,\theta,T)}{\partial\theta} \end{bmatrix}.$$

The matrix **Y** is periodic as the period $p_o = 2\pi$ is constant and it satisfies the condition for the absence of secular terms.

2. Perturbation in energy-angle variables

We now perturb equation (1) at $\mu \neq 0$. We vary the constant parameters taking $E = E(t)$ and $\alpha = \alpha(t)$.

Taking into account (4) we obtain the following system of equations, equivalent to system (1):

(7)
$$\frac{d\Psi}{dt} = \omega(E,T); \quad \theta(t) = \Psi(t) + \alpha(t)$$

(8)
$$\begin{bmatrix} \dfrac{dE}{dt} \\ \dfrac{d\theta}{dt} \end{bmatrix} = \begin{bmatrix} 0 \\ \omega(E,T) \end{bmatrix} + \mu\begin{bmatrix} G_r(E,\theta,t,T,\mu) \\ G_s(E,\theta,t,T,\mu) \end{bmatrix}$$

where $\begin{bmatrix} G_r \\ G_s \end{bmatrix} = \mathbf{Y}^{-1}\begin{bmatrix} -\dfrac{\partial x_b}{\partial T} \\ -\dfrac{\partial p_b}{\partial T} + F_v \end{bmatrix}$.

Here, the inverse matrix $\mathbf{Y}^{-1} = \begin{bmatrix} f(x_b, T) & p_b \\ \omega \dfrac{\partial p_b}{\partial E} & -\omega \dfrac{\partial x_b}{\partial E} \end{bmatrix}$ and correspondingly $\det \mathbf{Y} = -1/\omega$, i.e. the condition for the application of the perturbation approach, $\det \mathbf{Y} \neq 0, \infty$ is valid.

We will seek the solution (7) in the form of an asymptotic series:

$$\begin{vmatrix} E(t) = E_o(t) + \mu E_1(t) + \mu^2 E_2(t) + \dots \\ \theta(t) = \theta_o(t) + \mu\theta_1(t) + \mu^2\theta_2(t) + \dots \end{vmatrix} \tag{9}$$

Substituting (9) into (8), expanding in the powers of μ and equating the coefficients multiplying the same powers of μ^k, we obtain:

$$\begin{bmatrix} \dfrac{dE_k}{dt} \\ \dfrac{d\theta_k}{dt} \end{bmatrix} = \begin{bmatrix} 0 \\ \delta_k \end{bmatrix} + \begin{bmatrix} G_{r,k} \\ G_{s,k} \end{bmatrix}, \qquad k = 0, 1, 2, 3, \dots, \tag{10}$$

where δ_k reflects the necessary corrections to ω due to different order of approximation for E in $\omega(E,T)$, i.e.:

$$\mu^k \delta_k = \omega(E_o + \mu E_1 + \dots + \mu^{k-1} E_{k-1} + \mu^k E_k, T) - \omega(E_o + \mu E_1 + \dots + \mu^{k-1} E_{k-1}, T$$

$$G_{r,k} = \hat{G}_{r,k}(E_o, E_1, \dots, E_{k-1}, \theta_o, \theta_1, \dots, \theta_{k-1}, T)$$

$$G_{s,k} = \hat{G}_{s,k}(E_o, E_1, \dots, E_{k-1}, \theta_o, \theta_1, \dots, \theta_{k-1}, T)$$

Here $\boldsymbol{\hat{G}_{r,k}}$ and $\boldsymbol{\hat{G}_{s,k}}$ are differential operators which are applied to the obtained in the previous steps functions.

The complete determination of E_k is possible only when the coefficients of order μ^{k+1} are taken into account. The correction δ_k (10) contains E_k. This is why we solve the equation E_k simultaneously with the equation for θ_{k-1}, i.e. instead of solving (10) we should solve the system of equations:

$$\begin{vmatrix} \dfrac{dE_k}{dt} = G_{r,k}(E_o, E_1, \dots, E_{k-1}, \theta_o, \theta_1, \dots, \theta_{k-1}, t, T) \\ \dfrac{d\theta_{k-1}}{dt} = \delta_{k-1} + G_{r,k-1}(E_o, E_1, \dots, E_{k-2}, \theta_o, \theta_1, \dots, \theta_{k-2}, t, T) \end{vmatrix}$$

In (9) we do the following substitution:

$$(11)\qquad \left|\begin{array}{l} E_k(t) = L_k(t) + U_{rk}(t,T) \\ \theta_k(t) = \alpha_k(t) + U_{sk}(t,T)\,, \\ \dfrac{d\alpha_k(t)}{dt} = \omega_k(T) \end{array}\right. \qquad k=1,2,3,\ldots$$

where $U_{ro} = 0$, $U_{so} = 0$. This representation takes into account that E is a slow variable while θ is a quick variable. The quantity $L_k(t)$ is obtained only when the coefficients of order μ^{k+1} are considered.

Taking into account equation (11) the perturbation approach reduces equation (10) to:

$$(12)\qquad \left|\begin{array}{l} \dfrac{dL_{k-1}(T)}{dT} + \dfrac{\partial U_{rk}(t,T)}{\partial t} = G_{rk}(t,T) \\ \omega_k(T) + \dfrac{\partial U_{sk}(t,T)}{\partial t} = \delta_k(t,T) + G_{sk}(t,T) \end{array}\right.$$

We assume that the right-hand sides of (12) are expressed in functions the form of which was found in the previous steps.

From the condition of periodicity of U_{rk} and U_{sk} it follows that:

$$(13)\qquad \left|\begin{array}{l} \dfrac{dL_{k-1}(T)}{dT} = \langle G_{rk} \rangle_t \\ \omega_k(T) = \langle \delta_k + G_{sk} \rangle_t \end{array}\right.$$

where $< >_t$ means averaging with respect to time.

From (12) $L_{k-1}(T)$ and $\omega_k(T)$ are determined. Then we find U_{rk}, U_{sk} from the following system of equations:

$$\left|\begin{array}{l} \dfrac{\partial U_{rk}(t,T)}{\partial t} = G_{rk}(t,T) - \langle G_{rk} \rangle_t \\ \dfrac{\partial U_{sk}(t,T)}{\partial t} = \delta_k(t,T) - G_{sk}(t,T) - \langle \delta_k + G_{sk} \rangle_t \end{array}\right.$$

We should at this point note that instead of t we can use Ψ as an independent variable. In the case the system of equations (7) and (8) is equivalent to:

$$(14)\qquad \frac{dt}{d\Psi} = \frac{1}{\omega(E,T)}$$

$$(15)\qquad \begin{bmatrix} \dfrac{dE}{d\Psi} \\ \dfrac{d\theta}{d\Psi} \end{bmatrix} = \begin{bmatrix} 0 \\ 1 \end{bmatrix} + \mu\left(\frac{1}{\omega}\right)\mathbf{Y}^{-1}\begin{bmatrix} -\dfrac{\partial x_b}{\partial T} \\ -\dfrac{\partial p_b}{\partial T} + F_v \end{bmatrix}$$

The described above perturbation method can be used for the analysis of equations (14) and (15).

3. Perturbation in action-angle variables

Above we found a solution in energy-angle variables (E, θ). The crucial step was the treatment in variables x_b (E, θ, T) and p_b (E, θ, T), having a constant period $p_0 = 2\pi$ with respect to the angle (quick) variable θ. Here instead of energy E we will use the action I. Our goal is to transform canonically in such a way that the new action $I \equiv \overline{P} = const$ to be a constant while the new coordinate $\Psi \equiv \overline{X}$ is linear in time.

For the case in consideration the generating equation can be represented with the canonical equations of Hamilton:

$$\frac{dx}{dt} = \frac{\partial H}{\partial p} = P; \quad \frac{dP}{dt} = -\frac{\partial H}{\partial x} = -\frac{\partial V}{\partial x} = -f(x,T) \tag{16}$$

For the transition to action-angle variables and the achievement of the set above goal we introduce the generating function $W(x,I,T)$ such that:

$$P = \frac{\partial W(x,I,T)}{\partial t}, \quad \Psi = \frac{\partial W(x,I,T)}{\partial I}$$

$$W(x,I,T) = \pm\int_0^x \sqrt{2E(I,T) - 2V(x',T)}dx'$$

Then the new Hamiltonian is:

$\overline{H}(I,\Psi,T) = \overline{H}(I,T) = H(P,x,T) = E(T)$, where $E(T)$ is the energy integral, $E(T) = p^2/2 + \mathrm{V(x,T)}$.

The period in Ψ must be a constant and equal to 2π. The circular frequency in the generating solution is:

$$\omega_c(I,T) = \partial\Psi / \partial t = 2\pi / \Pi[E(I,T), T], \tag{17}$$

where the period in time $t = \Psi / \omega_c$ is:

$$\Pi(E,T) = 2\pi\frac{\partial I(E,T)}{\partial E} = 2\frac{\partial}{\partial E}\int_{\min x}^{\max}\sqrt{2E - 2V(x,T)}dx$$

We introduce the new functions:

$$\begin{cases} x = x_c(I,\theta,T) = x_b[E(I,T),\theta,T] \\ p = p_c(I,\theta,T) = p_b[E(I,T),\theta,T] \end{cases} \tag{18}$$

Taking into account (16)-(18), the system of equations (1) takes the form:

$$\left|\begin{array}{l}\omega_c(I,T)\left[\dfrac{\partial x_c(I,\theta,T)}{\partial\theta}\right]-p_c(I,\theta,T)=0\\ \omega_c(I,T)\left[\dfrac{\partial p_c(I,\theta,T)}{\partial\theta}\right]+f(x_c,T)=0\end{array}\right.$$

or

(19) $$\mathbf{Z}\begin{bmatrix}0\\ \omega_c\end{bmatrix}+\begin{bmatrix}-p_c\\ f(x_c,T)\end{bmatrix}=0$$

where $\mathbf{Z}(I,\theta,T)=\begin{bmatrix}\dfrac{\partial x_c(I,\theta,T)}{\partial I} & \dfrac{\partial x_c(I,\theta,T)}{\partial\theta}\\ \dfrac{\partial p_c(I,\theta,T)}{\partial I} & \dfrac{\partial p_c(I,\theta,T)}{\partial\theta}\end{bmatrix}$.

We seek the solution of the perturbed system of equations (1) by varying the constant parameters $I = I(t)$ and $\alpha = \alpha(t)$ as:

(20) $$\left|\begin{array}{l}x=x_c\left[I(t),\Psi(t)+\alpha(t),T\right]\\ p=p_c\left[I(t),\Psi(t)+\alpha(t),T\right]\\ \dfrac{d\Psi}{dt}=\omega_c\left[I(t),T\right]; \quad \theta(t)=\Psi(t)+\alpha(t)\end{array}\right.$$

Substituting (20) in (1) and taking into consideration (19) we obtain:

(21) $$\begin{bmatrix}\dfrac{dI}{dt}\\ \dfrac{d\theta}{dt}\end{bmatrix}=\begin{bmatrix}0\\ \omega_c(I,T)\end{bmatrix}+\mathbf{Z}^{-1}\begin{bmatrix}-\mu\dfrac{\partial x_c(I,\theta,T)}{\partial T}\\ -\mu\dfrac{\partial p_c(I,\theta,T)}{\partial T}+\mu F_v\end{bmatrix}$$

where $\mathbf{Z}^{-1}=\begin{bmatrix}\dfrac{1}{\omega_c}f(x_c,T) & \dfrac{1}{\omega_c}p_c\\ \dfrac{\partial p_c}{\partial I} & -\dfrac{\partial x_c}{\partial I}\end{bmatrix}$, $\det\mathbf{Z}=-1$.

The system (21) can be expressed as:

(22) $$\begin{bmatrix}\dfrac{dI}{dt}\\ \dfrac{d\theta}{dt}\end{bmatrix}=\begin{bmatrix}0\\ \delta\end{bmatrix}+\begin{bmatrix}G_v(I,\theta,t,T,\mu)\\ G_w(I,\theta,t,T,\mu)\end{bmatrix}$$

where δ is the necessary adjustment of ω_c.

We seek the solution of (22) in the form:

(23)
$$\left|\begin{array}{l} I = I_o(T) + \mu[I_1(T) + U_{v1}(t,T)] + \mu^2[I_2(T) + U_{v2}(t,T)] + \dots \\ \theta = \theta_o(T) + \mu[\theta_1(T) + U_{w1}(t,T)] + \mu^2[\theta_2(T) + U_{w2}(t,T)] + \dots \\ \delta = \mu\delta_1 + \mu^2\delta_2 + \mu^3\delta_3 + \dots \\ \dfrac{d\theta_o(t)}{dt} = \omega_o(T); \quad \dfrac{d\theta_1(t)}{dt} = \omega_1(T); \quad \dfrac{d\theta_2(t)}{dt} = \omega_2(T); \dots \end{array}\right.$$

where $U_{Vk}\ (t,T)$ and $U_{Wk}\ (t,T)$ do not contain secular terms, i.e.

(24)
$$\left\langle \frac{\partial}{\partial t} U_{vk}(t,T) \right\rangle_t = 0, \quad \left\langle \frac{\partial}{\partial t} U_{wk}(t,T) \right\rangle_t = 0, \quad k = 1, 2, 3, \dots$$

Substituting (23) in (22), developing in a series in the powers of μ and equating the coefficients multiplying the same powers of μ^k we get:

- in front of μ^o

$\dfrac{d\theta_o(t)}{dt} = \omega_{oo}(T)$, where $\omega_{oo}(T) = \omega_C(I_{oo}, T)$ the initial value I_{oo} is taken at the moment t = 0, i.e.

$$I_{oo} = I(T)\big|_{t=0}$$

or
$$\theta_o(t) = \int_0^t \omega_c(I_{oo}, T + \mu t')dt' + const$$

- in front of μ^1

(25)
$$\frac{dI_o(T)}{dT} + \frac{\partial U_{v1}(t,T)}{\partial t} = G_v(I_o(T), \theta_o(T), t, T, 0)$$

(26)
$$\omega_1(T) + \frac{\partial U_{w1}(t,T)}{\partial t} = \delta_1 + G_w(I_o(T), \theta_o(T), t, T, 0)$$

and accordingly
$$\delta_1 = \left[\frac{\omega_c(I_o(T), T - \omega_c(I_{oo}, T)}{\mu}\right]$$

$$\delta_2 = \left[\frac{\omega_c(I_o(T) + \mu I_1(T) + \mu U_{v1}(t,T)) - \omega_c(I_o(T), T)}{\mu^2}\right]$$

etc.

Averaging the two sides of (25) and (26) and taking into account (24) we obtain:

(27)
$$\frac{dI_o(T)}{dT} = \langle G_v[I_o(T), \theta_o(T), t, T, 0] \rangle_t$$

$$\omega_1(T) = \left\langle G_w[I_{oo}(T), \theta_{oo}(T), t, T, 0] + \delta_1 \right\rangle_t \tag{28}$$
$$\theta_1(t) = \int_0^t \omega_1(T_o + \mu t')dt' + const$$

The differential equation (26) can be resolved, i.e. through successive approximations and development of T in a power series. The determined by (27) quantity $I_o(\Psi)$ is then substituted in (28).

So, we have come on the approximation as follows:

$$\begin{bmatrix} \left\langle \dfrac{dI}{dt} \right\rangle_t \\ \left\langle \dfrac{d\theta}{dt} \right\rangle_t \end{bmatrix} = \begin{bmatrix} 0 \\ \omega_o \end{bmatrix} + \mu \left\langle \mathbf{Z}^{-1} \begin{bmatrix} -\dfrac{\partial x_c}{\partial T} \\ -\dfrac{\partial p_c}{\partial T} + \mu F_v \end{bmatrix} \right\rangle \tag{29}$$

where [$\omega_o = \omega_c$ [I$_o(T)$, T]= $\omega_{oo} + \mu\, \delta_1$

Then

$$U_{v1}(t,T) = \int_0^t \left[G_{v1} - \langle G_{v1} \rangle_t \right] dt' + const$$
$$U_{w1}(t,T) = \int_0^t \left[G_{w1} + \delta_1 - \langle G_{w1} + \delta_1 \rangle_t \right] dt' + const$$

4. Solution by Kuzmak's method in matrix form

In the two methods developed above we first transformed to functions with a constant period $p_o = 2\pi$ and only then introduced matrices **Y** and **Z**. This is why **Y** and **Z** turned out to be periodic. With Kuzmak's method [18] one proceeds in the reverse order: first, the functional square matrix Ξ is introduced and only then the transformation to constant period functions is performed. As a result, Ξ is not periodic but contains secular terms. In the analysis of the perturbed equation these terms compensate each other and the final solution is periodic. Here, we will develop a version of Kuzmak's method on the basis of a matrix presentation in application to an asynchronous non-linear oscillator.

The generating solution of the system of equations (1) when $\mu \equiv 0$ is assumed to be in form (2).

We introduce the matrix:

$$\Xi(E, t + t_o, T) = \begin{bmatrix} \dfrac{\partial x_o(E, t + t_o, T)}{\partial E} & \dfrac{\partial x_o(E, t + t_o, T)}{\partial (t + t_o)} \\ \dfrac{\partial p_o(E, t + t_o, T)}{\partial E} & \dfrac{\partial p_o(E, t + t_o, T)}{\partial (t + t_o)} \end{bmatrix}, \tag{30}$$

so that the following variation equation is satisfied:

$$\frac{\partial \Xi}{\partial t} + \mathbf{B}\,\Xi = 0, \text{ where } \mathbf{B} = \begin{pmatrix} 0 & -1 \\ \frac{\partial f}{\partial x_o} & 0 \end{pmatrix}. \tag{31}$$

Besides

$$\Xi = \mathbf{Y}\,\mathbf{H}\,[1 - (t+t_o)\,\mathbf{Q}\,], \tag{32}$$

where $\mathbf{H} = \begin{bmatrix} 1 & 0 \\ 0 & \omega \end{bmatrix}$ $\quad \mathbf{Q} = \begin{bmatrix} 0 & 0 \\ \frac{\partial \ln \Pi(E,T)}{\partial E} & 0 \end{bmatrix}$

Then $\det \Xi = -1$ and $\Xi^{-1}(E, t+t_o, T) = [1 + (t+t_o)\mathbf{Q}]\,\mathbf{H}^{-1}\mathbf{Y}^{-1}$.

The solution of the perturbed system of equations (1) we seek in the form:

$$\left| \begin{array}{l} x = x_b\ [E(T),\ \Psi(t) + \alpha(T), T\,] + \mu\, U_{1a}\ (t,T) \\ p = p_b\ [E(T),\ \Psi(t) + \alpha(T), T\,] + \mu\, U_{2a}\ (t,T) \end{array} \right.$$

where the constant parameters Ψ, E, α, θ, and dΨ/dt = ω(E,T) are varied. We lay down conditions U_{1a} and U_{2a} not to contain secular terms.

The following equation is satisfied:

$$\begin{bmatrix} \frac{dx}{dt} \\ \frac{dp}{dt} \end{bmatrix} = \begin{bmatrix} \omega \frac{\partial x_b}{d\theta} \\ \omega \frac{dp_b}{d\theta} \end{bmatrix} + \mu \mathbf{Y} \begin{bmatrix} \frac{dE}{dT} \\ \frac{d\alpha}{dT} \end{bmatrix} + \mu \begin{bmatrix} \frac{\partial x_b}{dT} + \frac{\partial U_{1a}}{\partial t} + \mu \frac{\partial U_{1a}}{\partial T} \\ \frac{\partial p_b}{dT} + \frac{\partial U_{2a}}{\partial t} + \mu \frac{\partial U_{2a}}{\partial T} \end{bmatrix}.$$

We also introduce the matrix:

$$\mathrm{U}_{\mathrm{a}}(t,T) = \begin{bmatrix} \mathrm{U}_{\mathrm{a1}}(t,T) \\ \mathrm{U}_{\mathrm{a2}}(t,T) \end{bmatrix}$$

We seek the solution in the form of an asymptotic series:

$$\left| \begin{array}{ll} \Psi(t) = \Psi_o(t) + \mu \Psi_1(t) + \mu^2 \Psi_2(t) + \ldots & \\ \alpha(T) = \alpha_o(T) + \mu\alpha_1(T) + \mu^2 \alpha_2(T) + \ldots & \\ \theta(t,T) = \theta_o(t,T) + \mu\theta_1(t,T) + \mu^2 \theta_2(t,T) + \ldots & \\ \theta_k(t,T) = \varphi_k(t) + \alpha_k(t), & k = 0, 1, 2, \ldots \\ E(T) = E_o(T) + \mu E_1(T) + \mu^2 E_2(T) + \ldots & \\ \mu U_a(t,T) = \mu U_1(t,T) + \mu^2 U_2(t,T) + \ldots & \\ U_k(t,T) = \begin{bmatrix} U_{k1}(t,T) \\ U_{k2}(t,T) \end{bmatrix}, & k = 1, 2, 3, \ldots \end{array} \right. \tag{33}$$

We set as a goal that U_{k1}, U_{k2} must not contain secular terms.

The generating solution has the form (5).

Substituting (33) in (1) and taking (5) into account developing in a series in the powers of μ and equating the coefficients multiplying the same powers of μ^k, we get:

- in front of μ^o

$$\frac{d\Psi_o(t)}{dt} = \omega(E_{oo}, T) \tag{34}$$

$$d\Psi_o = \int_0^t \omega(E_{oo}, T_o + \mu t')dt'$$

where E_{oo} is the initial value of $E_o(T)$ at the moment $t = 0$ and when $T = T_o$;

- in front of μ^k

$$\frac{\partial \mathbf{U}_k(t,T)}{\partial t} + \mathbf{B}\mathbf{U}_{k(}t,T) = \mathbf{\Phi}_k; \qquad \kappa = 1,2,3,\ldots \tag{35}$$

where $\quad \mathbf{\Phi}_k = col(\Phi_{k1}, \Phi_{k2},) \dfrac{d\Psi_k(t)}{dt} = \delta_k(T_o + \mu t), \qquad k = 1,2,3,\ldots$

$$\Psi_k(t) = \int_0^t \delta_k(T + \mu t')dt' \tag{36}$$

δ_k are the necessary adjustments of ω

$$\delta_1(T_o + \mu t) = \delta_1(T) = \frac{\omega[E_o(T),T] - \omega[E_{oo},T]}{\mu}$$

$$\delta_k(T_o + \mu t) = \delta_k(T) = \frac{\omega\left[E_o(T) + \mu E_1(T) + \ldots + \mu^{k-1}E_{k-1}(T)\right] - \omega\left[E_o(T) + \mu E_1(T) + \ldots + \mu^{k-2}E_{k-2}(T)\right]}{\mu^k}$$

,
k=2,3,4,.....

In particular, for the coefficient multiplying μ^1 we obtain:

$$\frac{\partial \mathrm{U}_1(t,T)}{\partial t} + \mathrm{B}\mathrm{U}_1(t,T) = \Phi_1;$$

where

$$\mathbf{\Phi}_1 = -\mathbf{Y}\begin{bmatrix} \dfrac{dE_o(T)}{dT} \\ \dfrac{d\alpha(T)}{dT} \end{bmatrix} + \begin{bmatrix} -\dfrac{\partial x_b}{\partial T} \\ -\dfrac{\partial p_b}{\partial T} + F_v \end{bmatrix} \tag{37}$$

Here $F = F(\frac{dx_b}{dt}, x_b, t, T, 0)$.

We seek the solution of equation (35) in the form:

$$\mathbf{U}_k(t,T) = \Xi \mathbf{V}_k(t,T), \qquad k = 1,2,3,... \tag{38}$$

where

$$\mathbf{V}_k(t,T) = \begin{bmatrix} V_{k1}(t,T) \\ V_{k2}(t,T) \end{bmatrix}, \qquad k = 1,2,3,...$$

Substituting (38) into (35) and taking (31) into account we get:

$$\mathbf{V}_k(t,T) = \mathbf{V}_k(0,T) + \int_0^t \Xi^{-1}(E, t'+t'', T)\Phi(t',T)dt' \tag{39}$$

From equation (14) it follows:

$$\mathbf{V}(t,T) = \mathbf{V}(0,T) + \int_0^t [1 + (t'+t_o)\mathbf{Q}]\mathbf{H}^{-1}\mathbf{Y}^{-1}\Phi dt' \tag{40}$$

$$= \mathbf{V}(0,T) + \int_0^t [1 + (t'+t_o)\mathbf{Q}]\{\frac{\partial}{\partial t'}[\mathrm{K}_1 + \mathbf{D}(T)t']\}dt'$$

where matrices $\mathbf{D}(\mathrm{T})$ and $\mathbf{K}_1$ have been introduced through the relations:

$$\mathrm{D}(T) = \left\langle \mathrm{H}^{-1}\mathrm{Y}^{-1}\Phi \right\rangle_t \tag{41}$$

$$\int_0^t \mathrm{H}^{-1}\mathrm{Y}^{-1}\Phi dt' = \mathrm{K}_1[\Psi(t), T] + \mathrm{D}(T)t$$

for $\mathbf{K}_1$ $[\Psi(0),\mathrm{T}] = 0$.

Integrating (40) by parts we get:

$$\mathrm{V}(t,T) = \mathrm{V}(0,T) + [-1 + (t+t_o)\mathrm{Q}][\mathrm{K}_1 + \mathrm{D}(t)t] - \mathrm{Q}[\mathrm{K}_2 + \mathrm{L}(t)t + \frac{Dt^2}{2}]$$

where $\mathbf{L}(t) = <\mathbf{K}_1>_t$ and

$$\int_0^t \mathrm{K}_1[\Psi(t'), T]dt' = \mathrm{K}_2[\Psi(t), T] + \mathrm{L}(T)t$$

Substituting in (38) and taking into account (32) as well as the fact that $\mathbf{Q}^2=0$, we obtain:

$$U(t,T) = YH\{\frac{QDt^2}{2} + [D - QL(T) - QV(0,T)]t + K_1 - QK_2 + (1 - t_0Q)V(0,T)\}$$

The matrix function $\boldsymbol{U}$ will be periodic in t if $\boldsymbol{QD}$=0 and $\boldsymbol{D}$(T) = $\boldsymbol{Q}$ [$\boldsymbol{L}$(T) + (0,T)] to the satisfaction of which it is sufficient to do the substitution:

(42), (43) $\qquad \boldsymbol{D}=0, \quad V(0,T) = -\boldsymbol{L}(T)$

In doing this we obtain:

(44) $\qquad \boldsymbol{U} = \boldsymbol{YH}\ [\boldsymbol{K_1} - \boldsymbol{QK_2} + (1 - t_0\ \boldsymbol{Q})\ \boldsymbol{V}\ (0,T)]$

Taking into account definition (41), condition (44) is equivalent to:

$$< Y^{-1} \Phi_k >_t = 0 \qquad k=1,2,3, \ldots$$

In particular, when k = 1 from (37) and (45) it follows:

(46) $$\begin{bmatrix} \dfrac{dE_o(T)}{dT} \\ \dfrac{d\alpha_o(T)}{dT} \end{bmatrix} = \Bigg\rangle Y^{-1} \begin{bmatrix} -\dfrac{\partial x_b}{\partial T} \\ -\dfrac{\partial p_b}{\partial T} + F_v \end{bmatrix} \Bigg\langle_t$$

In this way we obtained a system of equations (36), (43) and (46) which in addition serve as a basis of comparison with the results obtained with the non-canonical perturbation approach in energy-angle variables.

Conclusion

We conclude with the important observation that to first approximation the solution in energy-angle variables coincides with the solution to first order in action-angle variables as well as with the solution obtained by Kuzmak's method.

Indeed if in (29) we substitute $\omega = \omega_c = \dfrac{\partial E(I,T)}{\partial I}$ for $I = I_o\ (T)$, i.e. $\omega = \omega_o$ as well as $Z = Y\begin{pmatrix} \omega_c & 0 \\ 0 & 1 \end{pmatrix}$, we obtain:

(47) $$\begin{bmatrix} \omega\left\langle \dfrac{dI}{dt} \right\rangle \\ \omega\left\langle \dfrac{d\theta}{dt} \right\rangle \end{bmatrix} = \begin{bmatrix} 0 \\ \omega_o \end{bmatrix} + \mu \left\langle Y^{-1} \begin{bmatrix} -\dfrac{\partial x_c}{\partial T} \\ -\dfrac{\partial p_c}{\partial T} + F_v \end{bmatrix} \right\rangle_t$$

The comparison of equation (47) with the averaged equation (8) confirms the above conclusion. An analogous conclusion can be obtained through analysis of and comparison with equation (46).

The obtained results contribute in support of the idea that, in particular in the analysis of an oscillator under external asynchronous influence there isn't any significant difference between the non-canonical (non-Hamiltonian) and the canonical (Hamiltonian) methods. It is necessary, though, to mention that a number of other methods exist in the theory of non-linear oscillations which are not even to first order completely equivalent with the solution obtained by the considered above three methods.

References

1. Пуанкаре, А. Избранные труды в 3-х томах. Том I. Новые методы небесной механики. М., Наука,1971
2. Whitham, G. B. Linear and Nonlinear Waves, Wiley, 1977
3. Giacaglia, G. E. O. Perturbation Methods in Nonlinear Systems. Springer, 1979
4. Лихтенберг А., М. Либерман. Регулярная и стохастическая динамика. М., Мир, 1984
5. Павленко, Ю. Гамилтоновы методы в электродинамике и в квантовой механике. Изд. МГУ, 1985
6. Van der Pol B. On Oscillation Hysteresis in a Simple Triode Generator. Phil;. Mag., 43, 700-719
7. Крылов, Н. М. Н. Н. Боголюбов. Введение в нелинейную механику. Киев, АН УССР, 1937
8. Боголюбов, Н. Н., Ю. А. Митропольский, Асимптотические методы в теории нелинейных колебаний. М., Наука, 1974
9. Малкин, И. Г. Некоторые задачи теории нелинейных колебаний. М. Гостехиздат, 1956
10. Крускал, М. Адиабатические инварианты. М., ИЛ, 1962
11. Nayfeh, A. N. Perturbation Methods, Wiley, 1973
12. Андронов, А. А., А. А. Вит, С. Э. Хайкин. Теория колебаний. М., Наука, 1981
13. Мойсеев, Н. Н. Асимптотические методы нелинейной механики. М. Наука, 1981
14. Szebehy, V. Theory of Orbits: The Restricted Problem of Three Bodies, Academic Press, 1982
15. Stiefel, E. L., G. Scheifele. Linear and Regular Celestial Mechanics: Perturbed Two-Body Motion Numerical Methods, Canonical Theory. Springer, 1975
16. Roy A. E. Orbital Motion. Bristol, Adam Hilger Ltd., 1981
17. Самойло, К. А. Метод анализа колебательных систем второго порядка. М., Сов. радио, 1976
18. Кузмак, Г. Е. Асимптотические решения нелнейных дифференциялных уравнений второго порядка с переменными коеффицентами - Прикладная математика и механика. 23, 1959, №3, 515-526
19. Luke, I. C. A Perturbation Method for Non-Linear Dispersive Wave Problems, Proc.Royal Soc. London, Ser.A, 292, No.1430, 403-412
20. Ablowitz, M. J., D. J. Benney. The Evaluation of Multi-Phase Modes for Non-Linear Dispersive Waves. Stud. Appl. Mah., 49, 1970, No.3, 225-238
21. Gorschkov K. A., L. A. Ostrovsky, E. N. Pelinovsky, Some Problems of Asymptotic Theory of Nonlinear Waves. Proc. IEEE, 62, 1974, No.11, 1511-1517
22. Островский, Л. А., Е. Н. Пелиновский, Метод усреднения для несинусоидальных волн — ДАН СССР, 195, 1970, No.4, 804-806
23. Георгиев, П. Г., А. Я. Спасов. К вопросу о возмущениях нелинейных волн — Болг.физ.ж., 15, 1988, No.6, 531-544
24. Нелинейные волны: Стохастичность и турбулентность — В: Сб.статей, Горкий, 1980
25. Нелинейные волны: Самоорганизация — В: Сб.статей, М., Наука, 1983
26. Лем, Дж. Л. Введение в теорию солитонов, М., 1983
27. McLanghlin D. W., A. C. Scott. Solitons in Action, Academic Press, 1978

НЕЛИНЕЕН ОСЦИЛАТОР ПОД ВЪНШНО АСИНХРОННО ВЪЗДЕЙСТВИЕ: СРАВНЕНИЕ НА КАНОНИЧНИТЕ И НЕКАНОНИЧНИТЕ ПЕРТУРБАЦИОННИ МЕТОДИ ЗА АНАЛИЗ

Владимир Дамгов и Петър Георгиев

Резюме

В статията е представен неканоничен (нехамилтоновски) пертурбационен метод за изследване на нелинеен осцилатор под външно асинхронно въздействие с променливи "енергия-ъгъл". Като нови променливи са въведени итерационните константи на първоначалното решение. Прилагайки последователно метода на каноничните трансформации и получавайки функциите, е разработен каноничен метод с променливи "действие-ъгъл" за анализ на същата система в подобни условия. Двата метода се характеризират с извършване още в началото на преход към функции с постоянен период, като едва след това се въвеждат необходимите матрици на функционала. Същият проблем е изследван по метода на Кузмак, който се отличава с обратния подход - най-напред се въвежда квадратната матрица на функционала, и едва след това се осъществява прехода към функции с постоянен период. Направено е сравнение на резултатите, получени при използване на трите гореспоменати метода. Показано е, че решенията в първо приближение водят до еднакви резултати. Конкретно, това заключение е принос към идеята, че няма съществена разлика между неканоничните (нехамилтоновски) и каноничните (хамилтоновски) методи. Обръща се внимание, обаче, на факта, че другите методи, разработени в рамките на теорията на нелинейните колебания, не могат да дадат дори в първо приближение пълно съвпадение с решенията, получени при използването на трите гореспоменати метода.

Bulgarian Academy of Sciences. Space Research Institute
Aerospace Research in Bulgaria. 17.2003. Sofia

STUDY OF THE NEOTECTONICS AND GEODYNAMICS OF THE REPUBLIC OF BULGARIA

Hernani Spiridonov, Nikola Georgiev

Space Research Institute–Bulgarian Academy of Sciences

Abstract

In the paper, the modern tectonics and geodynamics of Bulgaria are studied. The specification of general tectonic units, its varied inner morphologic. tectonic structure, the borders between them and the recent geodynamics have been investigated by combination of two approaches: use and application of remote sensing information and general interpretation of data obtained by geodetic, geophysics, geologo-geomorphologic observations, measurements and different in scale maps, photographs and other materials.

Using the two approaches ring and linear structures on the territory of Bulgaria are established. The following important ring structures have been observed: Beloslatinska, Plevenska, Lukovitska, Popovska, Nikopolsko-Pavlikenska, Montanska, Velikotarnovska, Botevgradska, Central Srednogorska, Sakarska, Central Rhodopean. Some more important lineaments are: South-Moesian, Maritza, Olt–Ossamska and others.

On the territory of Bulgaria there are recent vertical movements. At present, the Danube plane (Moesian platform) generally sinks by 1-2 mm/year along the Danube river. All ring structures have risen by about 0,1-0,2 mm/year whereas some of them like the Pirin and the Rhodopes mountains have risen by up to 3-3,5 mm/year.

Key words: remote sensing, vertical movements, tectonics, geodynamics, geology, geomorphology.

1. Introduction.

In this publication, the modern tectonics and geodynamics of Bulgaria are studied. For the purpose, both remote sensing (aerospace) and ground-based data from the whole complex of Earth sciences are used.

The task was implemented on a polygon of Bulgarian territory comprising the central regions of the country from the Danube river as far as the Greek border. The polygon's width is 200 m. In the north, it stretches from the town of Lom on the west to the town of Russe reaching the White Sea coast to the south. The polygon was chosen in such a way as to cross transversely the major neotectonic units of Bulgaria: the Moesian platform or the Danube plane, the Predbalkan, the Stara Planina mountain, the Srednogorie region, and the Rhodopes massif. This polygon is known as the Balkanprob Project; it constitutes the southern deviation of the Europrob European geodynamic model.

The set task was theoretically based on the principles of new global tectonics (platetectonics). In view of the latest achievements in the field, Bulgaria and the Balkan peninsula are considered as an active outskirts (segment) of the European plate. In it first-class tectonic units are outlined: the Moesian platform, and the platform's deformed outskirts (Balkanides, Stednogorie and the autohtonous parts of the Kraishte, the Rhodopes, Sakar, and Strandzha). On the latter two areas, post-collage paleogen-neogen sediment basins are identified. Nowadays, space onlook onto Bulgarian territory becomes essential, since it provides both global and regional overview of the individual accretion blocks with various paleographic behaviour, which underwent and are still undergoing varied paleogeodynamic development.

In the methodological aspect, the task was accomplished using both aerospace (remote sensing) data as well as data from the classical Earth sciences..

2. Analysis of remote sensing, geologo-geomorphologic, and geodetic data.

2.1. Analysis of remote sensing (aerospace) data.

The studied territory comprises the central band of Bulgaria, from the Danube river to the Bulgarian-Greek frontier; it is 200 km wide and crosses well-known tectonic zones: the Danube platform, the Predbalkan, Stara Planina mountain, the Srednogorie, and the Rhodopes mountain.

As a result of the deciphering of space images of various scale and spectral ranges, linear and concentric structures were identified, and with respect to North Bulgaria, space images of scale M 1:100000 were also used. The latter allowed to outline some new structures, which will be considered, too.

In the course of work, a hypsometric map of Bulgaria was used, with height belts drawn at every 100 m (in scale M 1:1000000). The topographic background greatly assists the process of deciphering. Geologic and tectonic maps were used (M 1:500000; M 1:200000) and besides, some geophysical materials were interpreted, concerning the depth structure of Bulgaria.

In the process of structural-geomorphologic deciphering of space and photograph images of Bulgaria, most often, linear and ring structures are identified structures (Fig. 1, Fig. 2).

2.2. Analysis of linear structures.

On the neotectonic scheme (Fig. 1, Fig. 2), the linear structures are divided into two groups:

a) geologic faults known from other studies and confirmed by this interpretation;

b) space-tectonic lineaments, some of which have been identified with great certainty by a number of direct or indirect deciphering indexes.

An important and notable boundary of the Moesian platform is the North-Predbalkan or South-Moesian fault [3, 8]. The different sections of the South-Moesian lineament bear different names. Among them, the Vodoley-Draganovski segment is distinguished for its seismogeneity [7]. Recently, some authors assume that the South-Moesian fault is not a deep-penetrating in-depth fault reaching the mantle, but it is sooner an epidermal trass or a monoclinal slope with various manifrstations in the structural floors [7].

Another well-known fault structure is the Brestnishko-Preslavska flexure. In the southern direction, between Stara Planina mountain and the Srednogorie, the Zadbalkan fault is located, as well as the series of chariage along the southern slope of Stara Planina (Staroplaninski, Kashanski, Shipchenski etc.).

The next big fault structure is the Maritsa fault which serves as a boundary between the Kraishtensko-Rhodopes arc and the Srednogorie.

One of the lineaments identified by interpretation of space images and outlined by other authors as well is the Olt-Ossam lineament, which is delimited by the straight-line course of the rivers Olt in Romania and Ossam in Bulgaria. Actually, it series as a tectono-geomorphologiic boundary between the Lom depression and the North-Bulgarian (Ludogorsko) rise. The valley of the Ossam river ranks among the most ancient river valleys created yet during the upper Eocene, the Oligocene, and the lower Miocene, continuing its development but for short interruption periods until nowadays.

The other lineaments identified on space photos have no essential importance for the development of tectonic areas in Bulgaria.

2.3. Analysis of ring structures.

As a result of deciphering and interpretation of space images, combined with topographic maps of various scale, on the territory of the studied area, ring (concentric) structures of various form, size, depth, and orientation have been outlined. Among these are the structures in the Moesian platform, the Predbalkan, Stara Planina mountain, the Srednogorie, and the Rila-Rhodopes massif.

2.3.1. Ring structures in the Moesian platform.

Within the platform, the following structures can be identified: Beloslatinska, Lukovitska, Plevenska, Nikopol-Pavlikenska, Streletska, and Popovska.

The Beloslatinska structure is mentioned by many authors [5, 9]. It has a size of 45/25 km and represents an elongated oval pointing in the east-west direction. Most often, its formation is referred to the Troas period, in which a similar depression was formed. Within this structure, an industrial oil deposit was revealed (at the town of Knezha).

The Pleven oval structure is about 70 km long and up to 35 km. In depth of the structure, magma rocks with gabro-diorite compositions are revealed; whereas the positive structure was formed as a result of the slow squeezing of the magma body. Actually, the latter creates the biggest positive magnetic anomaly in Central North Bulgaria.

Another important structure is the Nikopol-Pavlikenska, sized 80/50 km. It is delimited by the rivers Ossam and Yantra, the northern half of being strongly eroded by the short tributaries of the Danube river. Among the most important structures to the east of the Yantra river are the Streletska and the Popovska structures, which are outlineded by the tributaries of the river of Rusenski Lom. The Popovska structure may be referred in depth to a magnetic body with gabro-diorite composition [11].

2.3.2. Ring structures in the Predbalkan and Stara Planina.

Within the Predbalkan and Stara Planina, the strongest deciphering indexes were the configuration of the hydrograph network as well as some tectono-geomorphologic indexes, the orientation of the tectonic structures (synclinal and anticlinal) against the linear chain outlook of the Predbalkan and Stara Planina. The major structural units here are: the Botevgradska, Montanska (Belogradchishka) and Tarnovska (Fig. 2) structures.

The Tarnovska regional morphostructure is emphasized mainly by a number of mountain-like elevations, risings, and hills. These orographic forms are part of Stara Planina and the lower mountains and elevations of the Predbalkan and the periplatform South-Moesian depression.

The morphostructure is about 200 km long from west to east, with an average width of 50-60 km and an area of about 12,000 km^2. In it, a central nucleus can be outlined, surrounded by a higher-terrain belt, followed by another, not well manifested and lower belt. The latter belt is closed to the south by the high terrains of Stara Planina (Fig. 2).

Another structure of this kind is observed in the Botevgrad region. It spreads to the west as far the Vrachanski Balkan, to the east – the Vassilyova Planina, and to the south – the Murgashko-Tetevenska Stara Planina. In its center, a depression is formed, which is occupied by the Botevgradska valley (Fig. 2).

Another important morphostructure is the Montanska one, which stretches from the Ogosta river to the river of Golyama Panega to the east. It coincides with the so-called Montanska anticlinal and represents a strongly elongated rising surrounded by depressions. To the north lies the Lomska depression, to the south – the Mezdrenska synclinal, and to the east – the Lukovitsko depression. The Montanska morphostructure is about 100 km long and up to 25-30 km wide. It is strongly partitioned by the rivers of Botunya, Skat, and Iskar.

2.3.3. Ring structures in the Srednogorie.

Within the Srednogorie, two big regional concentric structures can be outlined: the Panagyurska structure and Sarnena Gora. Among the smaller ring formations are the Chirpanski elevations, and the Manastirska structure whereas the latter one is negative. The typical thing about the first two regional morphostructures is that they are built up of magma and metamorphic rocks, and that, in the geophysical respect, they represent negative gravitational or magnetic anomalies (Fig. 2).

2.3.4. Ring structures in the Rhodopes massif.

Here, the most clearly outlined ring structure is the Rhodopes massif, and more precisely, the West Rhodopes. This structure is closed to the west and to the south by the Mesta river, to the north – by the Upper-Thracean trough, and to the east – by the valleys of the rivers Varbitsa and Borovitsa, tributaries of the Arda river. This is a big structure sized 150-90 km, built mostly of metamorphic rocks, paleogene sediments and vulcanites. The structure is a complex one, with depressed central part, where three depressions are formed: the Bratsigovo-Dospatsko, Smolyansko, and Vitinsko ones. The latter are filled with sediments, pyroclastites, and vulcanites and nowadays represent the highest terrains in the Rhodopes (Mount Perelik, 2191 m). Another similar structure in the Rhodopean massif is the Belorechko swelling, a positive structure built of pure crystalline rocks [3, 12, 13].

Another peculiarity of the Rhodopes massif and, in particular, the Eastern Rhodopes, are the volcanic structures: Dragoynovska, Nanovishka, Zvezdelska, Lozenska, Madzharovska, Irantepetska etc. Some of them are volcanic domes, others are typical volcano-tectonic depressions (Fig. 2).

3. Study of the modern geodynamics of Bulgaria.

The study of the geodynamic processes is a very topical problem, since it provides dataabout the dynamic processes taking place in the Earth's body, as well as of the dynamics of the lithospheric plates. Based on these facts, the horizontal and vertical movements of the Earth's crust can be determined with great accuracy throughout long periods of time, using various radiointerferometric, laser, or dedicated geodetic measurements. Space methods and equipment resulted in a boom of these studies, achieving in the recent years exceptionally high precision through the use of GPS measurements of the lateral and vertical position of points from the physical earth's surface. It is a great regret that the obtained data relates to the recent couple of years, covering only a short period of time which does not provide to carry out reliable analyses and interpretations.

For this reason, the vertical movements [12,14,15] on Bulgarian territory are studied by data from high-precision geodetic measurements dating since 1928 and comprising a relatively long period for which measurements throughout three epochs have been made.

At SRI-BAS, several annual measurements were performed of the neotectonics and geodynamics [12,14,15] of some detached geological structures on Bulgarian territory: namely: the Moesian platform, the Predbalkan with Stara Planina, and South Bulgaria [12,14,15]. The major objective of these studies was to reveal the correlation, if any, between the modern geodynamical processes and the relevant neotectonic and geologic structures in the mentioned regions whereas each region was studied individually and the obtained results were published.

The results were united in this paper, thereby providing a wholesome map of Bulgaria for the modern movements of the Earth's crust during the epoch 1930-1985 with isolines 0.5 mm/year apart. The neotectonic map (Fig. 2) and the map of modern movements (Fig. 2) finalize these multiannual studies. In the next study, the obtained results for the whole Bulgarian territory will be analyzed.

3.1. Reliability of the data used to determine the velocities of the vertical movements of the Earth's crust.

As already stated when discussing the study of the vertical movements of the Earth's crust, in the mentioned detached structural areas, mainly geodetic measurements were used, since the analysis of space data obtained by GPS measurements for middle-sized regions did not provide the needed accuracy to comply with the accuracy of the quantities obtained by geodetic methods.

Prior to their use, the obtained geodetic data was submitted to meticulous analysis aimed to identify potential errors caused by external factors that might deform the measurement results. Among these were the instrumentation errors obtained with the levelling procedure, the references' representativeness, the characteristics of the geological foundation (loess soils, possible slides) and for the references along the Danube river, the various water levels and, accordingly, the references' stability were studied.

To enhance data trustworthiness and to remove the possible systematic errors, initially, digital data was processed and then it was compared with the results from past epochs. Where the values' differences for two epochs with one and the same references were greater than modern movements, the data for both epochs and the references' reliability was verified.

Based on the data thus obtained, the data was processed anew and maps of the modern tectonic movements of the Earth's crust were drawn. Where deviations occurred, the references were studied anew and the factors deforming the results were removed. And only then the material was processed, the residual errors were removed and, based on these final results, the enclosed Appendixes were drawn.

3.2. Interpretation of the velocities of vertical movements.

In works [12,14,15], the velocities for three periods are interpreted: 1930-1985, 1930-1970, and 1970-1985, and the respective maps are drawn with isolines 0.1 mm/year apart. The obtained graphic material and the performed analysis revealed that the images obtained from the longest period, 1930-1985, were most trustworthy, with the least number of anomalies. This is a logical outcome since the available observed material is abundant enough to allow for occasional errors to be removed with processing. Accounting for these facts, the only drawn map of the vertical movements' velocities in Bulgaria was for the period 1930-1985 (Fig. 2).

Notwithstanding the visual idea of the modern movements on the whole territory one can get from the map, in pursuit of the set objective (to reveal the existing correlation between modern movements and neotectonic structures) we shall analyze the movements of the detached neotectonic structures.

3.2.1. Analysis of the modern movements of the Earth's crust for the Moesian platform.

The drawn map of the vertical movements' velocities displays the plane nature of the geodynamical processes taking place in the whole northern Bulgaria. It should be noted beforehand that the vertical movements comprising the Central part of the Danube plane confirm the general tendency of continuous sinking.

For the longest period (1930-1985) of generalization of the quantitative data, a general sinking (depression) of the central part of the Moesian platform is expected in the section along the Danube river, between the towns of Lom and Svishtov (Fig.2). The sinking comprises the part of the platform located between the great turns of the Danube river, at the towns of Vidin-Lom to the west and Svishtov-Russe to the east. The sinking has a clearly marked oval form (100-120 km) with elongation in the east-west direction. To the north it is parallel to the river bed of the Danube, while to the south, on Bulgarian territory, a deep bay is formed, passing through the boundary South-Moesian fault and penetrating the Predbalkan (the Balkanides). Typical of the period 1930-1985 is the tendency of increasing the Earth's crust vertical movements' velocities over a one-year period. These values are particularly great in the region of the settlements of Oryahovo and Baykal where they reach a velocity of $V_V = -2.5$ mm/year. To the north, on Roumanian territory, the isolines get quickly closer to each other. A similar pattern of the isolines with identical velocity is observed both to the east and to the west, while to the south they change smoothly, whereas the affected slowly-sinking area penetrates deep into the Predbalkan. The sinking comprises the depression that existed in the Upper Cretaceous and, in some respect, continues during the Neogene in the Lomska depression. A slightly manifested "swelling" is observed to the north-east in the Danube plane, forming the Nikopolsko-Pavlikenska, Popovska and Kubratska morphostructure.

Beyond this "swelling", eastward of the Nikopol-Gorna Oryahovitsa line, ring isolines are formed with maximal value of up to +1.0 mm/year. This formation correlates with the positive geologic structure, which comprises the whole of the Nikopol-Pavlikenska, Popovska and Kubratska morphostructure.

None of the ring arch-block and block structures within the scope of the Lomska depression affects the course of the vertical movements' velocities. The well-known South-Moesian fault is not represented on the vertical movements' velocity map, thus confirming the opinion of some researchers that it does not represent a deep-penetrating fault, but a monoclinal slope with fault manifestations in different structural-stratigraphic storeys [11,12,14,15].

3.2.2. Analysis of the Earth's crust modern movements for the Predbalkan and the Stara Planina mountain.

The study of the Earth's crust vertical movements' velocities for the regions of Kraishte, the Predbalkan, and the Stara Planina mountain for the period 1930-1985 provides a clear picture of the geodynamic processes taking place there. Thus, we have depressions in the region of Teteven-Etropole, corresponding to the central part of the sinking Teteven-Etropolska and Skravenska morphostructure. Slight sinking is observed within the scope of the Botevgradska structure, where the valley bearing the same name sinks by –1.0 mm/year. Eastward of these sinkings, within the Shipchenski and Kotlenski region, two "risings" are formed whose modern movement values reach up to +2.0 mm/year. In these regions, there is a significant correlation with the neotectonic structures.

3.2.3. Analysis of the Earth's crust modern movements for South Bulgaria.

The performed analyses of the vertical movements in South Bulgaria reveal a great variety of "sinkings" and "risings", whereas the velocities' positive values reach their maximum. In these regions we witness the greatest variety of high mountain chains: Pirin, Rila, the Rhodopes up to the Sakar mountain, plains and valleys, accordingly.

During the epoch (1930-1985). The vertical movements' velocities in the southernmost part of the Rhodopes massif reach up to +3.5 mm/year. These risings begin eastward of the valley of the Mesta river where the velocity is about +1.5 mm/year. The values in Pirin and Rila are also positive, but smaller: about 2.1 mm/year for Rila and about +4.0 mm/year for Pirin.

If we trace the isolines between the three mountains (the Rhodopes, Rila, and Pirin), we shall notice that along the valley of the Mesta river there is a clearly outlined fault band separating the Pirin mountain from the

Rhodopes, whose vertical movements are independent on each other. If we trace the isolines between the Rila and the Rhodopes blocks, we shall identify a clearly outlined "saddle" which delimits the different movement velocities of both mountains. The typical thing here is that each of them has its "own life", i.e. an individual rising velocity.

Eastward of the Pazardzhik-Chirpan line, an isoline configuration is formed which reveals a band of negative values. We point out to a feature characteristic of the period 1930-1985, namely the generation of an oval sinking with great velocity (-2.0 mm/year).

Northwards of the towns of Panagyurishte and Stara Zagora, during the same period, two closed ovals are outlined, with positive rising values of up to +1.0 mm/year (Fig. 2). In the south-east direction, a slight rising is observed, comprising the territory of part of the Zagorsko depression and the Sakar mountain, and having values of about +1.5 mm/year. Such a depression is also observed southward of the town of Burgas.

Here, yet another fact deserves to be noted, namely that in the period 1930-1985, a clear and notable tendency for severing of the West and the East Rhodopes. This saddle is observed on Bulgarian territory, in the region of the village of Podkova as well as at the town of Xanti in Northern Greece (the White Sea region).

Southward of the Nova Zagora-Elhovo line, a "sinking" starts which, in the immediate vicinity of the Burgas bay, reaches up to –3.0 mm/year.

4. Conclusion.

This work is an attempt to bind the results from the deciphering of space images and photos of the Moesian platform, Predbalkan, Stara Planina, Srednogorie, and Rhodopes, on the one hand, with the quantitative materials obtained from geodetic measurements, on the other hand. In parallel with this, the whole known data from geologic, geomorphologic, tectonic, geophysical, and geochemical data was used, as well as thematic maps of various scale and scope. The idea was to confirm or reject certain results or to show that the relation between them is not always a simple one, but various combinations or interpretations are possible. From our point of view the following more important conclusions may be made:

1. The drawn neotectonic map of the central part of Bulgaria which crosses different tectonic zones of Bulgarian territory, prepared on the basis of space images and photos, reflects the modern tectonic state-of-the-art and coincides fully or overlaps with the known neotectonic structures in the Predbalkan, Stara Planina, Srednogorie, and Rhodopes. Only for the Moesian platform it cannot be ascertained that there is complete coincidence

and that the deciphered neotectonic scheme coincides with the meso-cainosoic platform чехло.

2. The drawn maps of the vertical movements' velocities do not confirm all linear and ring structures obtained as a result of deciphering. For the Moesian platform, the existence of the Lomska depression is confirmed with respect to its area. Nowadays, it is slowly sinking with a maximal velocity of -2,5 mm/year., i.e. the neogene depression continues its development.

3. Linear structures can be passive or active. All fault linear structures in South Bulgaria (Marishka, Zadbalkanska) display typical modern activity, i.e. they are seismogenious, and in the Moesian platform such an effect is observed in the Vodoley-Draganovski segment of the South-Moesian fault.

4. The obtained map of the vertical movements' velocities for North Bulgaria reveals the slow oscillating pattern of its geodynamics, which is related mostly with its foundation and subcrust layers.

References

1. Атанасов, А., П. Боков, Г. Георгиев, И. Монахов. Основни черти в геоложкия строеж на Северна България във връзка с нефтогазоносната перспективност, Труд НИПИ, I, Техника, 1984.
2. Атанасов, А., П. Боков (редак.), Геология и нефтогазоносната перспективност на Мизийската платформа в Централна Северна България, 1983.
3. Бончев Е., Проблеми на българската геотектоника, Техника, 1971.
4. Вапцаров, И., Т. Дилинска. Морфотектонски проблеми на Родопския масив. Пробл. на географията, 3, 1980, 53-69.
5. Гочев П., Н. Кацков, Х. Спиридонов. Крупнейшие линеаменты и кольцевые структуры территории НРБ, Исследование Земли из Космоса, 2, 1982.
6. Гочев П. 1971. Тетевенски антиклинорий. В: Тектоника на Предбалкана. 229-324.
7. Дачев Х., Д. Гочев. Нови данни за тектонския строеж в Търновско по резултати от сеизмични проучвания, Год.УГП, 11, 1960.
8. Дачев Х., Строеж на земната кора в България. Техника, 1988.
9. Йосифов Д., П. Кацков, Д. Стойчев. О корреляции основных линейных элементов в геофизических полей и космических съемок на территории Болгарии – Геотектоника, тектонофизика и геодинамика, БАН, 1979.
10. Ненов Т., Х. Спиридонов, Л. Драгоманов, Д. Ангелова, В. Вълев, С. Нафтали, Е. Миков, Р. Косьовски. Неотектоника и геоморфология на Горнотракийската низина. В кн.: Методи и технологии за търсене на минерални суровини, 1, 162-172.
11. Спиридонов Х. Използване на дистанционна информация за изучаване на съвременните движения на земната кора. Национален семинар "Геодезически изследвания на съвременните движения на земната кора", 1985.

12. Спиридонов Х., Н. Георгиев. Анализ на дистанционни и земни изследвания на неотектониката и геотектониката на Мизийската платформа. International Symposium, New Surveying Instruments and Technologies, Sofia, 21-24 September 1993, 218-246.

13. Спиридонов Х. Неотектоника на Предбалкана и Стара планина. Сборник от докладите, изнесени на Националната научно-практическа конференция по география, София 9-10 април 1994, 95-108.

14. Спиридонов Х., Н. Георгиев. Неотектоника и геодинамика на Предбалкана и Стара планина, Аерокосмически изследвания в България, № 12, стр. 73 – 83 БАН С 1996.

15. Спиридонов Х., Н. Георгиев. Изследване неотектониката и геодинамиката на България . International Symposium on "Geodetic, Photogrammetric and Satellite Technologies "- Sofia, 08-09 11 2001, p.p.381-390.

16. Dabovski, Ch., A. Harkovska, B. Kamenov, B. Mavrudchiev, G. Stanlcheva-Vassileva, Y. Yanev. A geodynamic model of the Alpine magmatism in Bulgaria. Geologica Balcanica; 21, 4, 1991, 3-15.

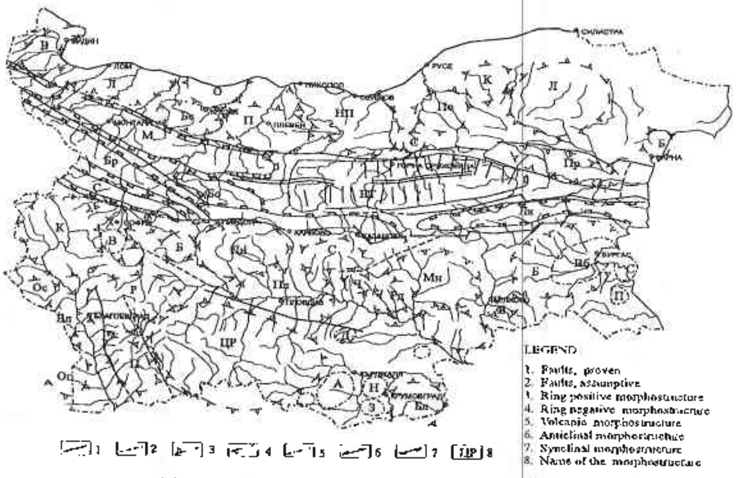

Fig. 1. A Decipherable neotectonic scheme of Bulgaria

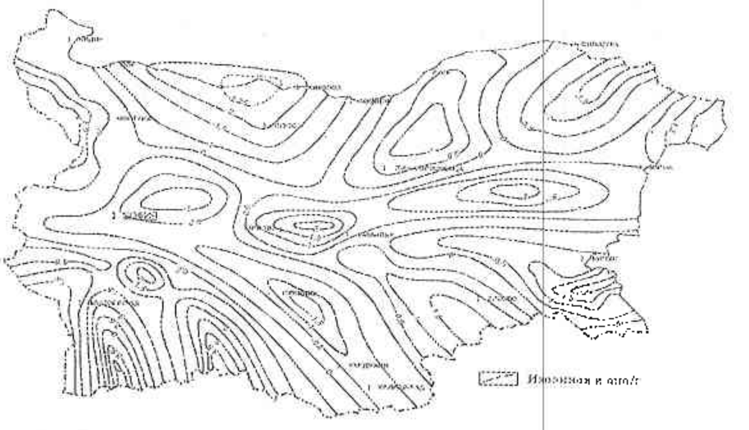

Фиг. 2. Карта на скоростите на вертикалните движения (мм/г) за периода 1930 - 1985

ИЗСЛЕДВАНЕ НА НЕОТЕКТОНИКАТА И ГЕОДИНАМИКАТА НА БЪЛГАРИЯ

Хернани Спиридонов, Николай Георгиев

Резюме

В публикацията се изследва съвременната тектоника и геодинамика на България. Уточняването на основните тектонски единици, тяхната разнообразна вътрешна морфоложка и тектонски изразителност, границите между тях, а така също и съвременната им геодинамика, се осъществява при съчетаване на два подхода: използване и приложение на дистанционна (аерокосмическа) информация и комплексна интерпретация на данни, получени от геодезични, геофизични, геолого-геоморфоложки наблюдения, измервания и различни по мащаб карти, снимки и др. материали.

Дистанционният (аерокосмическият) подход се основава на използването на аерокосмически данни: разнообразни по мащаб, разделителна способност и спектрален диапазон фотографии, сканерни изображения и магнитни ленти. При наличната аерокосмическа обезпеченост и при приложение на ландшафтно-индикационния метод на дешифриране успешно се оконтурват най-добре изявените по размери и площ неотектонски единици, а така също и разделящите ги главни разломни нарушения.

Вторият подход е класически и обхваща постиженията и резултатите от водените геодезични измервания, геолого-геоморфоложки, тектонски, геофизични, геотермични, хидроложки данни; наблюдения и публикувани карти, схеми и диаграми. Тук се използват както материали на редица ведомства, учени, публикации, така и собствени изследвания.

Bulgarian Academy of Sciences. Space Research Institute
Aerospace Research in Bulgaria. 17. 2003. Sofia

SPATIAL AND TEMPORAL ANALYSIS OF THE LANDUSE ON TWO TERRITORIES IN RAKOVSKI DISTRICT

Eugenia Roumenina

Space Research Institute-Bulgarian Academy of Sciences

Abstract

The paper is dedicated to landuse monitoring on the territory of Belosem and Shishmantsi villages, Rakovski district. To accomplish the set objectives and tasks, concepts and methodologies from Remote Sensing, GIS and landscape science are applied. The following tasks were set: development of GIS database, containing data of the landuse dynamics, soil differences, geology and topography; monitoring of the landuse, using multichannel images and the developed GIS database; composition of maps, presenting the landuse structure and determination and analysis of the spatial landuse dynamics for 1995 vs. 1978.

Environmental conditions and the prospects for their reclamation provide good preconditions for agricultural use of the land. Enforcement of the Law on Ownership and Use of Agricultural Land and Land Allocation to its Owners or Their Heirs may result in a change in landuse structure and environmental status. This called for monitoring of the territory, using the GIS database developed in this study.

Key words: remote sensing, GIS, landuse

An issue of present interest for modern society is ensuring and supporting a sustainable landuse, consistent with the environmental and socio-economic characteristics of the respective regions.

This called for periodical assessment of the utilization and use of territory in close relation with the processes of its transformation, applying modern technologies for rapid acquisition of accurate spatial information. The necessary data can be obtained by development of regional and local Geography Information Systems (GIS), which use multichannel images as information input.

The main **objective** of the current study is monitoring of landuse on the territory of Belosem and Shishmantsi villages. Here, the following **tasks** have to be resolved: 1. Development of a GIS database (GIS-DB), containing information for landuse dynamics, soil differences, geology and topography; 2. Monitoring of landuse, using multichannel images and the developed GIS-DB; 3. Composition of maps, presenting landuse structure; and 4. Determination and analysis of spatial landuse dynamics for 1995 vs. 1978.

The **object** of the present research are different landuse types on the territory of Belosem and Shishmantsi villages, Rakovski District. They are situated in the North part of the Upper Thracean Flat, north-east of Plovdiv town. They occupy area of 4,171.4 ha (Belosem) and 1,980.3 ha (Shishmantsi).

Materials and methods

To accomplish the set objectives and tasks, concepts and methodologies from Remote Sensing (RS) [Velikov V., 1995], GIS [Mitchell A., 1999] and landscape science [Petrov P, 1990; Popov A.,1989] are applied. The development of the digital models is performed in Arc View 3.2.a environment. The structural diagram of the study is presented in Fig. 1. It shows the relationship between different types of input data and their processing and transformation into GIS-DB; the generation of new thematic layers using the database and the thematic maps, composed using the obtained results i.

The information sources used in the process of development of the GIS-DB and the methods of composition of digital maps are presented on Table 1.

Table 1. Information sources and methods used for composition of digital maps

DIGITAL MAPS	INFORMATION SOURCES	USED METHODS
Basic Map	Topography Maps, scale 1:25000, Publisher: MTS; Data from Local Agronomists and Field Checks;	12 Themes are Digitized
Geology Map	Geology Map, scale 1:100000, Map Sheets Plovdiv and Chirpan; Publisher: IG-BAS and GSGMC; 3 Themes from the GIS-DB are integrated	2 Themes are Digitized
Geo-hazard Map	Geo-hazard Map in Bulgaria, scale 1:500000, Publisher. BAS, GMRA; 2 Themes from the GIS-DB are integrated	3 Themes are Digitized
Soil Map	Composed by scientists from SRA, MAF, scale 1:10000; 5 Themes from the GIS-DB are Integrated	1 Theme is Digitized
Landuse Map for 1978	Aerial Photos, Taken on 09.08.1978: Panchromatic: - Camera MRB, f-152 mm, scale 1:72000; Multichannel Camera MKF-6 MC, f – 125 mm, scale 1:32000, Spectral Ranges: 0,46-0,50 μm, 0,52-0,60 μm,0,58-0,62 μm, 0,64-0,68 μm, 0.70-0,74 μm, 0,79 – 0,89 μm; Data from Local Agronomists and Field Checks; 8 Themes from the GIS-DB are integrated.	Computer Aid Visual Interpretation of Panchromatic and Multichannel Images
Landuse Map for 1995	Panchromatic Aerial Photos, Taken on 30.06. and 6.07. 1995 , scale 1:21000; Satellite Image from Landsat TM, taken on 19.08.1992, Pixel Size for Channels 1-5 and 7 – 30x30 m, for 6th – 120 m; Spectral Ranges: 1. 0,45-0,52 μm 2. 0,52-0,60μm 3. 0.63-0,69 μm, 4. 0,76-0,90 μm 5.1,55-1,75 μm, 6. 10.40-12,50 μm, 7. 2,08-2,35 μm; Data from Local Agronomists and Field Checks; 8 Themes from the GIS-DB are integrated.	Computer Aid Visual Interpretation of Panchromatic and Multichannel Images
Change Detection Map for Landuse in 1995 vs. 1978	Information from the GIS-DB is uses - Landuse Maps for 1995 and 1978	Arc View GIS
Change Detection Map of the Soil and Landuse Categories for 1995 vs. 1978	Information from the GIS-DB is uses - Landuse Maps for 1995 and 1978 and Soil Map	Arc View GIS

Results and Comments

The analysis of the monitoring results and composed digital maps provides to identify the following main trends in landuse dynamics in Shishmantsi and Belosem villages.

The landuse structure established on the territory of the two villages is of agricultural type. The relative part of arable land (fields, permanent crops, pastures and meadows), compared to the total area of Shishmantsi is 80.7 % for 1978 г., displaying a slight trend for decrease in 1995 - 78.6 % (Fig 2). For the territory of Belosem this indicator remains unchanged. (80.1 % for 1978 and 79.7 % for 1995). Second comes build-up area, which shows some increase from 5.6 % (1978) to 7.1% (1995) for Shishmantsi and no change for Belosem with 8.7 % for both years. Third ranks infrastructure, which increases from 4.2 % (1978) to 4.8 % for (1995) for Shishmantsi and from 4.7 % (1978) to 5.3 % (1995) for Belosem. The other types of landuse for the territory of Shishmantsi are forests and water catchments - 4.7 % and 3.5 % accordingly, which have experienced no change during the study period.

For Belosem, the forth place is occupied by water catchments with 5.4 %, followed by forests with 0.9 % (1978) and 0.3 % (1995). The area occupied by industrial and mining waste and limestone-pits amounts to 1.3% of the territory of Shishmantsi and only 0.04 % of Belosem.

The most significant change is observed for the permanent crops category on the territory of Shishmantsi (Fig. 2.). In 1978, vineyards occupied 73.4 ha and decreased to 6.7 ha in 1995 (Table 2.). The industrial zones increased their area from 0.6 % in 1978 to 2.1 % in 1995. The reason is building of a (Table 2.) steelworks in the foot of the limestone hills, which are situated eastward of the village.

For the territory of Belosem (Fig. 3.), the greatest change is also observed in the permanent crops category. In 1978, the vineyards occupied 50.4 ha and in 1995 they were completely cleared off (Table 3.). The same trend is observed for rice crops. In 1978 they occupied 31.9 % of the total area and in 1995 they were grown no longer (Fig. 3., Table.3.).

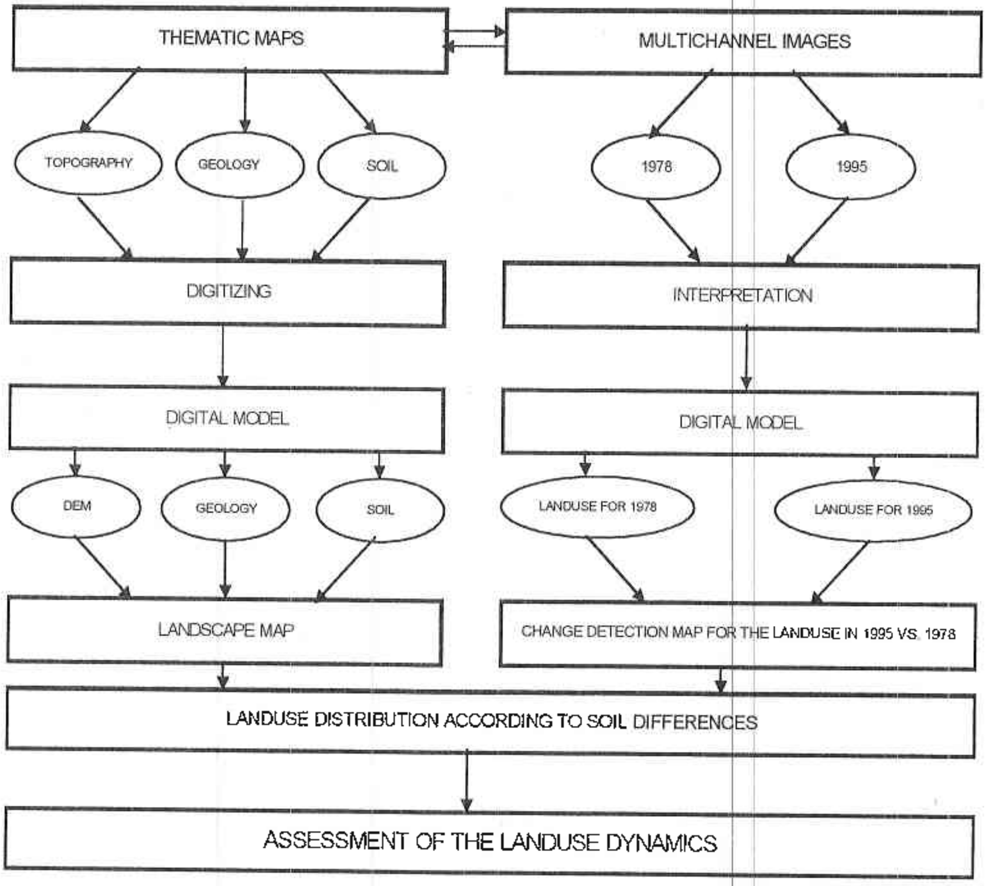

Fig. 1. Flowchart of the study

Belosem is the biggest village in Rakovski District. The provision of the local population with fields increased from 0.3 (1978) to 0.6 (1995) ha per person. This can be explained with increase of the fields in 1995, which comes from an area, occupied by rice and permanent crops in 1978.

The provision of the inhabitants of Shishmantsi with fields increased from 0.9 to 1.0 ha per person for the two years. The reason is again the replacement of permanent crops for fields.

The number of people in the two villages remains practically unchanged [National Statistics]. The provision-with-fields indicator for the studied villages differs essentially from the overall trends for Bulgaria as

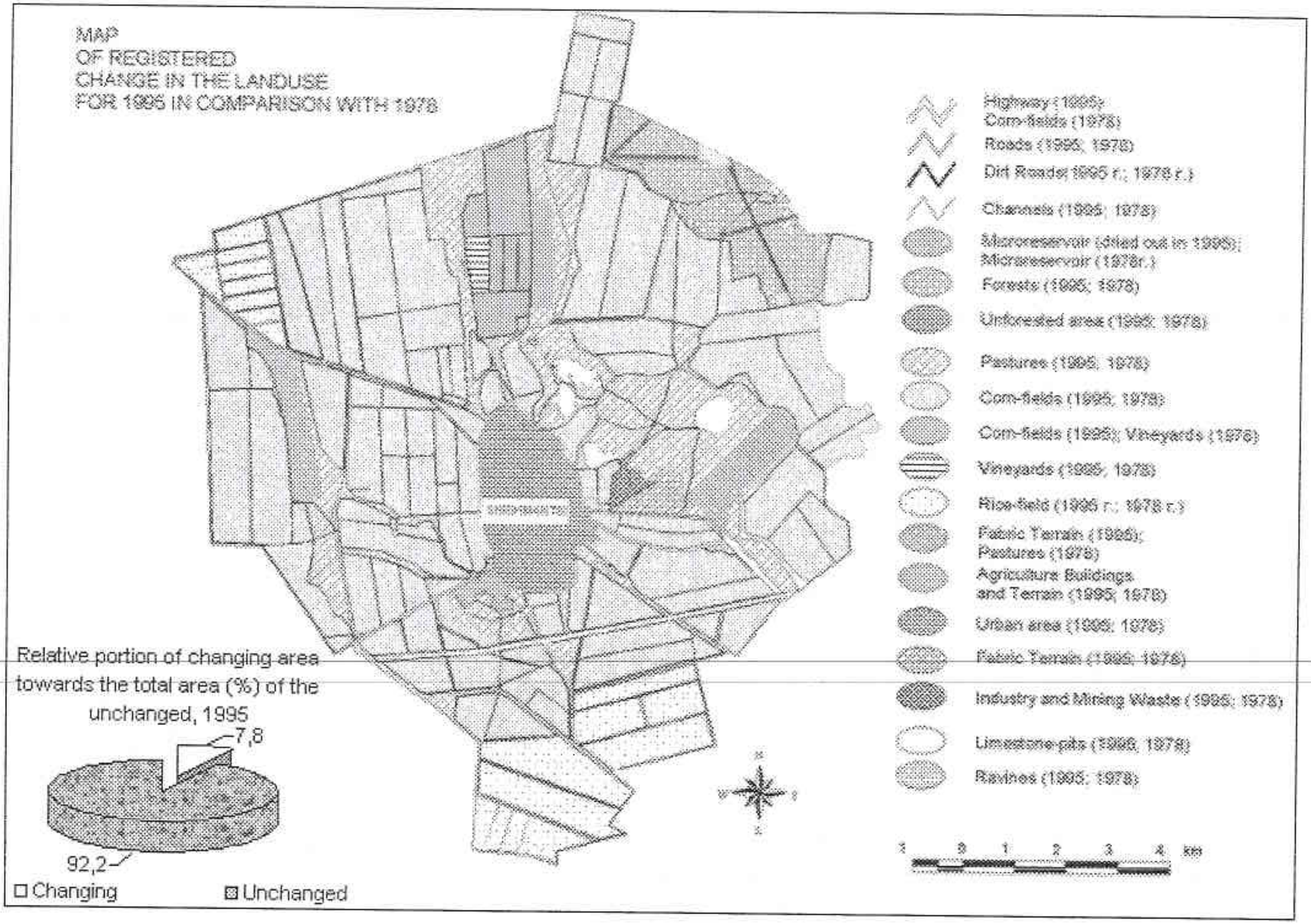
MAP
OF REGISTERED
CHANGE IN THE LANDUSE
FOR 1995 IN COMPARISON WITH 1978
Highway (1995);
Corn-fields (1978)
Roads (1995, 1978)
Dirt Roads (1995 r.; 1978 r.)
Channels (1995; 1978)
Microreservoir (dried out in 1995);
Microreservoir (1978r.)
Forests (1995; 1978)
Unforested area (1995; 1978)
Pastures (1995; 1978)
Corn-fields (1995; 1978)
Corn-fields (1995); Vineyards (1978)
Vineyards (1995; 1978)
Rice-field (1995 r.; 1978 r.)
Fabric Terrain (1995);
Pastures (1978)
Agriculture Buildings
and Terrain (1995; 1978)
Urban area (1995; 1978)
Fabric Terrain (1995; 1978)
Industry and Mining Waste (1995; 1978)
Limestone-pits (1995; 1978)
Ravines (1995; 1978)
1 0 1 2 3 4 km
Relative portion of changing area
towards the total area (%) of the
unchanged, 1995
7,8
92,2
□ Changing
▨ Unchanged

Fig. 2.

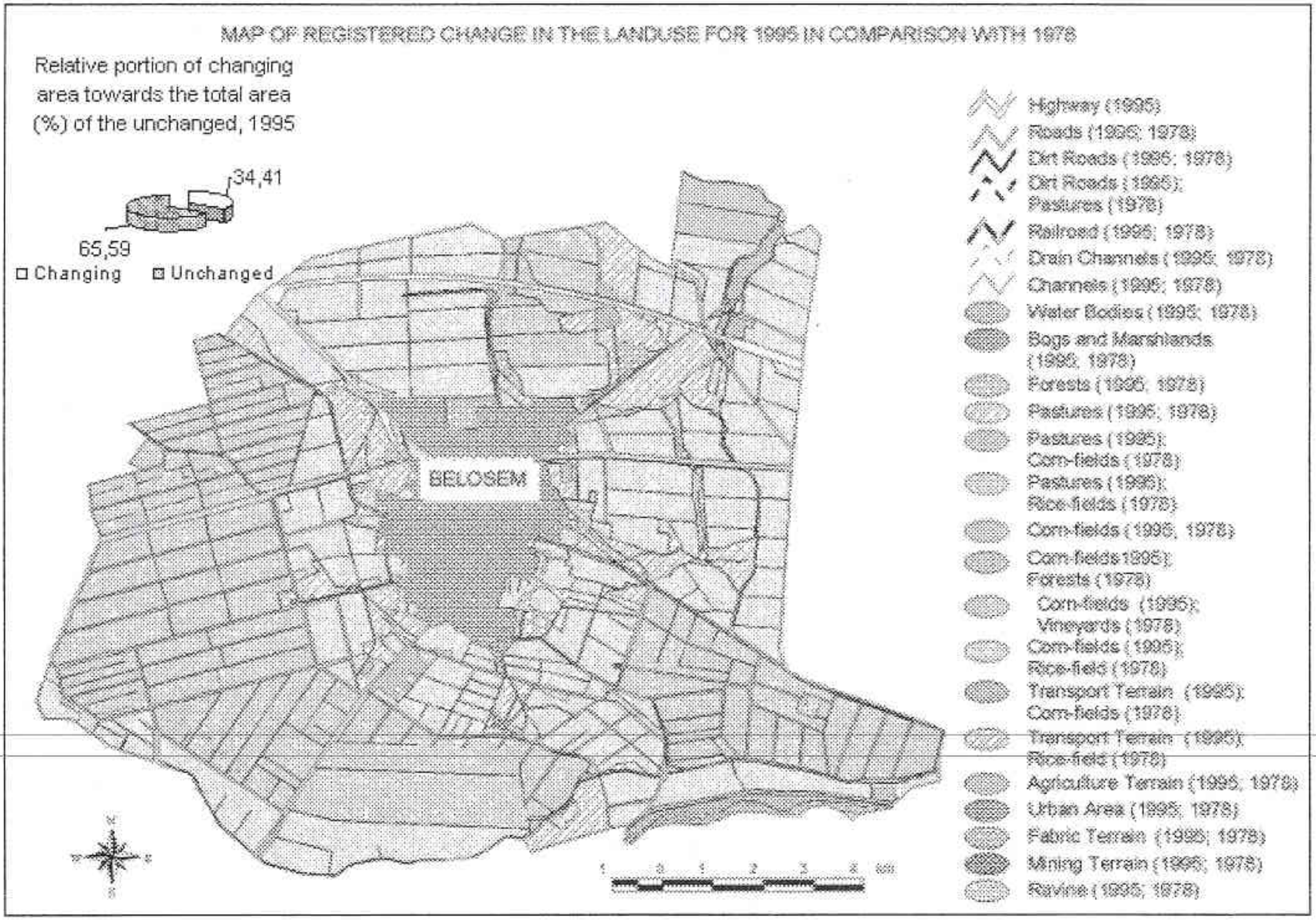
MAP OF REGISTERED CHANGE IN THE LANDUSE FOR 1995 IN COMPARISON WITH 1978
Relative portion of changing area towards the total area (%) of the unchanged, 1995
34,41
65,59
□ Changing
▨ Unchanged
BELOSEM
Highway (1995)
Roads (1995; 1978)
Dirt Roads (1995; 1978)
Dirt Roads (1995); Pastures (1978)
Railroad (1995; 1978)
Drain Channels (1995; 1978)
Channels (1995; 1978)
Water Bodies (1995; 1978)
Bogs and Marshlands (1995; 1978)
Forests (1995; 1978)
Pastures (1995; 1978)
Pastures (1995); Corn-fields (1978)
Pastures (1995); Rice-fields (1978)
Corn-fields (1995; 1978)
Corn-fields 1995); Forests (1978)
Corn-fields (1995); Vineyards (1978)
Corn-fields (1995); Rice-field (1978)
Transport Terrain (1995); Corn-fields (1978)
Transport Terrain (1995); Rice-field (1978)
Agriculture Terrain (1995; 1978)
Urban Area (1995; 1978)
Fabric Terrain (1995; 1978)
Mining Terrain (1995; 1978)
Ravine (1995; 1978)
1 0 1 2 3 4 km

Fig. 3.

Table 2. Area (ha) changes of land-cover categories for Shishmantsi Villag

1978 1995	1	2	3	4	5	6	7	8	9	10	11	12	13	14	15	16	17	Total 1995
1	84.8	0	0	0	0	0	0	0	0	0	0	0	0	0	0	0	0	84.8
2	0	8.	0	0	0	0	0	0	0	0	0	0	0	0	0	0	0	8.8
3	0	0	8.6	0	0	0	0	0	0	0	0	0	0	0	0	0	0	8.6
4	0	0	0	273.1	0	0	0	0	0	0	0	0	0	0	0	0	0	273.1
5	0	0	0	0	6.7	0	0	0	0	0	0	0	0	0	0	0	0	6.7
6	0	0	0	0	66.7	1033.0	0	0	0	0	0	0	0	0	0	0	0	1099.6
7	0	0	0	0	0	0	168.3	0	0	0	0	0	0	0	0	0	0	168.3
8	0	0	0	0	0	0	0	25.4	0	0	0	0	0	0	0	0	0	25.4
9	0	0	0	0	0	0	0	0	43.5	0	0	0	0	0	0	0	0	43.5
10	0	0	0	0	0	12.7	0	0	0	0	0	0	0	0	0	0	0	12.7
11	0	0	0	0	0	0	0	0	0	0	3.3	0	0	0	0	0	0	3.3
12	0	0	0	0	0	0	0	0	0	0	0	79.8	0	0	0	0	0	79.8
13	0	0	0	0	0	0	0	0	0	0	0	0	7.4	0	0	0	0	7.4
14	0	0	0	0	0	0	0	0	0	0	0	0	0	93.2	0	0	0	93.2
15	0	0	0	28.6	0	0	0	0	0	0	0	0	0	0	11.7	0	0	40.3
16	0	0	0	0	0	0	0	0	0	0	0	0	0	0	0	7.2	0	7.2
17	0	0	0	0	0	0	0	0	0	0	0	0	0	0	0	0	17.8	17.8
Total 1978	84.8	8.	8.6	301.7	73.4	1045.7	168.3	25.4	43.5	0	3.3	79.8	7.4	93.2	11.7	7.2	17.8	1980.3

1. Forests, **2.** Unforested Area, **3.** Ravine, **4.** Pastures, **5.** Vineyards, **6.** Corn-fields, **7.** Rice fields, **8.** Microreservoir, **9.** Channels, **10.** Highway, **11.** Roads, **12.** Dirt Roads, **13.** Agricultural Buildings and Terrain, **14.** Urban Area, **15.** Plants, **16.** Industry and Mining Waist, **17.** Limestone-pits

well as for Plovdiv region. The value of this indicator for Rakovski district is 0,5 ha per person for 1990 [M. Ilieva at al, 1997].

The diagram for Shishmantsi, (Fig. 4) showing the relative portion of soil types towards the total area of the fields, reveals that the most widely distributed soils are Calcixerollic Xerochrepts - 32.2 % and Typic Haploxeralfs - 21.5 %. They are suitable for growing grain and fodder crops, vineyards and orchards.

Second rank Fluventic Xerochrepts - 19.6 %. They are suitable for vegetables, permanent crops and meadows. Pastures grow mainly on Entic Haploxerolls. These soils feature with small depth, rocky composition, and great active carbonates content. They are of poor economic importance.

Table 3. Area changes of land-cover categories (ha)for BelosemVillag

1978 1995	1	2	3	4	5	6	7	8	9	10	11	12	13	14	15	16	17	18	19	Total 1995
1	15.8	0	0	0	0	0	0	0	0	0	0	0	0	0	0	0	0	0	0	15.8
2	0	2.7	0	0	0	0	0	0	0	0	0	0	0	0	0	0	0	0	0	2.7
3	0	0	2.9	0	0	0	0	0	0	0	0	0	0	0	0	0	0	0	0	2.9
4	0	0	0	387.4	0	2.6	3.2	0	0	0	0	0	0	0	0	0	0	0	0	393.2
5	0	0	0	0	0	0	0	0	0	0	0	0	0	0	0	0	0	0	0	0
6	20.3	0	0	0	50.4	1543.6	1318.3	0	0	0	0	0	0	0	0	0	0	0	0	2932.6
7	0	0	0	0	0	0	0	0	0	0	0	0	0	0	0	0	0	0	0	0
8	0	0	0	0	0	0	0	64.6	0	0	0	0	0	0	0	0	0	0	0	64.6
9	0	0	0	0	0	0	0	0	97.0	0	0	0	0	0	0	0	0	0	0	97.0
10	0	0	0	0	0	0	0	0	0	62.0	0	0	0	0	0	0	0	0	0	62.0
11	0	0	0	0	0	0	0	0	0	0	22.0	0	0	0	0	0	0	0	0	22.0
12	0	0.1	0	2.9	0	21.8	4.2	0	0.1	0.1	0	0	0.4	0	0	0	0	0	0	29.6
13	0	0	0	0	0	0	0	0	0	0	0	0	17.5	0	0	0	0	0	0	17.5
14	0	0	0	0	0	0	0	0	0	0	0	0	0	155.1	0	0	0	0	0	155.1
15	0	0	0	0	0	4.6	6.7	0	0	0	0	0	0	0	0	0	0	0	0	11.3
16	0	0	0	0	0	0	0	0	0	0	0	0	0	0	0	21.5	0	0	0	21.5
17	0	0	0	0	0	0	0	0	0	0	0	0	0	0	0	0	328.4	0	0	328.4
18	0	0	0	0	0	0	0	0	0	0	0	0	0	0	0	0	0	13.2	0	13.2
19	0	0	0	0	0	0	0	0	0	0	0	0	0	0	0	0	0	0	2.0	2.0
Total 1978	36.1	2.9	2.9	390.3	50.4	1572.6	1332.4	64.6	97.1	62.1	22.0	0	17.9	155.1	0	21.5	328.4	13.2	2.0	4171.4

1. Forests, **2.** Bogs and Marshlands, **3.** Ravine, **4.** Pastures, **5.** Vineyards, **6.** Corn-fields, **7.** Rice-fields, **8.** Water catchments, **9.** Drain Channels, **10.** Channels, **11.** Railroad, **12.** Highway, **13.** Roads, **14.** Dirt Roads, **15.** Transport Terrain, **16.** Agricultural Buildings and Terrain, **17.** Urban Area, **18.** Plants Terrain, **19.** Industry and Mining Terrain

Conclusions

As a result of anthropogenic activities, nowadays the landuse structure of the studied areas is highly disturbed and the anthropogenic influence increases over time.

Rice and permanent crops cultivation exhibit a clear trend of area decrease in 1995.

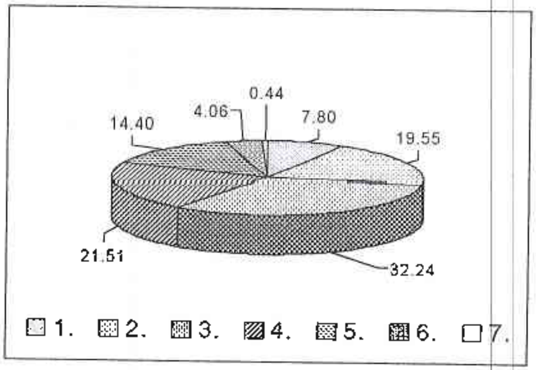

Fig. 4. Relative portion of soil types towards the total area (%) of the fields, 1995 г. 1. Typic Xerofluvents, 2. Fluventic Xerochrepts, 3. Calcixerollic Xerochrepts, 4. Typic Haploxeralfs, 5. Entic Haploxerets, 6. Typic Haploxerets, 7. Entic Haploxerolls.

The high provision of the population with arable land and the lack of working force will influence significantly plant-growing structure. It is necessary to grow less labor-consuming cultures with higher mechanization potential.

The environmental conditions and the opportunity for their reclamation provide good preconditions for agricultural use of the land. Enforcement of the Law on Ownership and Use of Agricultural Land and Land Allocation to its Owners or Their Heirs may lead to a change in the landuse structure and environmental status. This calls for monitoring of the territory, using the GIS database developed in the present study.

The GIS database provides the opportunity for rapid extraction of unbiased thematic information from multichannel images for the purpose of regular landuse monitoring of the studied areas.

Acknowledgments. I express my appreciation to the Soil Resources Agency of the Ministry of Agriculture and Forestry for the provided data.

References

1. Великов В., Д. Мишев, Е. Руменина, "Космос, ландшафти, екология", Изд. "Св.Св. Кирил и Методий", В. Търново, 1995.
2. Илиева М., Ил. Илиев, Б. Колев, "Обща характеристика на селското стопанство, мон. "География на България", Академично издателство "Проф. М. Дринов", С.1997.
3. Петров П., "Ландшафтознание", Изд. "Св. Кл. Охридски", С., 1990.

4. Попов А., “Влияние на някои ландшафтообразуващи фактори и процеси върху диференциацията на природните комплекси в Горнотракийската низина”, Известия на БГД, кн. XXV, Изд. "Наука и изкуство", С., 1989.

5. Mitchell A. The ESRI Guide to GIS Analysis, Volume 1: Geographic Patterns & Relationships, Published by ESRI, Inc., Redlands, California,1999.

6. Брой на населението по области, общини и населени места, Национален статистически институт, София, 1993.

ПРОСТРАНСТВЕН И ВРЕМЕВИ АНАЛИЗ НА ЗЕМЕПОЛЗВАНЕТО В ДВЕ ОБЛАСТИ НА РАЙОН ”РАКОВСКИ”

Евгения Руменина

Резюме

Статията е посветена на мониторинга на земеползването на територията на селата Белозем и Шишманци – община Раковски. При реализацията на поставените задачи и цели са използвани концепции и методики от дистанционните изследвания, ГИС и ландшафтознанието. Поставени са за решаване следните задачи: създаване на ГИС база данни за динамиката на земеползването, почвените различия, геологията и топографията с помощта на многоканални изображения и създадената база данни; съставяне на карти, изобразяващи структурата на земеползването и определяне и анализ на пространствената динамика на земеползването за 1995 година сравнена с 1978 година.

Екологичните условия и възможностите за тяхното възобновяване създават добри предпоставки за използване на земята за целите на земеделието. Прилагането на закона за собствеността и използването на земеделската земя и връщането на земята на нейните собственици и техните наследници може да доведе до промяна в структурата на земеползването и екологичния статус. Това поражда необходимостта от наблюдение на територията с помощта на базата данни, разработен в изследването.

Bulgarian Academy of Sciences. Space Research Institute
Aerospace Research in Bulgaria. 17. 2003. Sofia

LAST PLANT EXPERIMENTS IN THE "SVET" SPACE GREENHOUSE EQUIPMENT ONBOARD THE "MIR" ORBITAL STATION

Tania Ivanova, Svetlana Sapunova, Plamen Kostov, Ivan Dandolov

Space Research Institute-Bulgarian Academy of Sciences

Abstract

Unique results from the plant growth research under microgravity were achieved during the last experiments in the Bulgarian SVET Space Greenhouse (SG). It was launched onboard the MIR Orbital Station (OS) in 1990 and was the only equipment for long lasting plant experiments in the world till the end of MIR OS. A total of 680 days of experiments with different plant species were carried out on international programs. In 1989-1999 two Russian crews conducted the most productive several-month experiments with a new wheat variety. This more resistant variety allowed full life cycle plant development and even producing second generation "space" seeds. So, it was proved that there were no obstacles to grow the crop that is most important for the future Biological Life Support Systems (BLSS) during long-lasting missions. The last OS MIR crew conducted experiments with different leafy vegetables in the SVET SG in 2000. Plant samples were returned to Earth for analysis while the rest were eaten with pleasure by the cosmonauts to taste their flavour qualities.

1. Introduction

The research on plant growth under microgravity is of great importance since plants are a major element of Biological Life Support Systems (BLSS) for future long-term space missions. Plants can supplement the astronaut food and scrub the carbon dioxide in cabin air through their metabolism, thus regenerating the atmosphere. Besides, taking care of a garden in such extreme conditions has a significant psychological effect on the crew's emotional status, rapidly enhancing the astronauts' psycho-physiological condition.

The SVET Space Greenhouse (SG), an automated facility for plant growth under microgravity, was designed in the Space Research Institute, Bulgarian Academy of Sciences. It was tested and launched in space under a joint project with the Institute of BioMedical Problems (IBMP), Moscow, within the *Krystall* module, docked to the MIR OS on June 10, 1990. Since those times, SVET SG has been a regular equipment onboard the MIR OS till its plunge into the Pacific and was used to accommodate a series of total 680 days plant space experiments on different scientific programs in 1990-2000 (Table 1). Unique scientific results in the field of Space Biology were obtained from these experiments.

Table 1. Main plant experiments carried out in the SVET SG onboard the MIR OS in 1990-2000.

No	Year	Start–end	Days	Plant variety	Program
1	1990	16 Jun-8 Aug	54	Radishes, Chinese Cabbage	INTERCOSMOS
2	1995	10 Aug-9 Nov	90	Wheat *Super Dwarf*	MIR-SHUTTLE
3	1996	5 Aug-6 Dec	123	Wheat *Super Dwarf*	MIR-NASA-3
4	1996-97	6 Dec-17 Jan	42	Wheat *Super Dwarf*	MIR-NASA-3
5	1997	31 May-30 Sep	115	Mustard *Brassica Rapa* (3 veg.)	MIR-NASA-5
6	1998-99	18 Nov-26 Feb.	100	Wheat *Apogee*	RUSSIAN
7	1999	9 Mar-17 Aug	130	Wheat *Apogee* (2^{nd} generation)	RUSSIAN
8	2000	21 May-15 Jun	27	4 lattice crops-genus *Brassica*	RUSSIAN
		Total time:	**680**		

The first successful 2-month experiments with vegetable plants (radishes and Chinese Cabbage) carried out in 1990 proved the efficiency of Bulgarian hardware and technology [1,2]. In 1995, American scientists from the Utah State University (USU), USA and NASA/Ames Research Center designed the American Gas-Exchange Measurement System (GEMS) [3]. It was added to the SVET SG basic Bulgarian equipment to record more environmental factors to which plants are exposed. Three-month wheat (*Super Dwarf* variety) plant experiments were carried out in the SVET-GEMS equipment. The physiological and chemical analyses showed that the space plants, grown in these two experiments, though looking healthy, had been exposed to significant moisture and nutrient stress [4]. This made us direct our efforts to equipment optimization in order to provide more adequate environment for the plants - light intensity and spectrum and substrate (soil) moistening.

A set of the SVET-2 SG equipment (a greenhouse of a new generation) with considerably improved technical characteristics was designed by Bulgarian scientists on NASA's order and launched on board the MIR OS in early 1996. A succession of plant experiments on the "Greenhouse" Project were planned by the USU and IMBP and carried out in the SVET-2 SG equipment on the MIR-NASA program in 1996-97 [5]. The specific goals of these experiments were to grow plants through a complete life cycle in space "from seed to seed". Healthy plants of *Super-dwarf* wheat were grown through a complete life cycle during the "Greenhouse 2b" experiments conducted on MIR-NASA-3 program from August 1996 to January 1997 by the U.S. astronauts Shannon Lucid and John Blaha. Unfortunately, in these experiments wheat seeds were not produced in space. All 297 heads harvested on December 6, 1996 were sterile - not a single seed was detected. It was found that the ethylene gas in the cabin atmosphere of MIR OS had caused the sterility of the heads.

Another plant species - mustard plants (*Brassica Rapa*) with a very short life cycle were used in the next "Greenhouse 3" experiments. They were planned by the Louisiana State University, USU and IBMP and conducted by the astronaut Michael Foale on the MIR OS in 1997 under the MIR-NASA-5 program [6]. For the first time, a full plant life cycle "from seed to seed" was completed and seeds produced in space were planted, germinated and developed. A total of three successive generations of *Brassica Rapa* plants were grown and harvested.

Notwithstanding the indisputable success of these experiments - a complete life cycle "from seed to seed" achieved under microgravity - the problem of producing wheat seeds in space was still left open. Scientists directed their attention to wheat plants again as more important for the future BLSS and crew food during long-term space missions.

Experiments "Greenhouse 4 and 5" were performed on the MIR OS under the Russian national space research program in 1998-99. The main purpos of these experiments was to continue the studies of wheat reproductive function in microgravity and to grow crops of several wheat generations. The last experiment "Greenhouse 6" with leafy crops was carried out by the crew of the last MIR OS in 2000.

2. Results from the Last SVET-2 SG Experiments on the MIR OS

The plant experiments in the SVET-2 SG were continued in 1998-99 with another wheat variety *Apogee*. This variety was designed by scientists from the USU under the direction of Prof. B. Bagbee especially for greenhouses and has the ability to form seeds in the conditions of high ethylene concentrations. The *Apogee* wheat reaches average height, which is important for the conditions of a space flight. The **"Greenhouse 4"** wheat plant experiment was carried out between November 1998 and February

1999 by the 26th Russian crew. On November 18, 1998, the space "farmers" Genadiy Padalka and Sergey Avdeev planted 50 wheat seeds, but only 8 of them germinated due to insufficient initial substrate moistening. New seeds were sown again on November 30. In the beginning of December, they started to germinate and grew good sprouts. Later, about January 27, plants started to form heads, which seemed full with seeds. The scientists were excited. For the first time wheat seeds appeared to be obtained in space. The crew confirmed this at the time of video observations on February 2 (Fig.1).

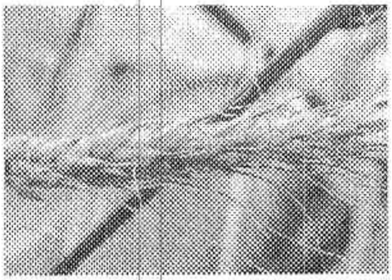

Fig. 1. A photograph of the Apogee wheat plants grown during the "Greenhouse 4" experiment in the SVET-2 SG on the MIR Orbital Station taken in February 1999.

All 12 plants with 29 ears had seeds [7]. On February 26, the life cycle was completed and the plants were harvested. All 29 ears were put in a bag and sent to Earth. On Earth, each ear with the seeds was packed separately and sent for detailed analysis. A total of 508 space-produced seeds were counted although the investigators anticipated getting no more than 100. The preliminary report said that the "space" seeds had similar structures to "earth" seeds and that they looked viable. Only 10 seeds were kept onboard for further sawing in order to produce second generation space seeds. 45 of the seeds that slipped out of the ears were packed and put aside to be planted on Earth. Fresh seeds usually require a long rest period (of several months) before planting. The scientists used another way in order to save time. On April 1, they soaked these 45 seeds for a day. 40 of them germinated and were put into a freezer. On April 5, the seeds were taken out and, on the next day, all 40 seeds were planted and further sprouted.

The same procedure was applied onboard the MIR OS. On March 3, 1999, the next **"Greenhouse 5"** wheat plant experiment was started by the 27th Russian space crew. The cosmonauts soaked 40 seeds (10 space-produced and 30 earth-produced). All the seeds germinated and, on the next day, they were put into a freezer for several days. On March 9, the seeds were planted in the SVET-2 SG. Unfortunately, at this time the temperature in the MIR OS was about 29°C while the wheat plants required an optimal soil temperature of 12-17°C. For that reason, only two out of the ten space seeds sprouted. Further, one of them died and the only remaining wheat plant developed and produced seeds. Nevertheless, this was a unique result. For the first time second-generation space seeds were produced in microgravity. In April, the new "space" seeds were returned to the MIR OS. They endured the landing and launch loading well and were planted in the vacant places in order to use the sowing area more effectively. The experiments were completed on June 7, 1999, but the plants were not harvested because of the risk of rotting. The equipment continued operating till August 17, when the plant samples were collected and returned to Earth for further detailed analysis. All the 5 second-generation space seeds were planted on Earth, germinated and produced healthy green plants. The experiments gave further evidence that wheat growth and development in microgravity follow the same pattern as on Earth. The period of vegetation as a whole was not extended. Neither were the individual phases of wheat development. Experiments "Greenhouse 4 and 5" yielded a total of more than 1000 "space" seeds and second-generation "space" seeds were obtained in the "Greenhouse 5" experiment. Table 2 presents data for the comparative analysis of two space generations wheat plants [8].On the whole, the only second-generation space plant was not morphologically different from the first-generation ones and the ground experimental samples (control).

Table 2. Characteristics of *Apogee* wheat in experiments "Greenhouse 4 and 5"

Parameter	Flight experiment "Greenhouse 4"	Flight experiment "Greenhouse 5"		Control without ethylene	Control with ethylene 1.1 mg/m^3
		I generation	II generation		
Period of the full cycle of vegetation, *days*	70-82	83-90	83-90	80-83	75-80
Dry mass of one plant, *g*	3.64	2.29	1.21	3.05±0.86	1.70±0.28
Number of shoots with heads per plant	2.4	2.1	2.0	2.8±0.4	3.0±1.0
Plant height, *cm*	35.3±3.1	33.9±5.9	27.0	44.8±2.8	27.7±1.1
Stem length, *cm*	26.2±2.0	27.1±3.1	22.0	36.2±3.1	18.9±4.2
Number of seeds per plant	42.3	20.7	5	68.3	13.2

This experiment was a great scientific success. A plant with a long life cycle was grown "from seed to seed" in space. Moreover, this was a wheat plant - a plant of great agricultural importance. Before the results of the "Greenhouse 4 and 5" experiments were received the retarding effect of microgravity on plant development was debatable. Now biologists drew the conclusion that retarding of plant development in space is caused not only by the lack of gravitational force, but also by the conditions existing in a closed space where there are many environmental pollutants whose concentration, though admissible for man, is harmful to plants.

The MIR OS was renewed after it had been empty for 223 days and the next **"Greenhouse 6"** plant experiment was carried out in the year 2000 under the Russian national space program. Seeds of 4 different species of lattice crops - genus *Brassica* were planted in the SVET-2 SG on May 21 by the 28th space crew (cosmonauts Sergey Zalyotin and Alexander Kalery) which grew normal biomass (Fig. 2).

The plants were chosen for their short vegetation cycle (leaves mature in 2-4 weeks after sowing). The experiment was completed on June 15. A sample of each plant was brought back to Earth, while the cosmonauts tested the rest.

In the 2000 experiment, four leafy vegetables were raised for 26 days, including Chinese cabbage (*Brassica rapa var. pekinensis*), Mizuna (*B. rapa var. nipposinica*), broccoli (*B. rapa var. utilis*), and mustard (*B. juncea*). The growth and development characteristics of the space-grown plants did not differ from their ground analogues. The comparison between the Chinese cabbage crop dry mass grown in the 1990 and 2000 space experiments demonstrated that productivity in the latter was 5 times higher.

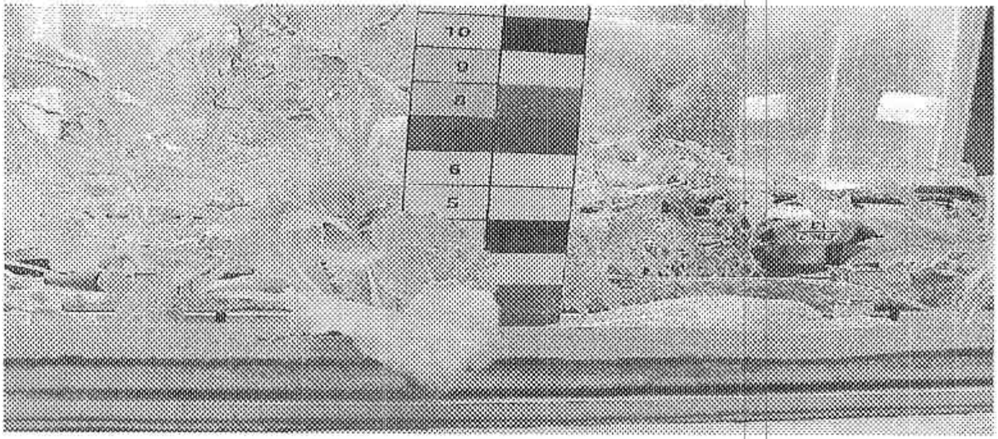

Fig. 2. A view on the green plants (4 lattice crops) grown in the SVET-2 SG in June 2000.

In the 2000 experiment, cosmonauts tested the flavour qualities of the received leaf vegetables and concluded that any of the four varieties would be a significant enhancement to their diet, and a worthy crop for a space production greenhouse, as they gave preference to Mizuna and mustard.

3. Major scientific results

More than 400 experiments were conducted on the MIR OS during its 14 years in orbit. And the "Greenhouse" experiments are considered to rank among the most important and successful ones.

The scientific results obtained during the SVET and SVET-2 SG experiments answered a number of questions concerning plant growth under microgravity [9]:

- Light completely replaces the gravity vector and plants turn towards the light as they sprout. The plants which are in the middle of the sowing area turn upwards while the others turn aside because of the reflecting surface (mailar) put on the walls within the chamber.
- Seeds must be orientated before sawing because if the root begins to grow towards the light, the plant will die.
- The roots fill up the entire substrate volume and they are orientated not to the gravity vector but to the areas with more nutrients and moisture.
- The nutrients flow away towards the tuber and this is not because of gravity but due to the capillary osmose (in 1990, radishes were grown).
- The space plants take the same time to flower and produce seeds in microgravity as they do under normal gravity conditions.

The results obtained during the biological flight experiments are fundamental. Reiteration of the "seed-to-seed" cycle was achieved and the environmental variables in a human space habitat (MIR OS) having an impact on plant growth and development under microgravity were determined.

The main result from the series of experiments in the SVET and SVET-2 SG on the MIR OS is that there is no "show-stopper" for plant growth in microgravity. The research conducted in this facility brought the scientists nearer to the possibility to grow plants for food in space. They proved the feasibility of BLSS development if appropriate equipment was designed.

The successful *Brassica Rapa* and *Appogee* wheat experiments showed that the lack of gravity is not an obstacle for normal plant development in space. The impact of microgravity as a stress operator on the second and third generation space-produced seeds in case of normal plant size and yields is possible to be found on a cellular level.

The vegetable plants grown onboard the MIR OS during the "Greenhouse 1" (1990) and "Greenhouse 6" (2000) experiments are of another important plant group that deserves special attention. Both experiments were conducted under severe water stress no matter that it was caused by different reasons. A few months before the MIR OS plunge into the Pacific (in March 2001), the crew tasted the green salads grown in the SVET SG for the first time.

4. Prospects for the ISS

The new International Space Station (ISS) will provide a perfect opportunity for conducting full life cycle plant experiments in microgravity, including measurement of more vital plant parameters during the next 15-20 years. Now, many countries (Russia, USA, Italy, Japan, etc.) are designing plant growth facilities for scientific research based on the SVET SG operational principles, scheduled for the ISS.

The designed biotechnological and technical equipment and the conduction of so many successful experiments make Bulgarian scientists preferred partners for future international collaboration to design facilities for plant microgravity research on the ISS. The universality of the equipment allows different international teams of biologists to use it for experiments planned on their own programs. There are different proposals for joint projects, but the most perspective is the Brazilian one.

In October, 1999, a Memorandum of Understanding was signed between the SRI and BRAZSAT (Brazilian Company in the area of space research and commercial space services). According to it, both parties will work together on the development of Equipment for Agricultural Research in Microgravity (EPAM) using Bulgarian space greenhouse experience. Two governmental institutions were involved in the Project: the Brazilian Space Research Institute (INPE) and the Brazilian Agricultural Research Company (EMBRAPA). In 2000, a Feasibility Study Contract was signed and now we are waiting for financial support for the next stages of the Project's development.

A new Concept for a new Space Greenhouse, based on the Bulgarian experience and "know-how" is being developed [10]. The absolute and differential plant chamber air parameters and some plant physiological parameters will be measured and processed on-line. Using transpiration and photosynthesis measurement data the controller will evaluate the plant status and perform adaptive environmental control in order to provide most favorable conditions for plant growth at every stage of plant development in autonomous mode during plant microgravity experiments.

The Bulgarian and Brazilian Governments support the negotiations - a bilateral agreement was signed in 2000 during the visit of the Bulgarian Foreign Minister in Brazil. The EPAM launch into space is scheduled for 2003-04 and will be probably connected with the flight of the first Brazilian astronaut. The aim of the experiments will be to test the effectiveness of the methods for fighting plant diseases and to grow more productive plant species in the conditions of microgravity. EPAM will be mounted in the ISS Brazilian allocation and will be accommodated in a double middeck locker in the upper half of the NASA developed EXPRESS Rack.

References

1. Ivanova, T.N., Yu. A. Bercovich, A. L. Mashinskiy, G. I Meleshko. The First Vegetables Have been Grown up in the "SVET" Greenhouse by Means of Controlled Environmental Conditions. Microgravity Quarterly (ISSN 0958-5036), 2, 1992, 2, 109-114.
2. Ivanova, T., S. Sapunova, I. Dandolov, Y. Ivanov, G. Meleshko, A. Mashinskiy and Y. Berkovich. "SVET" Space Greenhouse Onboard Experiment Data, Received from "MIR". Station and Future Prospects. Advances in Space Research (ISSN 0273-1177), 14, 1994, 11, 343-346.
3. Ivanova, T., P. Kostov, S. Sapunova, G. Bingham, S. Brown. Equipment for the Greenhouse SVET'95 Project and Some Optimisations for Future Experiments on Board the MIR Orbital Complex. Аерокосмически изследвания в България (ISSN 0861-1432), 1998, 14, 46-49.
4. Salisbury, F. B., G. W. Bingham, W. F. Campbell, J. G. Carmen et al., Growth of super-dwarf wheat on the Russian space station MIR, 26th Intern. Conf. on Environmental Systems, Monterey, CA, 8-11 July 1996 (SAE 961392).
5. Ivanova, T. N., P. T. Kostov, S. M. Sapunova, I. W. Dandolov, F. B. Salisbury, G. E. Bingham, V. N. Sytchov, M. A. Levinskikh, I. G. Podolski, D. B. Bubenheim, G. Jahns. Six-Month Space Greenhouse Experiments - a Step to Creation of Future Biological Life Support Systems. Acta Astronautica (ISSN 0094-5765), 42, 1998, Nos.1-8, 11-23.
6. Ivanova, T., S. Sapunova, P. Kostov, I. Dandolov. First Successful Space Seed-to-Seed Plants Growth Experiment in the SVET-2 Space Greenhouse in 1997. Аерокосмически изследвания в България (ISSN 0861-1432), 1999, 16, 12-23.
7. Levinskikh, M. A., V. N. Sychev, T. A. Derendyaeva, O. V. Signalova, I. G. Podolsky et. al. Growth of Wheat from Seed to Seed in Space Flight. *Aerospace and Environmental medicine*, 34, 2000, 4, 37-43.

8. Sychev, V. N., Ye. Ya. Shepelev, G. I. Meleshko, T. S. Gurieva, M. A. Levinskikh et. al. Biological Life Support Systems: Investigation Onboard the Orbital Complex MIR. Aerospace and Environmental medicine, 33, 1999, 1, 10-16.

9. Ivanova, T., P. Kostov, I. Dandolov, S. Sapunova. Results from Microgravity Experiments in the SVET Space Greenhouse Onboard the MIR Orbital Station, 51st International Astronautical Congress, Rio de Janeiro, Brazil, 2-6 October 2000, Rep. IAF-00-J.3.10.

10. Kostov, P., T. Ivanova, I. Dandolov, S. Sapunova, I. Ilieva. Adaptive Environmental Control for Optimal Results during Plant Microgravity Experiments. 52nd International Astronautical Congress, Toulouse, France, 1-5 October 2001, Rep. IAF/IAA-01-G.4.04.

ПОСЛЕДНИ ЕКСПЕРИМЕНТИ С РАСТЕНИЯ В КОСМИЧЕСКАТА ОРАНЖЕРИЯ "СВЕТ" НА БОРДА НА ОРБИТАЛНА СТАНЦИЯ "МИР"

Таня Иванова, Светлана Сапунова, Пламен Костов, Иван Дандолов

Резюме

Уникални резултати в изследванията, свързани с развитието на растенията в условия на безтегловност, са постигнати по време на последните експерименти в българската Космическа оранжерия (КО) СВЕТ. Тя е изстреляна на борда на Орбитална станция (ОС) МИР през 1990 г. и беше единствената апаратура за дългосрочни изследвания с растения в света до края на съществуването на ОС МИР. В нея са проведени общо 680 дни експерименти с различни видове растения по международни програми. В периода 1998-1999 г. двата руски екипажа на ОС МИР осъществиха най-резултатните няколко-месечни експерименти с нов сорт пшеница. Този по-устойчив сорт позволи осъществяването на пълен цикъл на развитие на растенията и дори получаването на второ поколение "космически" семена. Така бе доказано, че няма пречки да бъде отглеждана в условие на безтегловност и най-важната култура за биологичните системи за осигуряване на живота на космонавтите при бъдещите им дълготрайни полети. Последният екипаж на ОС МИР проведе експерименти с различни видове салатени култури в КО СВЕТ през 2000 г. Образци от растенията бяха върнати на Земята за изследвания, а останалите бяха изядени с удоволствие от космонавтите за да се тестват вкусовите им качества.

Bulgarian Academy of Sciences. Space Research Institute
Aerospace Research in Bulgaria. 17. 2003. Sofia

OPTIMIZED SYSTEM FOR COORDINATES DETERMINATION WITH ACCURACY FIRING AT GROUND TARGETS

Garo Mardirossian, Boytcho Boytchev, Boyko Ranguelov, Georgi Sotirov*

Space Research Institute - Bulgarian Academy of Sciences
**Geophysical Institute - Bulgarian Academy of Sciences*

Abstract

The paper is devoted to an automated seismological system determining the target coordinates with bomb casting. The basic problems are formulated and the options for their resolution are discussed. Unique method and equipment for automatic determination of the coordinates of bomb- or bullet-hit target are proposed. A brief optimization analysis is made, based on which the optimal block diagram of the equipment implementing the proposed method is synthesized.

1. Problem

The enhanced requirements for intensification and quality improvement of fight training in aviation require to have objective data for the crews' results with firing at ground-based targets. Such data can be provided by high-performance methods and instrumentation for objective control of bomb casting and firing at ground-based targets, automatic express analysis, and result assessment.

2. Problem resolving options

The problem for automatic express identification of a bomb- or shell-hit target can be resolved using various methods: seismic, acoustic, location, infrared etc. [3,13,14]. All of them feature some advantages and shortcomings, but some of them might be implemented effectively at a later time, when the new type of components needed for the purpose will appear.

The idea for using a seismological system to identify explosion targets with various types of firing is boosted by its relative simplicity, high performance, and cost effectiveness. Such systems allow to identify automatically the position of earthquake epicentres. Ready-made elements and units for construction of such systems are already available, as well as the related software [7].

In [4], the optional methods for identification of earthquake epicentres are discussed, using directly the recorded times of the first arrived seismic waves. The most popular of them are the Successive Iterations Method [8] and the Hyperbole Method [1,6].

Since the task lies in determination of fire-hit with polygon fighting, we can assume the source of seismic waves as being located on the ground surface, accounting only for the propagation of voluminous longitudinal waves. This allows to consider the problem in plane coordinate system.

3. Proposed method

In [4], a copyright-protected [5] method and an equipment are proposed, providing to identify automatically the epicentre position of earthquakes, explosions, bomb- or shell-hits etc., for epicentres whose depth is negligibly small compared to the epicentre's distance. Here, t_1, t_2, t_3 , …t_n are the recorded times of the first seismic waves arrived at recording sites P_1, P_2, P_3 ,….P_n.

In Fig.1, a plane coordinate system XOY is shown, with one exemplary arbitrary position of three recording stations, P_1, P_2 и P_3, with their respective coordinates, a_1b_1, a_2b_2 and a_3b_3, and the epicentre E (the bomb or shell's hit-position) with unknown coordinates, x and y. The arriving times of the first seismic waves, generated by the bomb or shell's hitting epicentre E at time t_o are t_1, t_2 и t_3 at the three recording sites, accordingly.

For basic geometric considerations, a system of 3 equations may be written, where v stands for seismic waves' propagation velocity throughout the earth's surface. Obviously, this velocity can be assumed constant within the firing-ground, where the surface ground layer is actually homogenous:

$$(1) \qquad \left| \begin{array}{l} (x - a_1)^2 + (y - b_1)^2 = v^2(t_1 - t_o)^2 \\ (x - a_2)^2 + (y - b_2)^2 = v^2(t_2 - t_o)^2 \\ (x - a_3)^2 + (y - b_3)^2 = v^2(t_3 - t_o)^2 \end{array} \right.$$

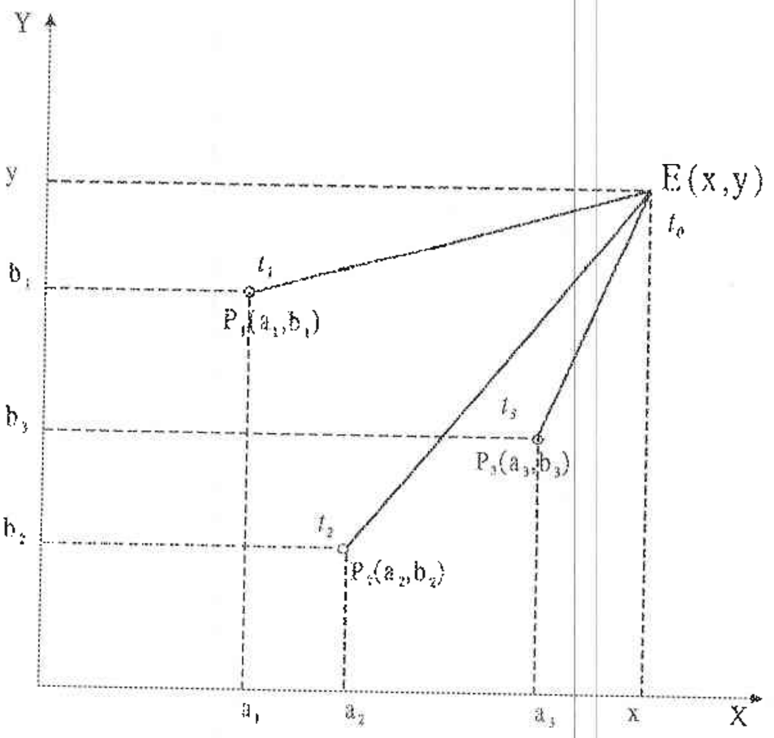

Fig. 1

Should the recording stations be positioned: one on the y axis ($a_1 = 0$), the other – in the origin of the coordinate system ($a_2 = 0$, $b_2 = 0$), and the third - on the x axis ($b_3 =0$), then, the system of equations (1) can be simplified:

(2)

$$\left|\begin{array}{l} x^2 + (y - b_1)^2 = \nu^2(t_1 - t_o)^2 \\ x^2 + y^2 = \nu^2(t_2 - t_o)^2 \\ (x - a_3)^2 - {b_3}^2 = \nu^2(t_1 - t_o)^2 \end{array}\right.$$

Since the distance from the epicentre to the recording stations is relatively small, a higher resolution is required for recording the times of the first arrived seismic waves, as well as for the system's overall speed of operation.

In Fig. 2, the position of the eight stations, P_1, P_2, P_3 ....P_8, along the firing ground's periphery and the central station *CP* are shown.

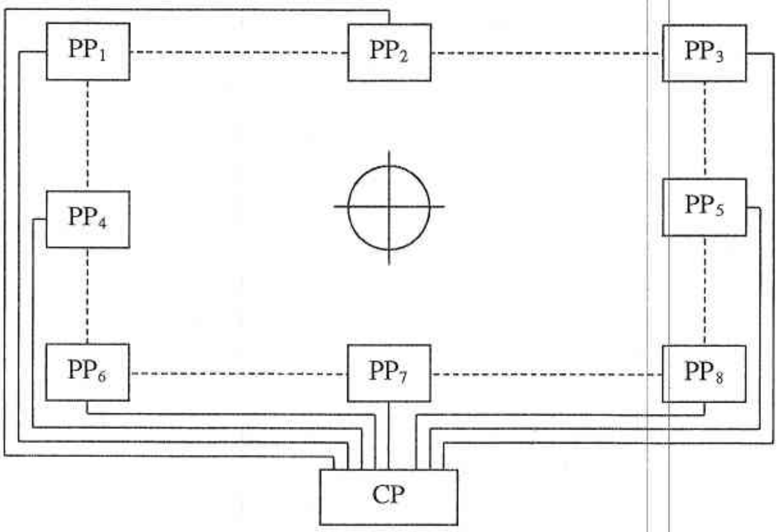

Fig. 2

4. Optimization analysis

A simple assessment reveals that, with assumed average velocity of seismic waves propagation of 3 km/s and acquired accuracy of hit target coordinates of the order of 10 m, the resolution at the time of recording the arrival of the first waves is of the order of 0,003 s. Though such time recording accuracy is no problem for modern chronometric systems, the possible differences in seismic waves propagation velocity and instrumentation errors in threshold blocks' activation at the recording stations might result in incorrect determination of the hit's position. This can be eliminated by software means and by increasing the number and optimizing the position of the recording stations [12]. The increased number of recording stations produces an overdetermined system of equations, thus eliminating the influence of local minimums with the minimization procedure and increasing significantly the accuracy in determining the unknown coordinates. Here, overdetermination of the system can be achieved by about 8 registration stations.

A major problem here is the choice of seismoreceivers. Depending on operation conditions, the problem can be solved using seismoreceivers with magnetoelectric transducer, capacity transducer, or piesoelectric transducer [4]. The analysis criteria are sensitivity, frequency bandwidth, damping, and calibration options. Magnetoelectric transducers feature highest sensitivity and best damping potential, but they are relatively large-sized, require adjustment at the time of assembly and current maintenance, and are relatively expensive. Here, high sensitivity is not decisive. The most important criteria are sameness of amplitude-frequency characteristics, maximal increment velocity of the electric signal at the sensor's output, maximal high-frequency bandwidth, and own resonance frequency outside the frequency band of the processed seismoreceiver electric signals.

Accounting for the above, and minding besides the cost and operation conditions (temperature and moisture in the first place), a seismoreceiver with piesoelectric transducer is suggested.

Since the sensors are positioned at some depth under the earth's surface, the disturbing influences should be eliminated, such as acoustic waves, generated by various sources, the bomb-casting airplane including. The influence of climatic factors (temperature, wind, moisture etc.) is also reduced.

The manner of discriminating (comparing) the arrival times of the first seismic waves at each sensor is essential. The available options are two – discrimination at each station or discrimination at the central station. The first option requires taking measures to preserve the front of the electric pulse, which in its turn necessitates coordination and using cables with precise wave resistance. The second option means transmitting the amplified actual analogue signal from the seismoreceivers along a shielded audio-instrumentation cable to the central station, whereas comparing takes place at the input of a dedicated analogue interface module, where data from all sensors is collected. Upon comparing, by the lag times of pulse fronts, time intervals are transformed into lag-equivalent digits, which are supplied through a standard interface to the computer inputs. In the dedicated interface module, the electric signals from the sensors are received, filtered, amplified, and discriminated. The first seismic wave front, propagating in the firing ground's surface layer, activates the sensors in a succession, depending on their distance from the hit point. As illustrated in Fig.3, the seismic wave arrives with time lags of $+\Delta t_1$, $+\Delta t_2$ etc., accordingly), which are function of propagation velocity and the relevant distance S_i. Equal time lags may be observed with several sensors positioned at equal distances away from the hit point (as with the case in Fig.2), as well as with pairs of sensors etc. Thus, for instance, with 8 seismosensors, the system measures 7 relative time lags with respect to the first activated, which is assumed to be "0".

In the dedicated interface module, the electric signals from the sensors are received, filtered, amplified, and discriminated. The first seismic wave front, propagating in the firing ground's surface layer, activates the sensors in a succession, depending on their distance from the hit point. As illustrated in Fig. 3, the seismic wave arrives with time lags of $+\Delta t_1$, $+\Delta t_2$ etc., accordingly), which are function of propagation velocity and the relevant distance S_i. Equal time lags may be observed with several sensors positioned at equal distances away from the hit point (as with the case in Fig.2), as well as with pairs of sensors etc. Thus, for instance, with 8 seismosensors, the system measures 7 relative time lags with respect to the first activated, which is assumed to be "0".

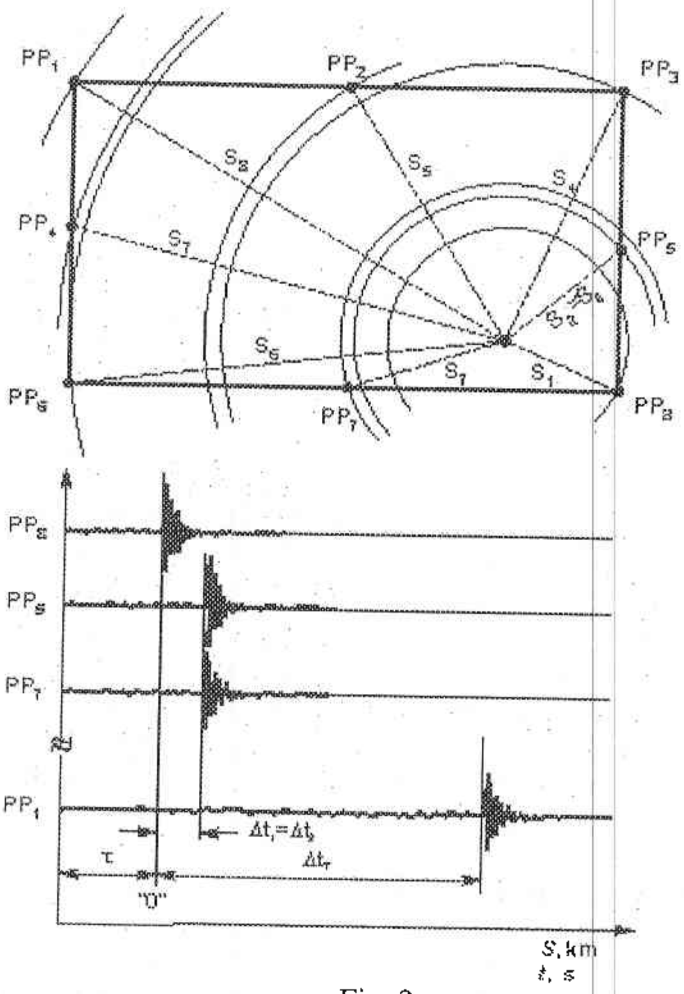

Fig. 3

The options for transmitting an electric signal from the peripheral stations are also two: along a wireless (radiochannel) or along a cable link. Undoubtedly, the lags over a radiochannel will be greater and of various size, and their compensation will be more difficult. Thus, a maximal cable length difference $\Delta L = 1200$ m between the closest and the farthest station,

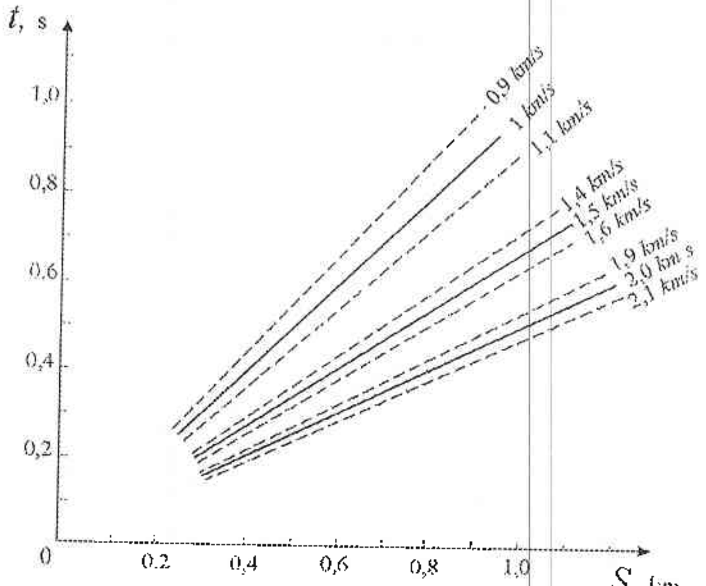

Fig. 4

will produce a time difference in passing this ΔL of the order of 3.10^{-6} s, i.e. within the microsecond range. Cables should be accordingly compensated for or harmonized, accounting for the time lags of the various peripheral stations.

With an assumed maximal difference of $\Delta v = \pm 0{,}1$ km/s in surface seismic waves' propagation velocities within the firing ground, for distances of the order of 0,5 km, time error will be of the order of $\Delta t = 0{,}03$ s. With respect to overall time, this amounts to about 6 %. The relationship $t = f(S)$ for three different velocities v is shown in Fig. 4.

5. Technical implementation

In Fig. 5, the overall block diagram of the SDS-2 is shown, synthesized based on optimization analysis. The major considerations in its synthesizing were that in IBM PC, the internal time signals cannot be used directly because they feature but a short-time accuracy and time resolution. Their appearance, irrespective of the operation system, varies from a couple of to dozens of milliseconds. To provide for accurate measurement of the times Δt_i with sufficient resolution, another accurate supporting generator is needed, with sufficiently high frequency. For the purpose, some supporting frequencies of the bus of the IBM PC may be also used. Under a relatively simple work algorithm (used in frequency-meters), the time intervals Δt_i are filled by the frequency f_b, whereas the number of these pulses may be processed by the computer, using adequate software under the algorithm already proposed. For such purposes INTEL and some other producers propose the integrated circuit 8254 (3 timers), which can process time intervals; it is a part of the hardware set and it is compatible with the office signals of all IBM PCs.

The structure and work algorithm of the SDS-2 according to the proposed structural diagram is as follows:

1. Filtration and amplification of the sensor-supplied signal for correct discrimination. This takes place in blocks HPF (very-high-frequency filter), Y (amplifier), and LPF (low-frequency filter). HPF is included to eliminate the possible direct-current level (which bears no data) originating from the sensors' amplifiers. HPF eliminates the noises outside the sensors' useful frequency bandwidth and is conjugated with them.

2. Because of the fact that the initial phase of the analogue signals supplied by the sensors is unclear, the provided comparers (K) are of the window type, with symmetrical comparing threshold with respect to the zero line, comparing above the noise level of the input signals. A great variety of such integrated elements is available.

3. An essential element in the operation of such a system is the comparing threshold. Depending on its level, false activation is possible with low threshold and missed activation - with high threshold. One possible solution is the floating activation threshold, which adapts itself to the input signal. For the purpose, the circuit is supplied with detectors of the mean and peak value of the signals obtained at the output of LPF; these detectors control the activation threshold of comparers K_I. The adequate control of the activation threshold makes the system adaptable to the input signals, prevents false activation, and may enhance measurements accuracy.

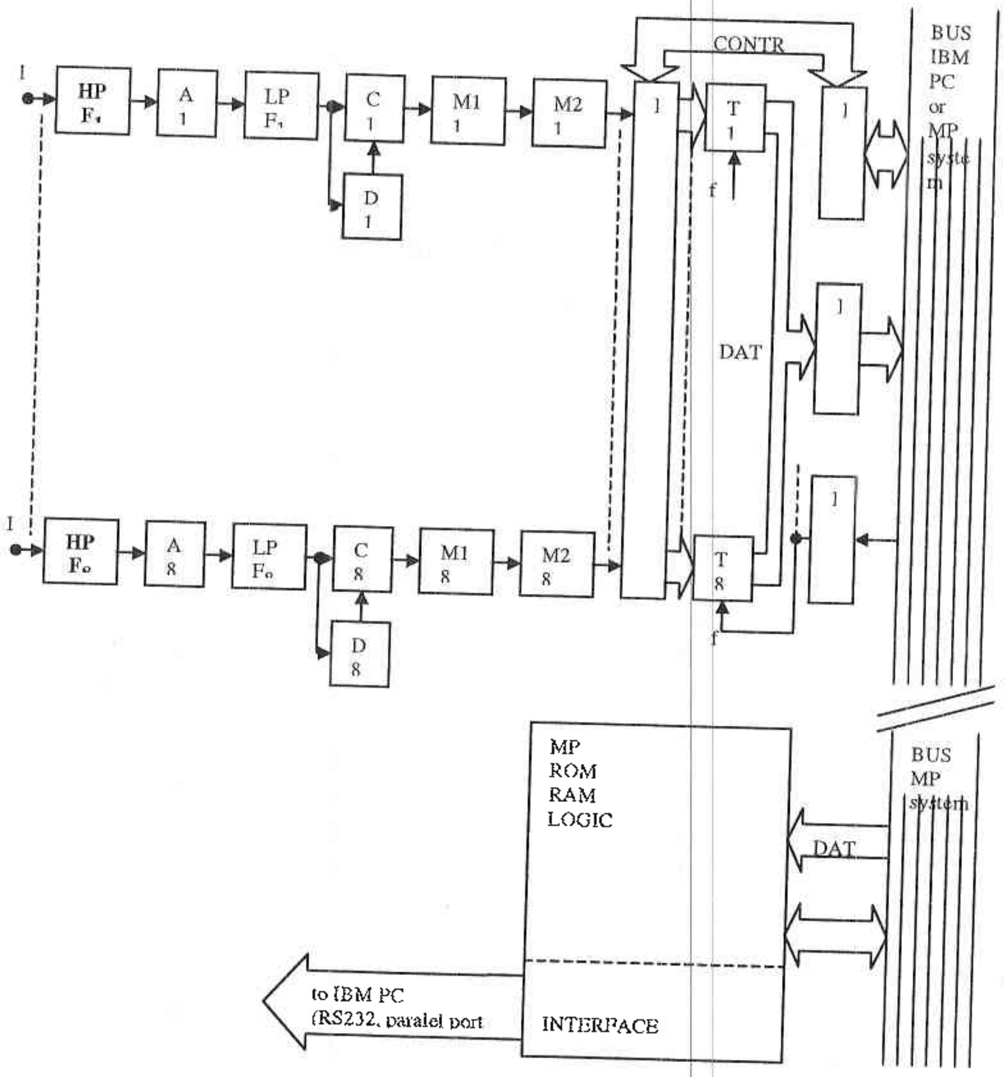

Fig. 5

4. The useful information is contained in the forefront of the first pulse at the output of comparers K_i for each individual channel. To simplify the operation of the next logic *L*, the pulse sequence should be transformed into one, wider pulse, preserving the forefront. This is carried out in blocks M_{1i}, which are, in fact, monovibrators.

5. To eliminate the error resulting from the different cable length from the sensors to the module's input, blocks M_{2i} are introduced, compensating for the different time lags of the signals along the cables.

6. The pulses obtained at the outputs of M_{2i} (in particular, their forefront) contain the whole data needed for accurate calculation of the hit coordinates. By the control logic *L*, the forefront of the first arrived pulse activates counting at all timers T_i, whereas the arrival of the forefront of each subsequent pulse at whichever channel stops the counting at this channel's timer. Each timer counts one number, whereas in the timer having started the counting this number is 0.

7. The digital data containing the channel's number and the result of counting is sufficient to calculate the hit coordinates. It is only this data that is transmitted by buffers (B) to the bus of the PC.

Another version is also possible, where the whole above-described module is part of a PC-independent microprocessor system. In it, the whole data, instead of being fed to the bus of the PC, is fed to the bus of the microprocessor system, consisting of microprocessor (μP), ROM, RAM and communication interface, say RS232, parallel port or USB. This option requires additional power-supply, a box, and own software.

On the structural diagram, both options are shown. In the first option, the module is positioned in the PC slot, provided with adequate software, while in the second option the microprocessor system communicates with the PC through standard interface.

A hit-matrix may be created, containing the relative actual time differences for each sensor and corresponding to each point of the firing-ground. Discretization depends on the needed recording accuracy of the hit. Here, no cable compensation or coordination is needed. The matrix also accounts for and eliminates the errors resulting from possible differences in the seismic waves' propagation velocities at different points of the firing ground.Knowing these different velocities at different points of the firing ground, the following algorithm may be adopted. After the initial identification of the hit position, the computer recalculates the coordinates, this time correcting velocity, and accordingly, the time for the seismic wave's arrival from the hit target to each PP.

The synthesized block diagram of the radioelectronic section of the COK-2, jointly with the determined basic technical-operation parameters, provides grounds for the system's technical design. Experiments in the field will verify the operability, accuracy, and applicability of the proposed system.

References:

1. Arhangelskii, Vvedenskaya, Manual for Data Processing and Analysis at Seismostations, vol.2, AN Publishing USSR, Moscow, 1964.

2. Vibrations in Technichs – Vol.5, Machinedesign, Moscow 1981.

3. Dorofeev, A., Aviation Munitions., BTC, Sofia, 1984.

4. Joffe, V. I., *Acoustics Handbook Swyaz, Moscow, 1979.*

5. Maksimov, L., S. Sheinin. Measurement of Equipment Vibrations, Stroyizdad, 1974.

6. Mardirossian, G., Mishev, D. Device for Automatic Express Determination of Earthquake Epicenter. BG Patent № 42808/1990.

7. Petkov, I. General Physics, vol.2. Science and Art, Sofia, 1987.

8. Software product HYPO, ver 7.1.

9. Savarenskii, E., Kirnos, D., Seizmology and seizmometry components, GITTL, Moscow, 1955.

10. Samardjiev, D., Hristoskov, L., National Operative Telemetry System for Seizmological Information (NOTSSI). Bulgarian Geophysics Magazine, N3 1980.

11. Sotirov, G., Todorov, S., Donov, G System for Co-ordinates Determination of Accuracy Firing on Ground Targets. In *Proceedings of International Military Conference "Hemus-1998"*, Plovdiv, Bulgaria, June 3-5, 1998.

12. Wilmore, P.L., Manual of Seismological Observatory Practice, Edinburg, 1970.

13. Skoko, D., Y. Sato. Optimal Distribution of Seismic Observation Points. Japan, 1967.

14. SMAD Advanced Digital Sound Ranging System. ALCATEL, Stuttgart, 1999.

15. TELESEIS STAR. Teleseis System Division. Houston, 1998.

16. Mardirossian, G, Sotirov, G., Rangelov, B., Getzov, P. An Automatic System for Co-ordinates Determination of Accuracy Firing on Ground Targets. In *Proceedings of Conference of Higher Military Air Force Academy 2001.*

ОПТИМИЗИРАНА СИСТЕМА ЗА ОПРЕДЕЛЯНЕ НА КООРДИНАТИТЕ ПРИ ТОЧНА СТРЕЛБА ПО НАЗЕМНИ ЦЕЛИ

Гаро Мардиросян, Бойчо Бойчев, Бойко Рангелов,Г. Сотиров

Резюме

В статията е описана автоматизирана сеизмологична система за определяне на координатите на целите при бомбомятане. Формулирани са основните проблеми и са разгледани възможностите за тяхното решаване. Предложени са оригинален метод и апаратура за автоматично определяне на координатите при бомбомятане и хвърляне на снаряди. Направен е кратък оптимизационен анализ, въз основа на който е синтезирана оптималната блок схема на апаратурата, реализираща предложения метод.

Bulgarian Academy of Sciences. Space Research Institute
Aerospace Research in Bulgaria. 17.2003. Sofia

MAN AS AN OBJECT OF GEOCHEMICAL AND GEOPHYSICAL INFLUENCES

Irina Stoilova

Solar Terrestrial Influences Laboratory-Bulgarian Academy of Sciences

Abstract

There are an increasing number of papers in the last years that evidence of a correlation between geochemical and geophysical factors and human health parameters and human behaviour. The basic factors that could affect human health and behaviour are: the geochemical composition of the geographical environment; the tectonic processes; the geomagnetic field variations (GMV), the climatic changes and the changes of the solar activity as well as the fact that all of them could influence mutually each other. The subject of this paper is the theoretical basis of the geochemical and geophysical influences on human health. The biological mechanisms according to which the geomagnetic field influences the psychological and behavioural reactions of people are not highlighted or identified yet. We present some of the existing suggestions and theories trying to explain these mechanisms. The studies performed in this area and the obtained results will be very useful in developing measures to protect man from the harmful influence of geochemical and geophysical factors.

Introduction

There are an increasing number of papers in the last years that evidence of a correlation between geochemical and geophysical factors and human health parameters and human behaviour. The data confirming the existence of this correlation become much more convincing. The ratio between the two groups of investigations: those confirming the correlation to those that do not prove it is approximately 4:1. "The effect of geochemical and geophysical factors on human behavior is not an artifact or an occasional event, but it is usually so complex that it could be easily omitted in the process of limited observations during the performed investigations" [1].

The basic factors that could affect human health and behaviour are: the geochemical composition of the geographical environment; the tectonic processes; the geomagnetic field variations (GMV), the climatic changes and the changes of the solar activity as well as the fact that all of them could influence mutually each other.

Geochemical Influences

The influence of the geochemical components on human health and behaviour is determined by the geochemical composition of the soil and the waters of a certain area; it is in direct relationship with the quantity of rock formations present in the same area. A number of geochemical components with regional variations are integral ingredients of blood, DNA and DRNA as well as of most of the human constitution enzymes [2]. There are a number of well-known cases demonstrating a close relationship between the geochemical composition in given geographical areas and human health as well as other cases known only to the specialists. But in all these cases, the existence of such a relationship is considered to be categorically proven. For example, there is a well-known relationship between the iodine content in human food diet and the development of endemic goitre which is a result of iodine deficiency.

The change of the copper (Cu) content in human constitution is considered as a consequence of the decrease of its quantity in soil. A disturbed copper metabolism in human constitution could cause the appearance of the Wilson disease (hepato-lenticular degeneration) as well as the symptoms of the Alzheimer's disease and old people dementia [4]. Copper is part of the content of some enzymes that are related with the Central Neural System (CNS) cell activity (dopamine, monoamine oxidase, cytochrome oxidase, etc.).

The high molybdenum (Mo) content of underground rocks in some Norwegian areas is considered as the main reason for the great number of cases of Multiple Sclerosis (MS) observed in these areas. Simultaneously, copper (Cu) and nickel (Ni) content in the environment is much less than the existing standards. It is considered that both metals have a balancing effect in respect to the great Mo content [5].

Aluminum (Al) is another soil, water and the food component related with the development of degenerative processes in some brain structures (Amyotrophyc Lateral Sclerosis – ALS). The frequent cases of this disease in some geographical areas are explained by the great aluminum content found in the soil [6].[1]

It is found that the low zinc (Zn) content causes memory disturbances and psychological derangements [7].

The healing effect of lithium (Li) in the cases of cardio-vascular diseases and psychological problems is well-known.

Selenium (Se) is used successfully in the cases of immune system derangements as well as for potency improvement. This data evidences of a close relationship between environmental geochemical content and human health and psychological activity.

Tectonic Processes

The tectonic processes are a factor that could also influence human psycho-physiological processes. It is found that precursors of tectonic activity could be observed days or even months before the event and surprisingly in areas located even at distances of several hundred kilometers away from its epicenter. Such precursors are: the electrical field changes, the low frequency variations, the specific smell of underground gases, the Geomagnetic Field (GMF) changes and the low and high frequency acoustic phenomena. Unfortunately, the phenomena usually observed and human behaviour perturbations are accounted for only retrospectively. The most frequently established fact is that the number of the various mysterious or unusual events has increased. For example, various light effects are often qualified as meetings with UFO. The cases of extrasensory or clairvoyant abilities as well as the appearance of poltergeists become much more frequent. These strange phenomena are quite often related with seismic activity [8]. The progressive increase of the number of these phenomena could assume epidemic character, which in its turn might result in a large-scale public panic [9].

Geomagnetic Influence

Geomagnetic (GM) variations could involve somatic and psychological health problems. GMF variations and especially low frequency (less than 100 Hz) variations penetrate easily live tissue, thus influencing all living organisms, including man.

---

[1] The review of the investigations concerning the influence of geochemical composition on human health in certain areas in Bulgaria is the subject of the present publication.

Earth GMF is about 0.5 gauss that corresponds to 50,000 gamma or 50 microtesla. Of coarse, it is not constant, but varies in the different geographical regions. It is approximately 25,000 gamma at the equator and about 70,000 gamma in the polar regions. The quantitative expression of these GMF intensity variations is presented by a variety of indexes – Kp, Ap, aa, Dst, etc.

Men possess varying degree of sensitivity to the GMF changes and perceive them in respect to both GMF waves intensity and their direction. There are people who can identify GMF changes of about 0.1 gauss/min. Some people even react to changes of 0.01 gauss/s.

Biological Mechanisms

The biological mechanisms after which GMF influence the psychological and behavioural reactions of people are not highlighted yet, albeit the various proposals and theories that have been forwarded. In ancient times, the magnetic forces were imparted a mysterious, supernatural and divine sense. In the Middle Ages, Parcelius used successfully the magnetic influences for medical treatment of various diseases. Later, in the middle of the 18th century (1766) F.A., Mesmer launched the idea of the existence of universal magnetic gravitation as well as of its influence on man. He explained all magnetic properties by the presence of a fluid causing magnetism. He even asserted that that fluid could not be seen or measured but it accounted for vital origin and it came from the universe depths, spreading over the planets and the earth and being felt by the people who passed it along to each other. He said that this fluid provided the reason, the feelings and the viability. Nobody could explain the origin of that fluid, but it really existed [10].

A much more real mechanism asserts that a very slight difference in the polarity between the CNS and the peripheral nerves of a degree of 15-29 mV could work like a primitive sensor in respect to the GMF change perceiving [11].

The electrical activity of some CNS structures and the endocrine glands is very sensitive to small changes of the GMF. Some of them are: pineal gland, thymus, gonads, thyroid gland, etc. These formations are involved in the cyclic recurrence of the psychological processes of live organisms and …"the circadian periodicity could influence basically as well as could increase the psychological malfunction" [1].

The presence of biogenic magnetite containing bioorganic iron compositions could be accepted as one of the possible ways for perceiving of

GM changes. Magnetite has been discovered in a number of microorganisms, fishes, birds, mammals and also in the human organism. The crystal lattice of the biogenic magnetite structure is different from the other ferrous compositions of inorganic origin [12]. Magnetite has been found in the adrenals, in the area over the eyebrows, etc. The conducted studies reveal that magnetite quantity increases proportionally with age. The presence of magnetite of biological origin…"allows us to regard the problems of magnetic perceiving from a new point of view initiating as well the idea of the existence of the so-called "Sixth Sense" which plays an important role in the behaviour of organic world representatives as well as in their evolution" [12].

There are some assumptions that the occurring atmospheric and geophysical changes influence the cells of live organism directly or indirectly by changes in water molecules, membrane permeability and the systems supporting homeostasis.

There is an interesting theory, which considers human constitution's neural lines as antennas perceiving the changes in geomagnetic waves and solar irradiation. It is namely in these antennas that the internal influences of certain intensity and frequency are transformed into neural impulses. The last ones influence the functions of the internal organs and the endocrine glands in human constitution by the vegetative neural system.

Modern Investigations

The electrophysiological studies reveal that the changes in GMF intensity influence the Central Neural System by a change in the frequency of the background electrical brain activity. The changes in this field are about 0.002 V/m and they change the frequency of brain rhythms by 1 Hz [13]. There are also changes in the vegetative functions, which are manifested by changes of the heart activity, the blood pressure values and the respiratory parameters.

The GMF pulsations such as Pc (pulsations continues) and Pi (pulsations irregular) could also have a biogenic meaning. For example, the Pc1 pulsations have a period from 0.2 to 5 s, which corresponds to the heart muscle shortening frequency. The appearance of these pulsations could essentially influence the activity of the biological system.

The continuous activity of the changed geomagnetism involves in a common reaction the neuroendocrine and endocrinology systems as well. This is proven by the identified changes in the hypothalamus-hypophysis system as well as in the adrenals. Some changes occur also in the peripheral blood and oxidation processes. Some more challenging investigations attempt to reveal the influence of earth magnetism on creative activity, talents and human genius [14].

While trying to highlight the influence mechanisms of the GMF on the CNS, Belov D. R. et al. found a positive correlation between the Ap index and brain electrical activity. The intensification of the synchronization processes during GMF changes were most clearly expressed in the frontal and central areas of the cortex [15]. The synchronization processes are considered a part of the total stress reaction involving biochemical and hormonal variations.

Nikolaev Y. S. et al. noted the influence of short-period GMF fluctuations which, in their opinion, are a main ecological factor influencing the biosphere. Their effect can be identified in both the amplitude increase as well as in the case of the fluctuation's complete disappearing [16]. An optimal level of the GM activity is necessary for a normal CNS activity. An abrupt GMF increase or its decrease to complete disappearing could result in various types of brain malfunction [17].

The vegetative neural system, playing an essential role in the function regulation of a number of human organism and systems is also sensitive to GMF changes. It is proven that the sympathetic vegetative neural system reacts mainly to slighter GM variations. The more abrupt and more intensive GMF changes cause a reaction of the parasympathetic vegetative neural system [18]. The duration of the activity of the GM parameter changes is of essential importance to all live organisms and especially to man. Thus, the idea of the need to determine the "dose" of GMF variations to which a live system is exposed originated. The need to design a "dosimetry" method regarding the cumulative exposure to unstable or abrupt GMF parameter changes was pointed.

The investigations aiming to identify the influence of the various geochemical and geophysical factors on human health and behaviour are as necessary as difficult to conduct because geophysical and solar phenomena are hard to isolate from the numerous physical factors of the environment as well as from the social and public cause-effect interrelations. "Further toxicological studies are required to assess the controls on the health effects of environmental hazards in different populations" [19]. In spite of the objective difficulties, the investigations in that area as well as the results obtained will be extremely useful in developing measures protecting man from the harmful effect of geophysical factors.

References

1. Persinger M. A. Geopsychology and geopsychopathology: Mental processes and disorders associated with geochemical and geophysical factors. Experientia 43, Birkhauser Verlag, Basel, Switzerland, 1987, 92-103.
2. Leet L. D., S. Judson, Physical Geology. Prentice-Hall, New Jersey, 1965.
3. Gaitan E., R. C. Cooksey, D. Mstthews, R. Presson, In vitro measurements et antithyroid compounds and environmental goitrogens. J. clin. endocr. Metab, 56, 1983, 767-773.
4. Bowman M. B., M. S.Lewis, The copper hypothesis of Schizophrenia: a review. Neurotics. biobehav. Rev.6, 1982, 321-328.
5. Layton W., Y. M. Sutherland, Geochemistry and multiple sclerosis: a hypothesis. Med. J.Aust. 1, 1975, 73-77.
6. Iwata S., Study of the effects of environmental factors on the local incidence of amyotrophic lateral sclerosis. Exotoxic. Åuvir. Safety, 1, 1977, 297-303.
7. Hess G. W. Chronic zinc deficiency alters neuronal function of hippocampal mossy fibres. Science, 205, 1979, 1005-1007.
8. Haraldson E. and L. G Issurarson. Does Geomagnetic Activity Effect Extrasensory Perception? - Personality and Individual Differences, 8, 1987, 745-747.
9. Persinger M., J. Derr, Geophysical variables and behavior: LXXIV. Man-made fluid injection into the crust and reports of luminous phenomena (UFO reports) - is the strain field an aseismically propagating hydrological pulse? Perceptual and Motor Skills, 77, 1059-1065.
10. Рожнов В., М. Рожнова. Гипноз от древности до наших дней. М. Изд. Сов.Россия, 1987, 304.
11. Baker R. R. Goal Orientation by Blindfolded Humans After Long-Distance Displacement: Possible Involvement of a Magnetic Sense. Science, 210, 1980, 555-557.
12. Клейменова Н. Г., В. А. Троицкая, Геомагнитные пульсации как один из экологических факторов среды. Биофизика. 37 (3), 1992, 429-438.
13. Стойнев А. и кол. Биоритми, 1991, Изд. Мед. и физк., С. 134.
14. Виноградов Е. Вопроси психологии. 1989, 6, 108-114.
15. Белов Д. Р. Зависимость пространственной синхронности ЭЭГ человека от геомагнитной активности в денъ опыта. Рос. Физиол. Ж. им. И.М.Сеченова, 84, No.8, 1998, 761-774.
16. Николаев Ю. С., Я. И. Рудаков, С. Р. Мансуров. Секторная структура межпланетного поля и нарушения деятельности центральной нервной системы. Проблемы космической биологии, Изд. Наука, М. 43, 1982, 51-59.
17. Белишева Н. К., А. Н. Попов, Н. В. Петухова, Л. П. Павлова, К. С. Осипов, С. Э. Осипов, С. Е. Ткаченко, Т. И. Баранова. Качественная и количественная оценка воздействия геомагнитного поля на функциональное состояние мозга человека. Биофизика, 40, 5, 1995, 1005-1012.
18. Braud W., S. Denis, Geophysical variables and behavior: LVIII, Autonomic activity, hemolysis and biological psychokinesis: Possible relationships with field activity. Perceptual and Motor Skills, 68, 1243-1254.
19. Fondyce F. Environmental geochemistry and health - global perspectives. Cogeoenvironment Newsletter, 16, 1989, 2000, 7-10.

ЧОВЕКЪТ КАТО ОБЕКТ НА ГЕОХИМИЧНИ И ГЕОФИЗИЧНИ ВЪЗДЕЙСТВИЯ

Ирина Стоилова

Резюме

През последните години значително нараства броят на публикациите, потвърждаващи корелацията между геохимичните и геофизичните фактори с параметри на човешкото здраве и поведение. Основни фактори, които могат да въздействат върху здравето на човека и неговото поведение, са геохимичният състав на географската среда; тектоничните процеси; вариациите на геомагнитното поле; климатичните промени и промените в слънчевата активност, като те взаимно влияят един на друг. Предмет на статията е обзорно представяне на някои теоретични постановки на геомагнитното и геохимичното влияние върху здравето и поведението на човека. Биологичните механизми, по които геомагнитното поле и геохимичният състав влияят върху физиологичните и поведенчески реакции на човека, не са изяснени и прецизирани, въпреки че съществуват различни предположения. Представени са някои от предложените в литературата теории и модели за обяснение на тези механизми. Изследванията в тази насока и резултатите, получени от тях, ще бъдат изключително полезни за разработването на защитни мерки, предпазващи човека от вредното влияние на геохимичните и геофизичните фактори.

Bulgarian Academy of Sciences. Space Research Institute
Aerospace Research in Bulgaria. 17. 2003. Sofia

OPTIMIZATION OF THE FUNCTION INJECTION MODELS IN THE MAGNETOSPHERE

Pavlina Ivanova

Geophysical Institute-Bulgarian Academy of Sciences

Abstract

Six function injection models in the magnetosphere are optimized. The minimum of the functional (least squares of the difference between experimental data and models) by different initial coefficient values of the studied mathematical models are found. Some examples of the model yield one minimum with the optimal coefficients.

Introduction

The carried out research on function injection is one of the main tasks of the International Programme STEP (Solar-Terrestrial Energy Programme). The thorough study of this problem is of great importance in the present decade (1995-2005; 23rd Solar cycle). The Polish astronomer Kopetckiy has qualified this decade as a "dangerous decade" due to the fact that, during it, an extremely high geomagnetic activity is expected.

Having in mind this fact, we optimized six existing models of function injection F, described in literature, [Feldstein et all., 1990, 1989, Dremuhyna et all., 1990, Ivanova P., 1992, Murayama, 1986, Bargadze, 1986, Akasofu, 1981], using one of the numerical methods, namely the simplex method (well known in experiment planning).

Models of the function injection F have been made by a lot of authors. For example, in [Feldstein et all., 1990], linear regression equations for a are obtained, which connect the velocity of entering energy to the ring current with various combinations of geoeffective parameters of the Solar Wind (SW) and the Interplanetary Magnetic Field (IMF). The highest correlation coefficient is equal to 0.8 and it is characteristic of the correlation between the magnetic field of the ring current of the function injection in the magnetosphere F_{exp} calculated by ground observations and its model F_{mod}.

Estimation method

We have studied six models of function injection F [Feldstein et all., 1990, 1989, Murayama T., 1986, Bargadze L. F. et all., 1986, Akasofu S. I., 1981], which are shown on Table No 1, where x_1, x_2, x_3 are their coefficients. SW and IMF take part in the models. The conditional designations are V and D - the velocity and the density of the SW. B, By, Bz are the module, the azimuthal and the vertical component of the IMF, ε is the power function of Akasofu and τ is the ring current decay constant.

We have improved the models by optimizing their coefficients. For this task we used the simplex method [Nelder J.A. et all., 1964] because of the simplicity and synonymy of its mechanism:
Let's take functional (1)

(1) $U=\sum_{i=1}^{N}(DR-DRM)^2$, where DR are the experimental values of the ring current, where DRM is the mathematical expression of the model M=1, 2, 3, 4, 5 and 6 respectively. M stands for the number of the optimized model.

The essence of the method lies in the fact that we make a random simplex (a body with N+1 pecks, k=1, 2,..., N+1, N are the parameters) of the computed value of functional U.

Further it changes under the influence of three operations:

a) reflection $P^*=(1-\alpha)P-\alpha P_k$, where $\alpha\in(0,1)$, P_k are the pecks of the simplex, k=1,...,N+1 ; $U_h=\max(U_k)$ for P_h, where U_h is the maximal value of the functional in pecks P_k. P is the central point of the simplex, α is a reflection coefficient, P_l is the simplex peck with minimal value of the functional U or we have the condition $U_L=\min(U_k)$ for P_L.

b) contraction $P^{**}=\beta P^*+(1-\beta)P$, where $\beta\in(0,1)$ is the contraction coefficient.

c) extension $P^{**}=\gamma P^*+(1-\gamma)P$, where $\gamma\in(0,1)$ is the simplex extension coefficient and P is its center. The simplex goes in the global minimum of the functional U with these operations, where its pecks are in one point, which gives the optimal values of our parameters.

We consider DRM-ring current for the investigation models in every iteration by the folowing expression:

$DRMj = (2\,FM_{j-1}+DRM_{j-1})[2-(1/\tau_{j-1})]/[2+(1/\tau_{j-1})]$

Further the consideration procedure goes to (1). The iterational process continues to the accuracye that we are expecting e. g. $U = 0,1.10^{-2}$ in our case.

Results

The results and the optimization proceses are shown in tables No 1, 2, 3 and 4. The experimental values for DR-ring current are from SSC 27 August 1978 14 UT , 30 August 1978 2UT and 23 March 1969 14UT.

On Table No 1 the investigation models are given. Given three coefficients are x_1, x_2 and x_3 , the values of which we can see in Table No 4. The value of the funcional U is shown in the last column of Table No 4 , from which the significant improvement of the studied models is seen. In all models, the value of the functional U is equal to 10^5, but in the ones obtained using a new coefficient the value of U is 10^{-2}.

Therefore, the obtained models are significantly improved and specified and they model the ring current function injection in the magnetosphere with really higher accuracy. Another contribution of the present studies is in the effective application of the optimization methods in this sphere of the space physics.

Table N^0 3 illustrates the results of the method. All examples begin from different initial values of the parameters. In the end of the optimization they yield the same value for the point in which the simplex is contracted.

This represents the solution of the task.

Conclusions

From the results we can draw the following conclusions:

1. Using the algorithm and program suggested in this paper, all numerical models of the function injection F in the magnetosphere producing the magnetic variations on the Earth's surface can be optimized.
2. The optimal models produce the best mathematical approximation of F_{exp} by F_{mod}.
3. The new models improve the coefficients of the correlation r between F_{exp} and F_{mod} (for example, $r_1 = 0,91$ $r_{1\ opt} = 0,97$ by F_1).

The author would like to express her gratitude to Prof. Dr. Feldshtein for the discussions and the analysis of the results, due to which this task has been solved successfully.

Table 1
Optimization models
$F1=x1.10^{-3}B_zV + x2$; if $B_z. V<1$ mV/m and $F1==-x3.10^{3}(V-300)$; if $B_z.V>-1$ mV/m;
$F2=-x1.B_T.V.\sin^2(Q/2).10^{-3} - x2$ if $B_T:V.\sin^2(\theta/2).10^{-3}>0,1$ mV/m, $F2=-x3.(V-300).10^{-3}$ if $B_T .V.\sin^2(\theta/2).10^{-3} .10^{-3}<0,1$ mV/m; where $\Theta=\mathrm{arcth}\ B_y/B_z$; $B_T =(B_z^2+B_y^2)^{1/2}$
$F3=-x1.10^{-6}.F_{mur} - x2$; if $F_{mur}>10^{6}$ $F3=-x3(V-300).10^{-3}$; if $B_z>0$ where $F_{mur}=B_s^{1,09}.V^{2,06}.D^{0,38}$; where $B_s=B_z<0$. D is density
$F4=-x1.10^{-3}.F_{bar} - x2$; where $F_{bar}=(D.V^2)^{1/6}.V.B_T.\sin^4(0 /2)$; $B_T=(B_z^2+B_y^2)^{1/2}$; $\theta=\mathrm{arctg}(B_y/B_z)$
$F5=-x1.10^{-18}\varepsilon - x2$; where $\varepsilon=2.10^{14}.B^2.V.\sin^4(\Theta/2)$;
$F6=x1.V.B_z.10^{-3}$; if $B_z<0$; and $(B_z+\sigma)<0$; $F6=x2.V.(B_z-\sigma)/2).10^{-3}$; if $B_z<0$ and $(B_z+\sigma)>0$; $F6=x2.V((B_z-\sigma)/2).10^{-3}$; if $B_z<0$ and $(B_z-\sigma)<0$; $F6=x3$; if $(B_z-\sigma) >0$; $B_z>0$; σ - dispersion of the IMF V, D, Bx, By, Bz - parameters of the SW and IMF.

Table 2
Optimal models
$F1=8,8.10^{-3}B_zV - 16$; if $B_zV<1$ mV/m and $F1=68,0.(V - 300).),002$; if $B_zV> -1$ mV;
$F2=-10,3.B_T.V.\sin^2(Q/2).10^{-3}+5,0$; if $B_TV\sin^2(\theta/2).10^{-3}>0.1$ mV/m; $F2=113.(V-300).10^{-3}$; if $B^TV\sin^2(0/2).10^{-3}<0,1$ mV/m.
$F3=-10,3.10^{6}.F_{mur}+5,1$; if $F_{umr}>10^{6}$ $F3=112.(V-300).10^{-3}$; if $B_z>0$ $F_{mur}=B_s^{1,09}.V^{2,06}.D^{0,38}$
$F4=-1,2.10^{-3}.F_{Bar}-30,4$; $F_{Bar}=(DV\ )VB\ \sin(4Q/2)$
$F5=-2,2.\varepsilon.10^{-4}+9,7$; $\varepsilon=2.10^{14}.B^2.V.\sin^4(Q/2)$
$F6=10,7.V.B_z.10^{-3}$; if $B_z<0$; and $(B_z+\sigma)<0$; $F6=9,1.V.((B_z-\sigma)/2).10^{-3}$; if $B_z<0$; and $(B_z+\sigma)>0$; $F6=9,1.V.((B_z-\sigma)/2).10^{-3}$; if $B_z<0$; and $(B_z-\sigma)<0$; $F6=0$; $(B_z-\sigma)>0$ and $B_z>0$.

Table 3

Examples, illustrating the optimization process:
initial and optimal values of the model coefficients

	x1	x2	x3	U
Initial values example 1 for M1	10,9	7,9	14,5	$0,27.10^{4}$
Initial values example 2 for M1	10,0	0,8	13,5	$0,5.10^{4}$
Initial values example 3 for M1				
Optimal values for all three examples	8,8	-16,0	-68,0	$0,3.10^{-2}$
Initial values example 1 for M2	19,4	0,4	14,4	$0,46.10^{5}$
Initial values example 2 for M2	15,0	0,8	13,0	$0,5.10^{5}$
Initial values example 3 for M2	19,0	1,0	15,0	$0,15.10^{6}$
Optimal values for all three examples	10,3	-5,0	-113,0	$0,1.10^{-1}$
Initial values example 1 for M3	5,8	0,5	14,5	$0,1.10^{5}$
Initial values example 2 for M3	5,0	0,8	13,0	$0,3.10^{5}$
Initial values example 3 for M3	4,0	1,0	14,0	$0,5.10^{5}$
Initial values example 4 for M3	4,4	1,5	15,0	$0,6.10^{5}$
Optimal values for all three examples	10,3	-5,1	-112,0	$0,3.10^{-2}$
Initial values example 1 for M4	6,4	7,4		$0,9.10^{5}$
Initial values example 2 for M4	5,0	4,8		$0,7.10^{5}$
Initial values example 3 for M4	4,0	5,0		$0,2.10^{5}$
Initial values example 4 for M4	8,5	4,0		$0,4.10^{6}$
Optimal values for all three examples	1,2	30,0		$0,4.10^{-1}$
Initial values example 1 for M5	6,4	7,4		$0,8.10^{6}$

Initial values example 2 for M5	5,0	4,8		$0{,}1.10^{7}$
Initial values example 3 for M5	4,0	5,0		$0{,}7.10^{6}$
Initial values example 4 for M5	8,5	4,0		$0{,}4.10^{7}$
Optimal values for all three examples	2,2	-2,7		$0{,}2.10^{-1}$
Initial values example 1 for M6	6,8	7,5		$7{,}5.10^{4}$
Initial values example 2 for M6	5,9	5,0		$0{,}2.10^{5}$
Initial values example 3 for M6	5,4	5,3		$0{,}3.10^{5}$
Initial values example 4 for M6	10,4	4,5		$0{,}1.10^{5}$
Optimal values for all three examples	10,7	9,1		$0{,}3.10^{-1}$

Table 4

Coefficients of the old and the new (optimal) models

Old coeff.	x1	x2	x3	U
M1	8,9	7,0	14,1	$0{,}3.10^{4}$
M2	19,8	0,6	14,1	$0{,}5.10^{5}$
M3	3,7	0,4	14,1	$0{,}3.10^{5}$
M4	3,8	2,8	-	$0{,}6.10^{5}$
M5	7,2	3,1	-	$0{,}4.10^{5}$
M6	5,4	5,4	-	$0{,}2.10^{5}$
New (optimal) coefficient				
M1	8,8	-16,0	-68,0	$0{,}3.10^{-2}$
M2	10,3	-5,1	112,0	$0{,}1.10^{-1}$
M3	10,3	-5,1	112,0	$0{,}7.10^{-2}$
M4	1,2	30,5	-	$0{,}5.10^{-1}$
M5	2,2	9,7	-	$0{,}2.10^{-1}$
M6	10,7	9,1	-	$0{,}3.10^{-1}$

References

1. Feldstein Ya. I., Ya. Pisarski, A. Prigancova, P. Ivanova. The ring current injection function and its relation to interplanetary parameters, Studio geophys. et geod., 34 (1990), p.129-136.
2. Дремухина Л.А., П.К. Иванова, Я.И. Фельдштейн. Развитие кольцевога тока и его моделирование на обсерватории Панагюриште, Геомаг. И астроном., т.30, No 5, (1990), стр.862-865.
3. P. K. Ivanova. Ring current and parameters of the Solar Wind, Compt. rend. Bulg. Acad. Sci., v.45, No 9, 1992, p. 45-47.
4. Nelder J. A., R. Mead, Compt. J., v. 7, 1964, 303.
5. Feldstein Ya. I., V. Yu. Pisarskij, N. M. Rudneva, A. Prigancova, Ring current and interplanetary medium parameters, Studio geoph. et geodet., 33 (1989), p. 61-80,
6. Murayama T. Coupling function between the solar wind and the Dst-index in "Solar wind-magnetosphere coupling". Terrapub., Tokio, 1986, 119.
7. Bargadze L. F., R. L. McPerron, D. N. Baker, Solar wind magnetosphere energy input functions. "Solar wind- magnetosphere coupling", Terrapub., Tokio, 1986, p.101.
8. Akasofu S. I., Prediction of development of geomagnetic storms using the solar wind-magnetosphere energy coupling function ε, Plan. Space Sci., 29 (1981), p.1151.

ОПТИМИЗАЦИЯ НА ФУНКЦИОНАЛНИ ИНЖЕКЦИОННИ МОДЕЛИ В МАГНИТОСФЕРАТА С ПОМОЩТА НА СИМПЛЕКС МЕТОДА

Павлина Иванова

Резюме

Оптимизирани са шест инжекционни модела в магнитосферата. Използвайки различни стойности на началните коефициенти на изследваните математически модели е намерен минимума на функционала (метод на най-малките квадрати на разликата между експерименталните и моделните данни). Някои примери на модела дават един минимум с оптимални коефициенти.

Bulgarian Academy of Sciences. Space Research Institute
Aerospace Research in Bulgaria. 17. 2003. Sofia

OBSERVATIONS OF OPTICAL EMISSIONS AND MAGNETIC FIELDS ABOARD OF INTERBALL-2 SATELLITE

Kunyo Palazov, Stefan Spasov, Alexander Bochev, Petar Baynov

Solar-Terrestrial Influences Laboratory-BAS

Abstract

In the work, the Bulgarian experiments aboard of the INTERBALL-Auroral probe satellites, namely the investigation of optical emissions in the ultra violet (UV) range (UVSIPS spectrometer) and the magnetic field experiment (IMAP-3 magnetometer), are described. To ilustrate the common analysis of data from both units, the observations during the October 19, 1996 geomagnetic storm are analised.

The Bulgarian experiments aboard of the INTERBALL-Auroral probe satellite (briefly INTERBALL-2) include investigations of optical emissions in the UV range (UVSIPS spectrometer) and the magnetic field (IMAP-3 magnetometer). Optical emissions are closely related to precipitated electrons and ions, which ionize high atmosphere. Magnetic field disturbances are indicative of field-aligned currents which are generated in the magnetosphere boundary region; their closure currents flow in the ionosphere.

The physical bases of optical and UV-diagnostics of auroral ionosphere is as follows: auroral electrons and ions of various energies, which precipitate from the magnetosphere, as well as the secondary electrons produced by them, excite atoms, molecules and ions in the ambient media which begin to emit light quanta. By measuring the intensity of auroral emission distribution in the visible (VIS), UV and X-ray spectrum regions, or at least in only one of them, and using the relation between emission intensity and differential energy distribution of precipitating charge particles, we may obtain the distributions of precipitating electrons' characteristic energy Eo and energy flux Qe (Frank et al., 1981).

The major advantage of space experiments is the possibility to measure these parameters on large area, determined by the unit's view field and the satellite's height. Measurements of emission intensity distribution in the vacuum UV region have advantages compared to measurements in the VIS range, as UV –radiation is absorbed by the underlying layer of molecular oxygen in the region of Schumann-Runge continuum. This atmospheric effect creates beneficial natural conditions to observe aurora from satellite in the dayside of the Earth. The contrast of the emission auroral intensity at the background of the dayglow of the upper atmosphere varies with the different spectral lines and, as a rule, exceeds their double value (Kuzmin et al., 1985). This is an advantage of the UV method, which became a decisive factor for implementation of the UVSIPS spectrometer aboard of INTERBALL-2.

The INTERBALL project is an inherent part of a large cooperation between several space missions in the framework of the International Solar-Terrestrial Physics Program. The INTERBALL-2 was launched in 1996 to an orbit with apogee (perigee) 20,000 (800) km respectively, inclination 65 deg and period 6 hours. The spectrometer UVSIPS aboard of the INTERBALL-2 was designed to measure in three spectral intervals centred to wavelengths 1304 A°, 1356 A° and 1493 A°. The spectrometer apparatus function is 32 A°, which is an important advantage of the experiment. The first channel measures the most intensive emission of atomic oxygen (triplet 1302-04-06 A°). The second spectral interval of the spectrometer (channel 2) is centred to wavelength 1356 A° (line of atomic oxygen spin-forbidden doublet with wavelength 1356-9 A°), excited in the polar oval. The doublet of the atomic nitrogen 1492,6-1495 A°, radiated from level N1(2p) gets into the third spectral interval (channel 3), centred to wavelength 1493 A°.

The spectrometer was mounted on the outside surface of the satellite. Due to the rotation of the spacecraft, period 120 sec, the spectrometer scans in the rotational plane, perpendicular to the direction of the Sun. Based on the location and attitude of the satellite, a construction was designed in order to direct the device towards the footprint of the local magnetic field line 120 km above the Earth's surface. The control of the operation mode followed a cyclogram, fixed by radio commands. The UVSIPS performs 36 measurements (36 pixels) for a given exposition which takes 0.15-0.6 sec and sends 20 bytes per pixel, i.e. 36 x 20 = 720 bytes stored in 6 blocks of digital arrays.

The flux-gate magnetometer IMAP-3 measures the three components of the magnetic field along the satellite's construction axes continuously throughout the whole orbit. The device was designed and manufactured by a proprietary technology in the Scientific Industrial Laboratory for Special Sensors and Systems ("SDS" Lab's), Bulgarian Academy of Sciences (BAS), Sofia, Bulgaria, and the Solar-Terrestrial Influences Laboratory (STIL) - BAS, Sofia, Bulgaria (Arshinkov et al., 1985). The magnetometer data is transmitted by the satellite telemetry system with a sampling rate of 1 vector per 3 sec or 8 vectors/sec depending on the operation mode, which can be controlled by ground commands. Upon its receiving at the ground stations, telemetry data is distributed via Internet by the IKI- Moscow to the respective P.I.s.

It is known that under small perturbations, the spacecraft spin axis is misaligned from the nominal rotation axis. That is why data processing, in particular UVSIPS and IMAP-3, needs adequate attitude information provided by the satellite systems. Apart from the data from the scientific equipment, the following attitude parameters are also distributed:

(1) Coefficients A1, A2, A3, A4 and B1, B2, B3, B4 which define the ellipse along which the kinematics moment rotates with respect to the nominal axis of rotation (towards the Sun); *w*1 – angular velocity of the satellite rotation around the nominal axis, period ~ 120 sec; *w*2 – the angular velocity of rotation of the angular momentum relative to the satellite (this angular momentum relative to the satellite is moving along the surface close to the elliptic cone), period ~ 68 sec.

(2) "Top of spin" the time instance when the direction to the North Pole of the ecliptic passes through the XY plane of the satellite.

Based on both the geographic position of the satellite and attitude data, foot point of local magnetic field lines, and view field of UVSIPS with respect to the local magnetic field line, the components of the measured magnetic field in field-aligned coordinates and other geophysical coordinate systems are determined.

To illustrate the common analysis of the data from both units, let us examine a geomagnetic storm registered on 19.10.1996 (orbit 216 - Fig.3). UFSIPS has performed a scanning at 22:49 UT (Fig.1,2,3) with registered intensive emissions. The emission profile displays a high intensity zone in 1304 A° line with width of 3 sec, reaching more than 10 KR. (Fig.1). This part of the profile is like a chord through the oval, approximately 2,000 km long (Fig.3). By geometric considerations it can be said that this arc is at least 150 km wide. The profile analysis leads to the conclusion that at equatorial direction from the arc there is a weak glow halo whose width is of the same order. According to the expectations, such intensities are possible with precipitating particle energy fluxes with energy of about 50-100 erg/cm^2, observed during polar aurora.

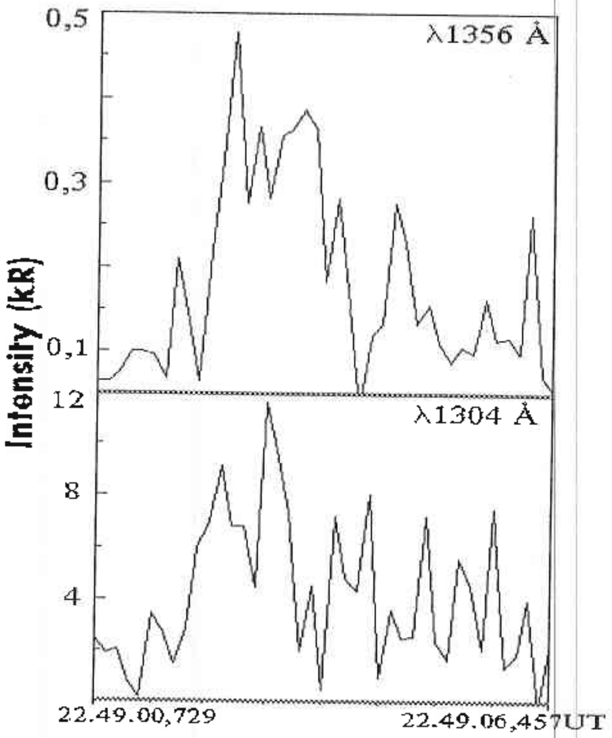

Fig.1. Intensity of lines 1304 A° and 1356 A°

The magnetogram begins with a calm interval (Fig. 4) which continues until 22:45 UT. The magnetic disturbances observed after that may be connected with current layers crossing. At the near-equator portion, from 22:45 UT until 22:50 UT, changes in the field up to 10 nT can be seen which might be treated as small-scale layers. The minimum width of such a structure may be of the order of 10 km. In the near-pole half from 22:50 UT until 22:56 UT, the field change is two times greater which is connected with a large-scale current structure crossing. The width of such a current layer is about 130 km reduced to atmospheric altitudes (at the footpoint). A comparison is made of the optical emissions measurements and the magnetic field. At the moment of optical emissions scanning, the satellite passed through the main zone of the field-aligned current layers. Their physical carriers are mainly low-energy (E~1 KeV) electrons. These particles degrade by energy at altitudes, higher than the atmospheric altitude, generating the observed optical effects. Here, we pay attention that a little before the encounter with this region, i.e. at 22:45-22:46 UT an increase of the magnetic field is observed of the order of several nT, corresponding to a re-stricted current structure. It is namely this interval that corresponds to the intensive emissions zone. We conclude that a localized discrete auroral arc was observed at the poleward edge of the auroral oval and that the main current region occurred polward of it. Our observations support the view that field-aligned current region in some cases can be displaced poleward from the auroral oval discrete arcs in the night-morning sector of the auroral oval.

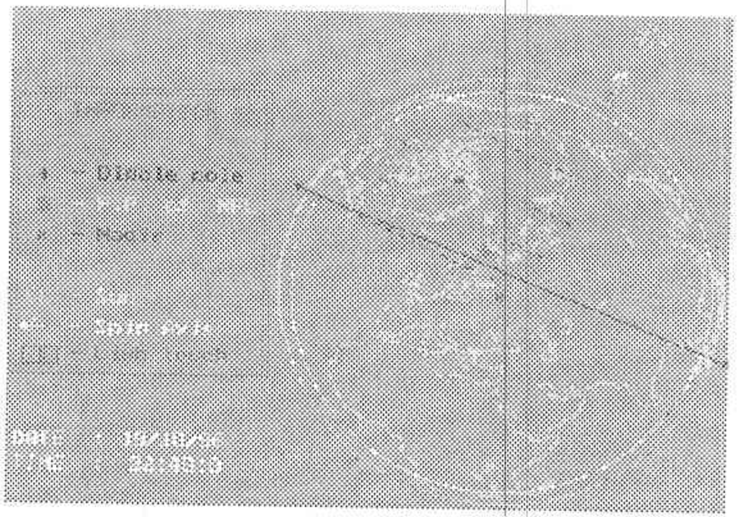

Fig.2. The northern hemisphere seen by the satellite at the moment of measurement. The symbols +, • , and Ò correspond to the dipole pole, the northern geographical pole, the point of intersection of the vector to the Earth centre, and the footpoint of the magnetic force line where the satellite is at that moment. The auroral oval is shown for forced geomagnetic conditions with index Kp=5+. The position of the terminator shows that the larger part of the auroral oval is situated in the shade. The position of the scan projection is marked by two arrow vectors. The view field of UFSIPS crosses the auroral oval through the chord in such a way that the intersection goes from the morning to the night section. Because of the deviation of the axis X-satellite-Sun, the footpoint occurred in the morning section out of the field of view. The coordinates of the footpoint are (at 22.49.03 UT for H = 150 km) 74.3° latitude, 32.7° longitude, MLT=3.04 h (Fig.3), H shade = 647 km.

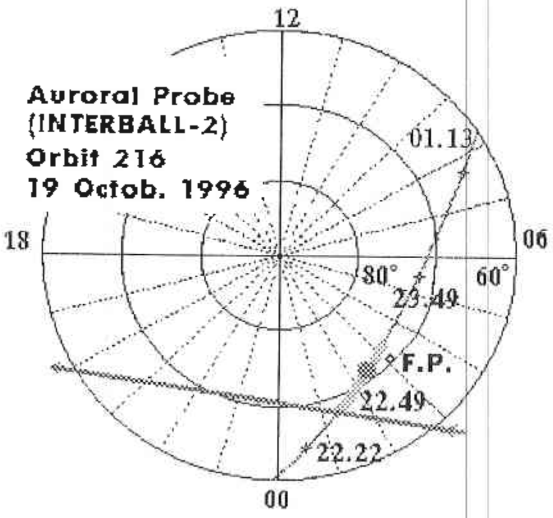

Fig.3. IMAP-3 magnetogram. It begins with a calm interval until 22:45 UT. The disturbances observed after that may be related with current layers crossing. At the near-equator half from 22:45 UT until 22:50 UT, changes in the field up to 10 nT can be seen which might be treated as small-scale layers. At 22:45-22:46 UT, an increase of the magnetic field is observed of the order of several nT. It is namely this interval that corresponds to the intense emissions zone. The main field-aligned current region is poleward (22:50 –22:56 UT).

INTERBALL-2 IMAP-3 19.10.1996

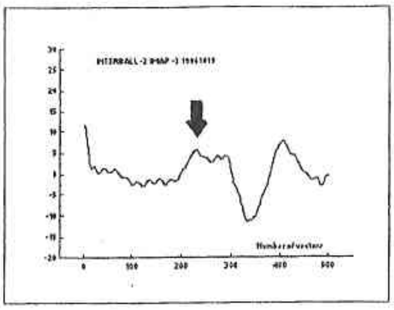

Vector No	0	100	200	300	400	500
UT	22:35:00	22:40:00	22:44:59	22:49:59	22:54:59	23:00:00

Fig.4.

References

1. Frannk L.A., J.D. Craven, K.L. Ackerson, M.R. English, E.H. Eather, R.A. Carovillano, Global auroral imaging instrumentation for the Dynamics Explorer mission, *Spce Sci. Instr.*, 5, 1981, 369-393.
2. Kuzmin A.K., T.V. Fomicheva, A.V. Kondabarov, K.N. Chikov, S.A. Dubkovski, V.V. Good, V.N. Krasavtsev, K.D. Lozev, A.N. Sandakov, I. Nedkov, K. Palazov, N. Petkov, S. Spasov, R. Verner, V. Ivanov and Sergienko, UV-spectrometer in INTERBALL project to map ionospheric characteristics in the magnetic field line footpoint from the satellite Auroral Probe. *INTERBALL-Mission and payload*, Russ.Sp.Agency (IKI) and Fr.Sp.Agancy (CNES), May 1995, 401-409.
3. Arshinkov I.S., Z.N. Zhuzgov, A. Bochev, E. Zakharieva, V. Velev, V.A. Styazhkin, P. Baynov and N. Abadjiev, Magnetic field experiment in the INTERBALL project (experiment IMAP). *INTERBALL-Mission and payload*, Russ.Sp.Agency (IKI) and Fr.Sp.Agancy (CNES), May 1995, 222-228.

НАБЛЮДЕНИЯ НА ОПТИЧНИ ЕМИСИИ И МАГНИТНИ ПОЛЕТА НА БОРДА НА СПЪТНИКА ИНТЕРБОЛ-2

Куньо Палазов, Стефан Спасов, Александър Бочев, Петър Байнов

Резюме

В работата е дадено кратко описание на двата български експеримента на борда на спътника ИНТЕРБОЛ-Авроралнa сонда, а именно: изследване на оптичните емисии в ултравиолетовия диапазон на светлината (спектрометър УВСИПС) и изследване на магнитного поле (магнитометър ИМАП-3). За илюстрация на съвместния анализ е направен анализ на данни от двата уреда по време на геомагнитната буря от 19 октомври 1996 год.

Bulgarian Academy of Sciences. Space Research Institute
Aerospace Research in Bulgaria. 17. 2003. Sofia

BRIGHT SPOTS SELECTION IN TV-IMAGES

Valentina Tzekova, Emil Tzekov

Space Research Institute-Bulgarian Academy of Sciences

Abstract

The aim of the present work is to propose a technique for separation of bright spots in TV-image background at low object signal to background signal ratio. It is shown that selection can be effected based on the front duration, using a differentiating circuit.

In television control systems it is necessary to separate some objects from the surrounding background. Sometimes, they represent bright points in the television image. Quite often, these objects are separated by the method of amplitude selection. The method is accomplished rather easily, but it needs a high object-signal to background-signal ratio.

In the paper, an approach is suggested for selection of bright point objects in television images with small object-signal to background-signal ratio, even when this ratio is less than 1. The object selection is based on three parameters and can be accomplished quite easily.

According to [1], the television image is described by function I = f (x, y), which expresses the image brightness in a point with coordinates (x, y). In television systems, brightness is represented by the amplitude of the videosignal $u_1(t)$.

If in the television transmitter, progressive monolayer scanning is used, the videosignal of one series of the monolayer scanning may contain pulses from different bright objects and look as shown in Fig.1, where:

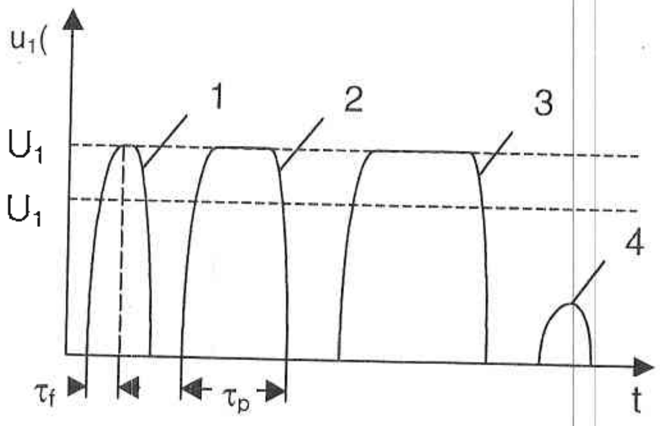

Fig. 1

1 - bright point object; 2 - object with fuzzy fronts; 3 – large-size object; 4 - point object of small brightness.

Let us assume that the pulse is obtained from a bright point object given its duration τ_p, front duration τ_f and amplitude U_p, satisfy the following conditions:

$$\begin{aligned} &\tau_{pmin}<\tau_p<\tau_{pmax}, \\ &\tau_{fmin} < \tau_f < \tau_{fmax}, \\ &U_p \geq U_{pmin}. \end{aligned} \tag{1}$$

According to conditions (1), bright point objects may be selected by applying the flow chart shown in Fig.2, where: 1 – front duration selector; 2 - amplitude selector; 3 – pulse duration selector.

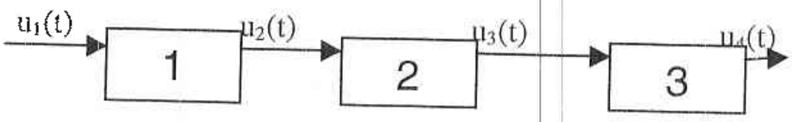

Fig. 2

The assumed sequence of parameter sign inspection was determined by the following reasons. In the process of selection by some specific parameter, the input signal is converted and part of the information contained in it will be lost. Since front duration selection is the most difficult, it is reasonable that signal processing starts with it. In contrast to it, pulse duration selection does not require information about the signal's amplitude, therefore it can be done in the end of signal processing.

Front duration signal selection can be most easily accomplished by a simple differential RC circuit. Let us define the conditions for this selection with predetermined time constant of the RC circuit and videopulse front shape. With practically sufficient accuracy it may be assumed that the videopulse fronts have exponential form:

(2) $$u_1(t) = U_1(1\ u_1(t)\ - e^{-t/\tau f}) \text{ when } t \geq 0.$$

The output signal of RC cell will be:

(3) $$u_2(t) = U_1(e^{-t/\tau f} - e^{-\beta t/\tau f}) / (\beta - 1),$$

where: $\beta = \tau_f / RC \neq 1$.

With $\beta = 1$, the output signal is determined by the formula:

(4) $$u_2(t) = U_1\, e^{-t/\tau f}\, t / \tau_f \text{ when } t \geq 0.$$

Function $u_2(t)$ has maximum at:

(5) $$t = \tau_f \ln\beta / (\beta - 1)\ ,\ \beta \neq 1 \text{ and}$$

(6) $$t = \tau_\phi\ ,\ \text{ when } \beta = 1.$$

From (3), (4), (5) and (6), we shall obtain the amplitude of output signal:

(7) $$U_2 = U_1(e^{-\ln\beta/(\beta-1)} - e^{-\beta\ln\beta/(\beta-1)}) / (\beta-1),\ \beta \neq 1 \text{ and}$$

(8) $$U_2 = U_1 / e \approx 0{,}37U_1\ ,\ \beta = 1.$$

The dependence of ratio U_2/U_1 on β is shown in Fig.3.

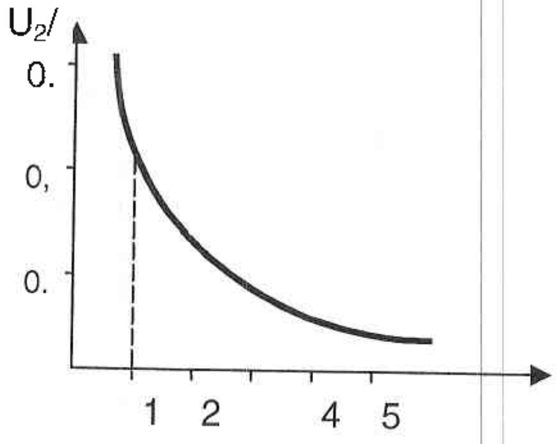

Fig. 3

Let us denote the background signals maximum amplitude by U_{1f}. For these signals, $\beta_f > \beta_{max} = \tau_{fmax} / RC \neq 1$.

Then, when the background signal is fed up, the output signal of the differential circuit will have the amplitude:

(9) $$U_{2f} < U_{1f} (e^{-\ln\beta max/(\beta max-1)} - e^{-\beta max \ln\beta max/(\beta max-1)}) / (\beta_{max} - 1) = k_f U_{1f} .$$

From inequality (9) it is seen, that the front duration selection task is reduced to the easy-to-perform amplitude selection of signals at the output of the differential circuit after the rule:

(10) $$\tau_f \leq \tau_{f\,Max} \text{ , при } U_2 \leq k_f U_{1f} .$$

Let us assume that $RC = \tau_{fMin}$, i.e $\beta_{min} = 1$ and let us find the minimum amplitude U_{1min} of a pulse with front τ_{fmin}, providing for satisfaction of condition (10). According to (8) and (10), we obtain:

$$U_{2\,min} = U_{1min} / e = k_f U_{1f}, \text{ or}$$
$$U_{1\,min} = k_f e U_{1f}.$$

From these equations it is possible to find the minimum object-signal to background-signal ratio for selection of bright point objects:

(11) $$U_{1\,min} / U_{1f} = k_f e.$$

It may be shown that, by increasing β_{min}, the minimal object-signal to background-signal ratio slowly decreases, but simultaneously with it, the output signal amplitude decreases, too. To obtain a large enough amplitude U_2, it is reasonable to assume $RC = \tau_{f\ min}$. Then, the minimal signal/background ratio will be:

$$U_{1\,min} / U_{1f} = 0{,}68 \quad \text{with} \quad \beta_{max} = 2$$
and
$$U_{1\,min} / U_{1f} = 0{,}53 \quad \text{with} \quad \beta_{max} = 3.$$

It should be noted that the signals from back and front fronts of the videopulse have different polarity, which should be accounted for in applying rule (10).

In the cases where the minimum amplitude U_0 of the bright point object videopulse should be greater than U_{1min}, rule (10) will change:

(12) $$\tau_f \leq \tau_{fmax} \quad \text{and} \quad U_0 > U_1 \quad \text{at} \quad U_2 \geq U_0 / e.$$

Thus, rule (12) provides for a simultaneous selection by front duration and by amplitude.

Videopulse duration selection is no particular challenge; it may be accomplished by any of the methods described in literature.

With satisfaction of condition (1), except for the bright point objects, bright vertical or slanting lines in a TV image may be also selected. The selection of such objects is a rather difficult task, necessitating additional pulse analysis throughout several adjacent series of the monolayer scanning.

Conclusions:

1. Conditions for selection of bright point objects by videopulse within one series of monolayer scanning are formulated.
2. It is shown that the front duration selection task may be accomplished using a differential circuit.
3. Rules for selection of bright point objects are proposed.
4. It is shown that bright point objects can be selected with a signal/background less than 1.

References

1. Розенфельд А. Т. Разпознавание и обработка изображений, "Мир", 1972.

СЕЛЕКТИРАНЕ НА ЯРКИ ТОЧКОВИ ОБЕКТИ В ТЕЛЕВИЗИОННО ИЗОБРАЖЕНИЕ

Валентина Цекова, Емил Цеков

Резюме

Целта на настоящата работа е да се предложи начин за отделяне на ярки точкови обекти от околния фон в телевизионното изображение при малки отношения на сигнала от обекта към сигнала от фона. Показано е, че селекцията по продължителност на фронтовете може да се извърши чрез използването на диференцираща верига.

Bulgarian Academy of Sciences. Space Research Institute
Aerospace Research in Bulgaria. 17.2003. Sofia

AUTOMATIC CONTROL OF VIDICON SENSITIVITY IN THE TELEVISION SENSOR OF AEROSPACE CONTROL SYSTEMS

Valentina Tsekova, Emil Tsekov, Georgi Sotirov

Space Research Institute - Bulgarian Academy of Sciences

Abstract

In the present work a flow chart of vidicon sensitivity automatic control in TV-sensor is proposed, which provides to achieve the maximal possible accuracy in identification of bright point objects. The major system parameters are defined which ensure system stability and speed.

In television coordinators determining the coordinates of bright point objects, the useful information is contained only in the videosignal they produce. The other signals are noise signals preventing to achieve maximum accuracy in determining the objects' coordinates. In application TV cameras, with a view to more precisely transmit brightness relations, vidicon sensitivity is regulated based

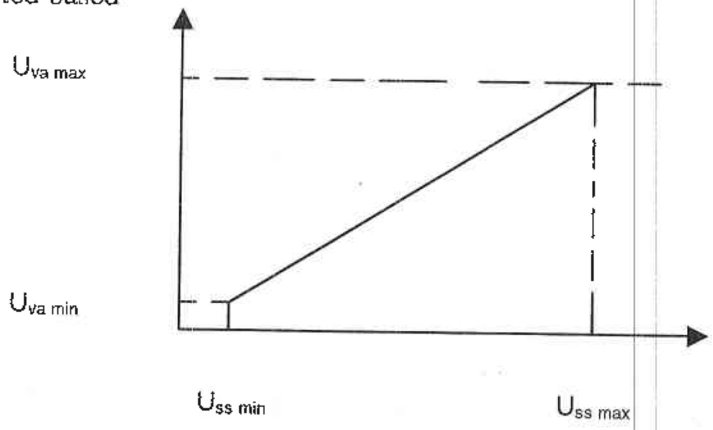

Fig. 1

on the average illumination of the vidicon target. In this case, the signals of the brightest objects are restricted, i.e. with this type of automatic control of vidicon sensitivity (ACS), the useful-signal to noise-signal ratio decreases.

Therefore, it would be more reasonable if vidicon ACS in television coordinators was based not on the average target illumination, but on the maximal amplitude of the videosignal in each frame. Vidicon sensitivity in the working area is a linear function of the signal slice voltage U_{ss} as shown in Fig.1 [1]. Therefore, the maximal amplitude of the videosignal from the bright spot object may be preserved by changing U_{ss} depending on the vidicon's illumination E, as shown in Fig.2.

The ACS system may be synthesized after the flow chart shown in Fig.3, where 1 is the optical system projecting the object images on the vidicon target. The videosignal obtained at the output of vidicon 2 is amplified by videoamplifier 3 and and is fed to coordinator 4, where the coordinates of the bright point object are determined. From 3, the videosignal is fed to the peak detector 5, whose charge time constant is very small, as a result of which the output voltage reaches its maximum within a shorter time interval than the duration of the videosignal from the point object.

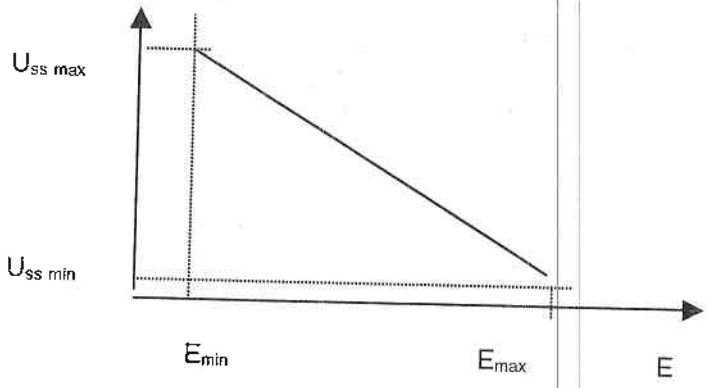

Fig. 2

Since the discharge time constant of peak detector T_{pd} is big enough, its voltage U_{pd} does not change essentially within one frame T_{fr}. This voltage is amplified in the direct-current amplifier 6 by the amplifying coefficient K_a

and is then averaged in the low-frequency filter 7, whose time constant T_f is big enough ($T_f >> T_{fr}$).

In the considered flow chart, the amplitude of the output voltage of the peak detector in a stable mode will be:

$$U_{pd} = U_{vid}K_{va}K_d. \qquad (1)$$

The voltage amplitude of the signal slice will be:

$$U_{ss} = U_{ss\,max} - U_{vid}K_{va}K_a K_d = U_{ss\,max} - U_{va}K_a K_d. \qquad (2)$$

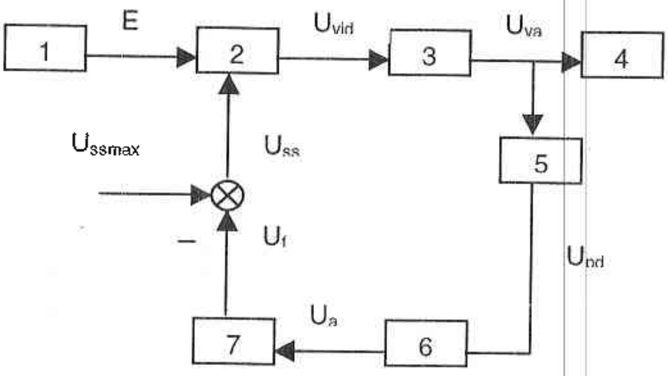

Fig. 3

From equality (2), the maximal amplifying coefficient of the direct-current amplifier in the ACS may be determined:

$$K_{a\,max} = (U_{ss\,max} - U_{ss\,min}) / K_d U_{va\,min}. \qquad (3)$$

In the cases where K_a is bigger than the coefficient obtained from formula (3), the ACS system will be unstable. Then, its oscillations could be removed provided only the time constant obtained from formula (15) is very big (2 - $3T_{fr}$). In this case, the system becomes so inert that it can not respond to possible rapid changes in the object's luminosity (e.g., changes within time interval 3 - $5T_{fr}$).

If the regulation characteristic of the television sensor (vidicon and video amplifier), shown in Fig.4 is assumed linear, that it can be written in the following way:

$$K = K_{min} + \alpha (U_{ss} - U_{ss\,min}), \tag{4}$$

where: K - the transmission coefficient of the television sensor;
α – the steepness of the control characteristics, and

$$\alpha = \mathrm{tg}\,\varphi = (K_{max} - K_{min}) / (U_{ss\,max} - U_{ss\,min}). \tag{5}$$

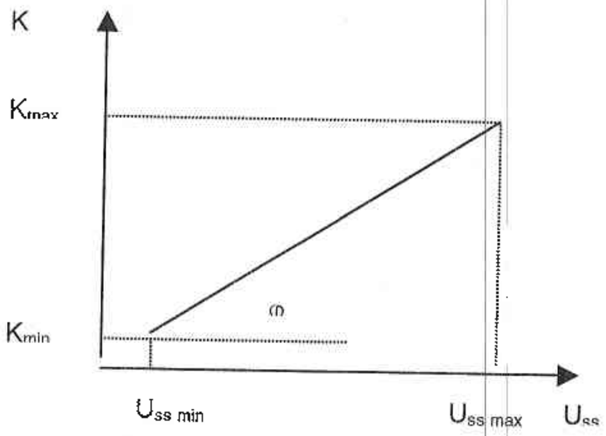

Fig. 4

Usually, the transmission band of the television sensor is much greater that the transmission band of the ACS. Therefore, it may be assumed that the amplitude U_{va} varies simultaneously with the change of the sensor amplifying coefficient, which is determined by U_{ss}, whose operating range is: $U_{ss\,min} < U_{ss} < U_{ss\,max}$.

In practice, in preliminary calculation, the following parameters should be assessed: the transmission coefficient of the television sensor, the range within which it should change, and the steepness of the control characteristics. Here, the following initial data is used: the possible change of illumination of the vidicon target by the bright point object (it should not exceed the illumination's work range, indicated in the vidicon certificate) and the range of voltage variation of the signal slice (also indicated in the vidicon certificate).

The output amplitude of the video amplifier will be:

(5) $$U_{va} = KE,$$

where E is the target illumination in lx. Therefore, the maximal and the minimal value of the transmission coefficient, accounting for the work of the ACS, will be:

(7) $$K_{max} = U_{va\,min} / E_{min},$$
(8) $$K_{min} = U_{va\,max} / E_{max}.$$

This coefficient will change within the range:

(9) $$\Delta K = K_{max} - K_{min} = (U_{va\,min}E_{max} - U_{va\,max}E_{min}) / E_{max}E_{min}$$

Provided the frame frequency is great enough, so that the ACS regulation time T_{reg} is much greater than the frame time, i.e. $T_{reg} >> T_{fr}$ [2], with changing the object's brightness, the voltage of the signal slice will be expressed as follows:

(10) $$U_{ss}(t) = U_{ss\,max} - K_aKEe^{-t/tpdd}(1 - e^{-tf}).$$

Since in television sensors the frame time is preset, the discharge time constants of peak detector and filter may be represented in the following way:

(11) $$t_{pdd} = aT_{fr}\ , \qquad t_f = bT_{fr},$$

where a and b are arbitrary positive constants.

From (10) and (11), the voltage variation of the signal slice corresponding to an illumination change of ΔE will be:

(12) $$\Delta U_{ss}(n) = K_aK\Delta Ee^{-n/a}(1 - e^{-n/B}) > 0,$$

where n = 1,2,3... is the number of frames upon change of illumination by ΔE.

The values of a and b are chosen by a compromise. The greater the value of a and the smaller the value of b, the more rapidly will U_{ss} achieve its stable value. With very great values of a the reactivity of the ACS system decreases, and with very small values of a, it becomes unstable, whereas within one frame, the following inequality is fulfilled:

(13) $$\Delta U_{ss} < K_d K_a \Delta U_{va}.$$

From (6) and (12) it follows that the following conditions must be satisfied:

(14) $$a < - 1/ \ln K_d,$$
(15) $$b > 1/ \ln(1 - K_d e^{1/a}).$$

So that the ACS system might preserve its stability and sufficient adaptivity.

Conclusion

1. A flow chart of the automatic control system of vidicon sensitivity at maximal illumination of the target is proposed. The system may be used in television coordinators to determine the coordinates of various space objects.
2. An analysis is made and the major system parameters are defined: transmission coefficient and time constants.

References

1. PHICIPS. Data Handbook, Electron tubes, 1975.
2. Гривицки Б. Х. Автоматические системы радиотехнических устройств, Госэнергоиздат, 1962.

АВТОМАТИЧНО РЕГУЛИРАНЕ НА ЧУВСТВИТЕЛНОСТТА НА ВИДИКОНА В ТЕЛЕВИЗИОНЕН ДАТЧИК НА АВИОКОСМИЧЕСКИ СИСТЕМИ ЗА УПРАВЛЕНИЕ

Валентина Цекова, Емил Цеков, Георги Сотиров

Резюме

В настоящата работа е предложена блокова схема на система за автоматично регулиране чувствителността на видикона в телевизионен датчик, която позволява достигане на максимална възможна точност при определяне на координатите на ярки точкови обекти. Определени са основните параметри на системата, които осигуряват нейната устойчивост и бързодействие.

Bulgarian Academy of Sciences. Space Research Institute
Aerospace Research in Bulgaria. 17.2003. Sofia

A VARIATIONAL PROBLEM FOR TIME OPTIMIZATION OF CUMULATIVE CHARGE FOR PSEUDOMETEORITE PARTICLES

Hristo Hristov, Viktor Baranov, Ivan Getsov***

Defence Advanced Researches Institute, Sofia, Bulgaria
**Tula State University, Tula, Russia*
***Vazov Engineering Plants, Sopot, Bulgaria*

Abstract

A variational problem with unconditional extremum for time maximization of forming shaped charge pseudometeoritical clouds is formulated. The maximal time action of pseudometeoritical clouds particles is used as input parameter. An Euler equation is derived and an intermediate integral for the varied parameter - the profile function of the inside lining is obtained.

The high performance and the small overall dimensions of cumulative charges used to form pseudometeorite particles combined with their low price make them a perspective means to test body robustness of various spacecraft in laboratory conditions. In this connection, a topical problem is studying the options for enhancing the efficiency of cumulative charges by optimizing the impact of the pseudometeorite cloud formed by them. One of the optimized parameters is the time of cloud impact on the craft's protection barrier. Here, two parameters are accounted for: the original deformation with the cumulative lining's collapse as well as the subsequent deformation with the cloud's movement, which enhances the adequacy of the selected physical model.

Using hydrodynamic cumulation theory [1], we shall analyze the metal lining's plane-radial scheme of explosive deformation for the cases where cumulative charge cloud is formed, whose geometry can be described by the following equations in a Cartesian coordinate system *y0x* [2]: $y=F(x)$;

$y = \Phi(x)$; $y = \varphi(x)$ and $y=f(x)$ for the body, charge and line couple, accordingly. All functions are continuous, smooth, the last two functions have positive first derivatives.

The following expression is known for the stress-load coefficient in a fixed charge section, as a function of charge geometry [1, 2]:

$$\beta = \beta(x) = \frac{o_1 F^2 \Phi 2 + o_2 F^2 \varphi^2 + o_3 \Phi^4 + o_4 \Phi^2 \varphi^2 + o_5 \varphi^4}{o_6 F^2 \varphi^2 + o_7 F^2 f^2 + o_8 \Phi^2 \varphi^2 + o_9 \Phi^2 f^2 + o_{10} \varphi^4 + o_{11} \varphi^2 f^2 + o_{12} f^4}$$

;

where $o_1, \ldots, o_{12}$ – some ratios of the densities of the body, explosive and lining materials.

Let us consider the original (with collapse) and the subsequent (with the cloud's movement) deformation of the lining - Fig.1. Points A and B launch an inside surface element of the lining $y=f(x)$ with length dx, to a distance x from the origin of the coordinate system (top of lining). The collapse velocities of this element's both ends are $W_0(x)$ and $W_0(x) + dW_0(x)$, accordingly. In time:

$$t_{AC} = \frac{f(x)}{W_0(x)}$$

point A reaches axis $0x$ and the element forms with axis $0x$ collapse angle $\alpha(x)$. The cumulative cloud's compactness and velocity depend on this angle's value [3]. For this time, B point is passes distance:

$$BB' = (t_{AC} - \frac{dx}{D})(W_0(x) + dW_0(x))$$

being apart from axis $0x$ by the distance:

$$B'C' = f + df - BB'$$

and forming angle $\alpha(x)$:

$$\alpha(x) = arctg\,\frac{B'C'}{dx}$$

where

$$t_{B'C'} = \frac{B'C'}{W_0(x) + dW_0(x)}.$$

With the element's full collapse the cut-off $C'K'$ is formed, with length (to simplify the expression (x) is omitted):

$$C'K' = \frac{W_1}{W_0 + dW_0}\left[f + df - \left(\frac{f}{W_0} - \frac{dx}{D}\right)(W_0 + dW_0)\right] - dx$$

,

where $W_1(x) = W_0/tg(x)$ – the element's launch velocity with collapse. Let us demand that: $tg\alpha = K = const$, where K is the tangent of angle α at which one may purposefully influence the cloud's compactness or discreteness [3, 4].

Then, the initial relative deformation in the end of the collapse will be:

$$\varepsilon_0(x) = \frac{C'K'}{dx}. \qquad (1)$$

The cut-off $K''C''$ is determined by expression:

$$K''C''(x,t) = W_1(x)t(x) - W_1(x + dx)\left(t(x) - \frac{dx}{d}\right) - dx$$

But $\quad t(x) = t - \left(\frac{x}{d} - \frac{f}{W_0}\right).$

Then, the deformation may be expressed as:

$$\varepsilon(x,t) = \frac{K''C''(x,t) - \sqrt{dx^2 - df^2}}{\sqrt{dx^2 - df^2}}.$$

Finally, after transformations we obtain:

$$\varepsilon(x,t) = \frac{\frac{dW_1}{dx}\left(\frac{x}{D} + \frac{f}{W_0} - t\right) + \frac{W_1}{D} - \frac{f'^2}{2} - 2}{1 + \frac{f'^2}{2}} = [\varepsilon], \qquad (2)$$

where $[\varepsilon]$ – the stress-load deformation's marginal value for the lining material.

Then, the general time functional of cumulative lining collapse, accounting for the allowed lining material deformation will have the form:

$$T = \int_0^H S(x, f, f')dx \qquad (3)$$

where

$$S(x, f, f') = \frac{1}{D} + \frac{2}{D}\frac{f'\beta(2+\beta) - f\beta'}{\beta\sqrt{\beta(2+\beta)}} + \frac{1}{D}\frac{\beta'^2 - \beta''\beta'(2+\beta) + \beta'^2(1-\beta)}{\beta'^2} -$$

$$-\frac{(2+\beta)}{\beta'^2\sqrt{\beta(2+\beta)}} tg\alpha \frac{1}{D}\{(1+[\varepsilon])[\beta(2+\beta)(f''\beta' - f'\beta'') + (1-\beta)f'\beta'^2] -$$

$$-2(2+[\varepsilon])[\beta''\beta(2+\beta) - \beta'^2(1-\beta)]\}.$$

With the adopted symbols, Euler's equation will be [5]:

(4) $$S'_f - S''_{xf'} - S''_{ff'}\frac{df}{dx} - S''_{f'f'}\frac{d^2 f}{dx^2} = 0;$$

(5) $f(0) = f0;\ f(H) = fH,$

where H is the cumulative lining's altitude.

Since in the right-hand side of (3) x does not participate immediately, in the left-hand side of (4) the second term, $S''_{xf'} = 0$, is missing, and we can write the intermediate integral [5]:

(6) $$S - S'_{f'}\frac{df}{dx} = C_1,$$

which yields:

(7)

$$\frac{1}{D} + \frac{2}{D}\frac{f'\beta(2+\beta) - f\beta'}{\beta\sqrt{\beta(2+\beta)}} + \frac{1}{D}\frac{\beta'^2 - \beta''\beta'(2+\beta) + \beta'^2(1-\beta)}{\beta'^2} -$$

$$-\frac{1}{D} tg\alpha(1+[\varepsilon])(2+\beta)\frac{\beta(2+\beta)(f''\beta' - f'\beta'') + (1-\beta)f'\beta'^2}{\beta'^2\sqrt{\beta(2+\beta)}} - f'\{\frac{2}{D}\frac{\beta(2+\beta) - f(\beta')'_{f'}}{\beta\sqrt{\beta(2+\beta)}} +$$

$$+\frac{1}{D}\frac{1}{\beta'^4}\{\{2\beta(\beta')'_{f'} - (2+\beta)[(\beta'')'_{f'}\beta' + \beta''(\beta')'_{f'}] + 2(1-\beta)\beta'(\beta')'_{f'}\}\beta'^2 - 2[\beta'^2 -$$

$$
\begin{aligned}
&-\beta''\beta(2+\beta)+\beta^2(1-\beta)]\beta(\beta')'_{f'}\}-\frac{1}{D}tg\frac{\alpha}{2}(1+[\varepsilon])\frac{2+\beta}{\sqrt{\beta(2+\beta)}}\frac{1}{\beta^4}\{\{\beta(2+\beta)[f''(\beta')'_{f'}-\\
&-\left(\beta''+f'(\beta'')'_{f'}\right)]+(1-\beta)\left(\beta'^2+2f'\beta'(\beta')'_{f'}\right)\}\beta'^2-2[\beta(2+\beta)(f''\beta'-f'\beta'')+\\
&-(1-\beta)f'\beta'^2]\beta'(\beta')'_{f'}+\frac{2}{D}tg\frac{\alpha}{2}(2+[\varepsilon])\frac{2+\beta}{\sqrt{\beta(2+\beta)}}\frac{1}{\beta'^4}\{[\beta(2+\beta(\beta'')'_{f'}-\\
&-2(1-\beta)\beta'(\beta')'_{f'}]\beta'^2-2[\beta''\beta(2+\beta)-\beta'^2(1-\beta)]\beta'(\beta')'_{f'}\}=C_1
\end{aligned}
$$

where C_1 is the integration constant;

$\beta', \beta'', (\beta')'_{f'}, (\beta'')'_{f'}$ are derivatives of the stress-load coefficient.

As a result, the variational problem for time optimization of a pseudometeorite cloud cumulative charge effect is formulated and an intermediate integral (7) is obtained. The problem requires locating the unconditional maximum of functional (3) with edge conditions (5). The varied parameter is the function describing the inside surface lining profile. It makes no problem to change this varied parameter for another parameter of the cumulative charge geometry. The problem is interesting in that, in functional (3), there is an option to control the cloud's digitization rate by varying parameter $[\varepsilon]$.

References

1. Physics of Detonation. K.P. Stanjukovitch, Moscow, Science, 1973, 703.

2. H.I. Hristov, Ph.D. Thesis, Tula University, Tula, Russia, 1993, 146.

3. N. A. Zlatin, About Maximum Speeds of a Solid Condensed Cumulative Charge Jets. Problem of Mathematics and Mechanics. Novosibirsk, Science, 1983.

4. S. K. Godunov, A. A. Derybas, I. V. Maly, About Influencing Material Viscosity in the Process of Jets Formation at Impact of Metallic Laminas. - Physics of Combustion and Detonation. Novosibirsk, Science, 1975, No.1, 3-18.

5. J. B. Zeldovitch, A. D. Mishkis. Members of Applied Mathematics. Moscow, Science, 1967.

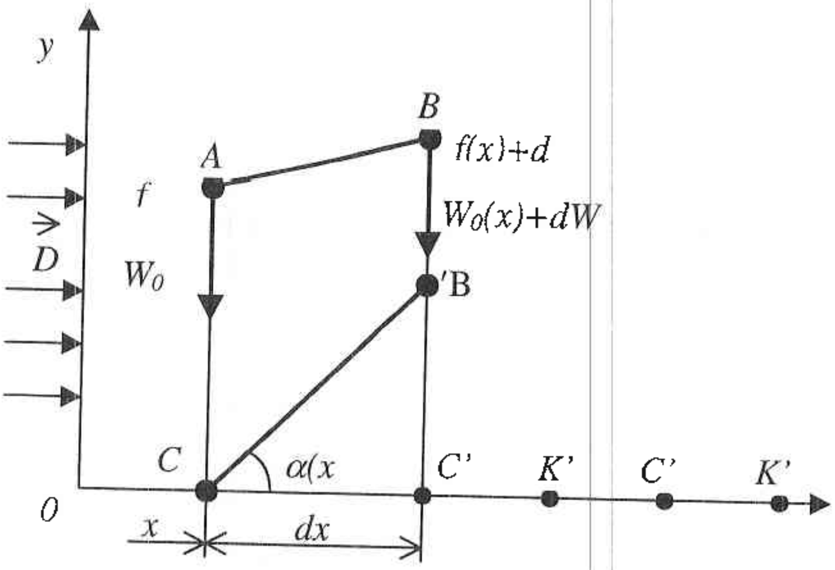

Fig. 1. The scheme of the initial and subsequent deformation of the cumulative lining.

ЗАДАЧА ЗА ОПТИМИЗАЦИЯ ПО ВРЕМЕТО НА ЕФЕКТА ОТ ДЕЙСТВИЕТО НА ПСЕВДОМЕТЕОРИТЕН ОБЛАК

Христо Христов, Виктор Баранов, Иван Гецов

Резюме

Формулирана е вариационна задача с безусловен екстремум за оптимизация на кумулативен заряд за псевдометеоритни частици по параметър максимално време на действие на облака от псевдометеоритни частици, изведено е уравнение на Ойлер и е получен промеждутъчен интеграл за параметъра на варирането – функцията на профила на вътрешната повърхност на облицовката.

Bulgarian Academy of Sciences. Space Research Institute
Aerospace Research in Bulgaria. 17. 2003. Sofia

PROBLEMS AND CONCEPTS OF THE DEVELOPMENT OF SOLAR POWER SATELLITES

Milen Zamfirov

Postgraduate student on the program
"Aerospace Methods in the Ecology and the Environment"
of the New Bulgarian University

Abstract

Solar radiation is a renewable and ecologically pure source of energy. The amount of solar power is huge but the use of that power for the production of electricity involves great difficulties, the major ones being the low density of solar radiation on the Earth's surface and the impermanent nature of that radiation (clouded skies, nighttime). A certain way to overcome those obstacles are the already developed energy accumulators and the combined solar-thermal energy systems, as well as the devices concentrating solar power and increasing its density. Unfortunately, these solutions are not widely applicable and are not competitive to conventional electric power stations. However, giving up ground-based solar electric power stations and placing them in a geosynchronous or low equatorial orbit would produce essentially different results.

1. Introduction

In 1968, P. E. Glaser [1], Head of the Technoscientific Department of the firm Arthur D. Little Inc. (USA) proposed a project for the development of a solar power satellite (SPS) on a synchronous orbit. The solar power satellite transforms solar radiation into electricity with the help of semiconductor photocells and sends the energy to the Earth as microwaves [2].

The SPS in Glaser's project has a number of merits: registration of the increased density of the solar radiation stream, dispersion of the thermal background in space (ruling out any danger of heat "pollution" of the Earth), lack of contact with the Earth's biosphere.

2. Current relevance

Currently, mankind uses annually about 10 billion tons of fuel and this figure is constantly rising – primarily in the developing countries which seek to provide to their citizens living conditions on a par with those in the highly developed nations [3]. In the USA, the daily per capita use of electric power is 10 kWh [4]. The consumption level in the developing nations is tens of times less while these countries account for 2/3 of the global population. If the tendency to close this gap continues, the total consumption of energy will grow several-fold and by the year 2020 it will reach 34 billion tons of fuel [5]. The steep rise of power generation is very dangerous: it could cause thermal "pollution" of the Earth and irreversible climate changes. Mankind's need of energy grows with the growth of technology. At present, fossil fuels provide the bulk of power: oil, natural gas and coal. But their deposits underneath the Earth's crust are not limitless. Given the current rate of explotation, they are bound to dry up in a few hundred years's time. Besides that, these fossils are needed by the chemical industries. Fossils can partially be replaced by nuclear fuel. The deposits of uranium are not limitless, either, while those of deuterium in the oceans are huge. In spite of that, no profitable controlled thermonuclear reactors have been developed so far. The use of all fuels enumerated on Table 1 [6], except for the solar and geothermal power station, pollutes the environment and harms Nature.

Table 1

Balance sheet of the output of electric energy in the world

Type	Per cent
Thermal electric power stations (coal, oil, natural gas)	63
Hydroelectric stations	19
Nuclear power station	17
Geothermal electric station	0,5
Solar, wind electric stations	0,1

The solution of the global ecological and power problems through pure energy is a serious and difficult task. One of the topical modern opportunities is the development of a project for building a system of solar power satellites. These discussions arise from the growing needs of ecologically pure power at the expense of the traditional power sources, which endanger the ecological balance.

3. SPS orbits

Powell [7] proposes launching of a platform with photocell panels onto a geosyncronous or solar-synchronous orbit, 35,800 km away from the Earth. At an angle of 23.5° between the orbit and the ecliptic, the panels will be illuminated by the Sun, which is the prime advantage of the SPS [8, 9]. A key problem is the location of the SPSs and their consumers. Glaser's original idea [1] was to launch geosyncronous equatorial orbit (GEO) actively controlled SPSs, containing solar panels and equipped with relay antennae; these would constantly face the Sun, sending directed microwave rays to ground-based reception stations (Fig.1)

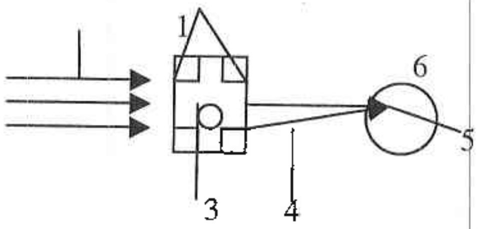

Fig. 1. 1 – solar radiation; 2 – photovoltaic cells; 3 – transmitting antenna; 4 – microwave beam; 5 – receiving station; 6 - Earth

A number of authors [10, 11, 12] propose the use of a low-earth-orbit (LEO) instead of GEO. This reduces the difficulty of transporting materials from the ground. In recent years, most intensive consideration [13, 8] was given to LEO and to orbits of the "Molniya" ("Lightning") type, the main problem being to deal with the economic aspect. On the one hand, LEO is a compromise as to the reduction of the difficulties and expenses inherent to GEO, and on the other, the technological and economic risks are easier to predict. The orbit of the "Molniya" type is a Russian satellite system of communication, which uses satellites along strongly eccentric orbits designed to establish radiocommunication between two ground stations [8]. Another widely discussed orbit is the one using a laser system for the transmission of energy (Fig.2). The slight divergence of the ray provides an opportunity to employ mirror relay stations of not big mass of size d. In this case of transmitting power to the ground the relay stations can operate on geosynchronous or high elliptical orbits and in this way it is enough for an SPS to be launched into a low solar-synchronous orbit which will allow to substantially reduce loss during transportation while establishing the station [8].

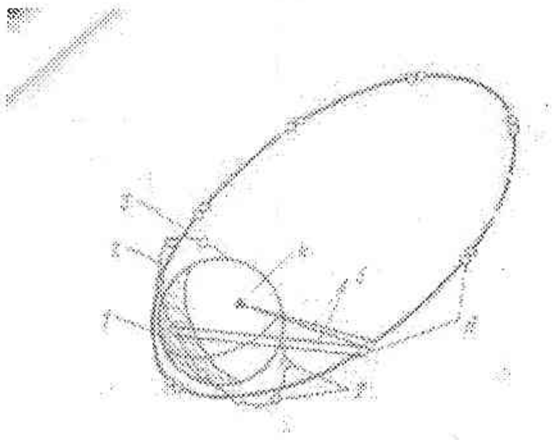

Fig. 2. (Lukuanov). 1 – Earth; 2 – SPS orbit; 3 – high elliptical orbit of the relay station; 4 – consumer; 5 – laser radiation; 6 – relay station; 7 – SPS.

3.1. Relaying reprocessed energy from an SPS

With the help of SPS's, enormous power (up to 10-15 GW or more) can be generated and relayed to any region of the Earth and the space around it.

The concentration of power, obtained from an SPS, and the possibility to transmit power from an SPS to reception stations situated at various places along the way of a rapid reorientation of the ray, allows for a considerable increase of the economic efficiency of the ground-based grid [14].

Types of systems for relaying power:

1. Relaying power through microwave radiation.
2. Relaying power through laser radiation.

1. *Transforming solar power on the basis of microwave rays (according to Grilihes)*

First version. Solar radiation is directly received by the surface of a converter, which generates electric power; this power is then concentrated using an electric commutation system and is transferred to the generator by a monochrome ray, and from there, via free space, to the transmitting system.

Second version. Transforming solar power into electricity using a generator of radio-frequency emission, which through waveguides is concentrated and is then brought to the receiving system-antenna.

Third version. Contains concentrators of solar radiation which:

i) transform it first into electric power and then into a directed monochrome ray;

ii) transform it directly into radiation within an optic or radio range.

Advantages:

- high efficiency of energy transformation;
- minimal losses in transmitting microwave radiation through the atmosphere.

Shortcomings:

- the great wavelength (10-12 cm) also presupposes great divergence of the ray which requires the establishment of large-area ground receiving stations;
- impossibility of transmitting energy to moving objects such as satellites, orbital transporting devices, etc;
- radio frequency interference is a real problem facing SPSs. It has become clear that SPSs will radiate so much energy that no communication system could operate in the 2.45 GHz sector at a distance of several kilometers from the receiving antenna on the ground [16].

2. Transmitting energy on the basis of powerful lasers

The specific peculiarities of the transformation of solar power into a laser beam have to do with the low density of solar radiation in the outer space, which presupposes the use of concentrators in the power emitting systems. But the theoretically attainable density of the stream of concentrated solar radiation does not exceed 16 mW/m^2 and is insufficient for effectively pumping the lasers [16]. An analysis of the suitability of various substances to be used as active media for SPS lasers with optical pumping indicates that these substances can be divided into three groups:

1. Admitting optical pumping and radiating in the visible range.
2. Permitting pumping by visible light and radiating in the infrared range.
3. Pumping and radiating in the infrared range.

In the first group are molecular substances J_2, Na_2, Br_2, Te_2, Li_2, HgBr and the lasers with solutions of organic dyes. In the second group are

CF_3J, $Br+CO_2$, J_2+CO_2; in the third are CO, CO_2, N_2O, HF, DF, G_2H_2. Of greatest interest are the substances of the third group and in particular CO, CO_2, N_2O. The examined substances of the first and second group have considerable disadvantages: the former necessitates an excessively high density of the radiated stream; and the latter features unacceptably low transformation efficiency because the energy transformed in the process of pumping exceeds considerably emitted energy. The only exception is the molecular compound CF_3J, which is regarded as one of the possible active media [9]. At the same time, the cited results cannot be considered final because the search for suitable working substances is going on.

Advantages:

- smaller ray divergence (1-10 micrometres)
- possibility of using mirror relay stations.

Shortcomings:

- high level of laser absorption by the Earth's atmosphere.

4. Modern projects

The USA is a historical leader in experimenting and demonstrating cableless energy transmission. Developments in radio in the 1950s have led to discussions on the development of microwaves in aviation. G. Brown [16] from Rayton Corp. with the assistance of the US Air Force was the first to construct a series of electrically powered helicopters for a demonstration of the advantages of microwave driving and directing flying vehicles (FV).

Nevertheless, the SPS projects were not implemented because no state was yet ready to fund such stations due to military estimates which indicated that such programs would be inoperable [16].

But the recent power black-outs in California made the USA take a fresh look at the power supply problem. Now the situation is rather complicated and the need of electricity needs is outrunning available resources. According to NASA's plan (www.sel.noaa.gov/info/SolarMax.pdf), in 2006-2007, the International Space Station will be used to test cableless power transmission. Besides, it is planned that at the same time the first trial electric station of 100 kW should be built. By 2011-2012, NASA plans the launch into outer space of a platform which would be essentially a megawatt electric station and would be capable of transmitting power both to other space vehicles and to the Earth. In future, the output of the electric station will grow and, according to preliminary calculations, in 15-20 years it will reach 10 MWatt (http://spacepwr.jpl.nasa.gov/solar.htm).

In 1994, Japan launched a 100-year plan called "Action Plan – Earth 21" [17]. It aims to reduce carbon dioxide in the Earth's atmosphere through the so-called carbon sinks. The program seeks to give electric power to photovoltaic systems based on the Earth and in space.

This blueprint [18] envisages the installation of systems, which could provide power from space to the world electric grid in 2040 at the earliest.

The ground plan envisages a series of solar power satellites, each of which will transmit 1GW of electric power to ground-based stations. The satellites will use microwave radiation of 2.45 GHz [18].

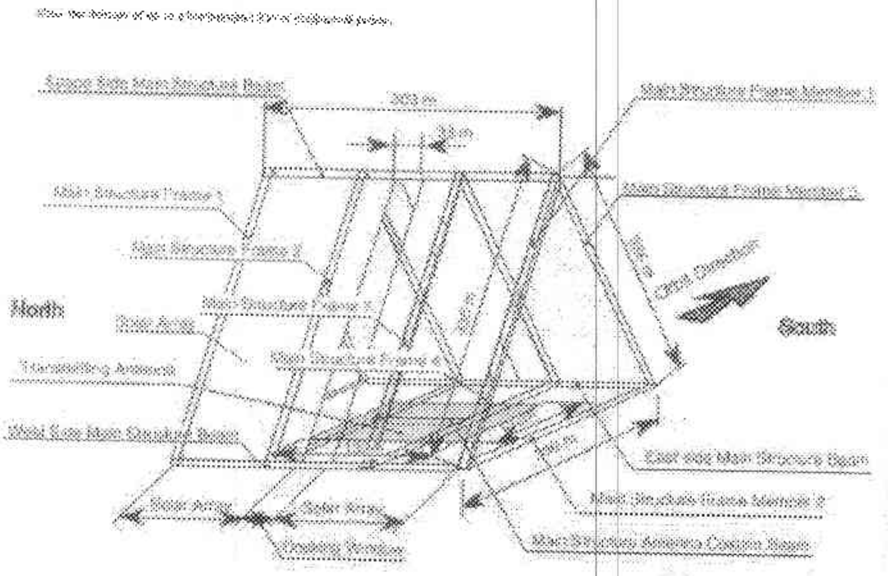

Fig. 3. (Nagamoto, Sasaki and Naruo)

SPS-2000 is a frame constructed of light aluminum in the shape of a triangular prism, sized approximately 300 m, carrying about 18 hectares of amorphous silicon batteries in a saddle-like configuration so as to render unnecessary active directing [19]. One square of the 130-metre phase transmitting antenna is connected to a satellite side facing the Earth in the lower part and provides about 10 MW of 2.45 GHz energy with a ray whose cross-section diameter is about 2 km to the Earth's surface [18]. The beam could be directed ± 30° to the West or to the East and can supply energy within 200 sec. to the receiving antenna within 3° of latitude from the equator. This provides for the supply of up to several hundred kW of continuous energy. A 1,100-km high equatorial orbit will be used. This choice minimizes transport expenses and the distance for transmitting energy from space [18].

5. Conclusion

SPS design and construction is a challenging techno-scientific task. Of the developed projects, the most discussed ones are SPSs processing solar power and transmitting energy in the form of microwave rays. Notwithstanding the large investments, the development of new branches of science and new technologies, the efficiency of the more-promising projects for the transmission of solar energy on the basis of powerful lasers is not as yet sufficiently well studied.

References

1. Glaser, P., Power from the sun: its future. Science, 1968, vol.168.
2. Glaser, P., Perspectives on satellite solar power. AIAA Pap.; New York, 1977.
3. Симеонова, К., Христов, Хр., Василев, Хр., Тодоров, С., Глобалните проблеми и България - Национален координационен център за глобални проблеми при БАН. София, 1999.
4. State of world. A worldwatch institute report on progress toward a sustainable society. New York, 1997.
5. Мировая энергетика: Прогноз развития до 2020 года. Под ред. Й.И. Страшинова, Енергия, Москва, 1990.
6. Ахмедов, Р., Нетрадиционные возобновляемые источники энергии. Хелиотехника, 1, Москва, 1990.
7. Powell, B., Spaceflight, X, New York, 1959.
8. Лукянов, А., Пленочные отражатели в космосе. Москва, 1997.
9. Подшивалов, В., Иванов, Е., Муратов, Л., Энергетические установки космических апаратов. Энергоиздат. Москва, 1981.
10. Prisniakov,V.F., Lyagushin, S. F., Statsenko, I. N, On the way to creating system of distant power sun for space vehicles. Solar energy, Special issue: Wireless Power Transmission. Vol.56, No 1.
11. Maryniak, G., Status of international experimentation in wireless power transmission. Solar energy, Special issue: Wireless Power Transmission, 56, No.1.
12. Collins, P., Purwanto.Y., Chuang, X., Future demand for microwave power from space in China and Indonesia. 49th IAF Congress, Sept.28-Oct.2, 1998, Melbourne, Australia.
13. Драбкин, Л., Солнечные электростанции. Физика, Москва, 1999.
14. Лучков, Б л., Солнечная энергетика. МИФИ. Москва, 2001.
15. Грилихес, В л., Солнечная энергия и космические полеты. Москва, 1984.

16. Osephuk, J., Health and safety issues for microwave power transmission. Solar Energy, Special issue: Wireless Power Transmission. Vol.56, No 1.

17. Nagamoto, M., An approach to develop space solar power as a new energy system for developing countries. Solar energy, Special issue: Wireless Power Transmission. Vol.56, No 1.

18. Nagamoto, M., Sasaki, S., Naruo, Y., Conceptual study of a solar power satellite, SPS 2000. Symposium on space technology and science. Yokohama, Japan, may 1994.

19. Matsuoka, H., Nagamoto, M., Collins, P., Global cooperation for equatorial SPS pilot plant. On clean and inexhaustible space solar power, Vienna, 27 July, 1999.

20. www.sel.noaa.gov/info/SolarMax.pdf

21. http://spacepwr.jpl.nasa.gov/solar.htm

ПРОБЛЕМИ И ИДЕИ ЗА РАЗВИТИЕТО НА СПЪТНИКОВИ СЛЪНЧЕВИ ЕЛЕКТРОЦЕНТРАЛИ

Милен Цветков

Резюме

Слънчевата радиация е възобновяем и екологично чист енергиен източник. Количеството на слънчевата енергия е огромно, но използването на този източник за производството на електричество е свързано с големи трудности, като основните са ниската гъстота на слънчевата радиация върху земната повърхност и непостоянният характер на тази радиация (облачност, нощ). Един от начините за преодоляване на тези пречки са вече разработените енергийни акумулатори и комбинираните слънчево-топлинни енергийни системи, както и устройствата за концентриране на слънчевата енергия и увеличаване на гъстотата ѝ. За съжаление, тези решения не са широко приложими и не са конкурентноспособни на обикновените електростанции. Отказът от наземните слънчеви електроцентрали, обаче, и поставянето им на геосинхронна или нискоекваториална орбита, може да доведе до съвсем различни резултати.

Bulgarian Academy of Sciences. Space Research Institute
Aerospace Research in Bulgaria. 17. 2003. Sofia

ANALYTICAL EFFECTIVE METHOD FOR VERIFICATION OF A SATELLITE PASS OVER A REGION OF THE EARTH SURFACE

Atanas Atanassov

Solar-Terrestrial Influences Laboratory, Stara Zagora Department

Abstract

An analytical method is proposed in this work for verification whether an artificial earth satellite during its orbital motion passes over a region of the earth surface. The method is based on undisturbed Keppler's approximation of the orbit and approximation of the region by a circular segment S. In order to define the situational condition, a conic surface is used with apex in the earth centre, cutting out the circular segment. The tangents of the conical surface with Keppler's plane determine the time intervals in which the satellite trace on the earth surface occurs inside the segment S. The transformation of these tangents in the plane of Keppler's orbit and the determination of their crossing points with Keppler's ellipse lies in the basis of the examined method.

1. Introduction.

A number of cases exist when, during space experiments, it is necessary to know the time of a satellite pass over a definite region of the earth surface. Thus, for example, in synchronous satellite and ground-based measurements, it is important when the satellite passes over a definite territory where the ground-based station is located. When problems of meteorological character are solved on the basis of sate-llite information, it is significant when the satellite is going to pass over a definite territory or a meteorological structure (cyclone centre, front). The solution of many other problems, connected with the study of the earth surface from space is connected with the determination of the temporal interval pass over a specific region. This is necessary in some of the cases for experiments planning. In other cases, the analysis is needed to schedule the seances for receiving satellite information. In both cases this is important for the quality of the conducted experiments, and from economical point of view.

The problem for determining a satellite pass over a definite geographic region has a standard solution. It is obtained on the basis of the imitation modelling by selecting a proper geometrical model for region V which determines the situational condition. The discretization of the solution of the artificial earth satellite motion equation and the respective analysis, as concerns the model of the region, allow to determine whether the satellite passes over the region as well as the moments of crossing its borders.

For the equation of the artificial earth satellite motion in geo-equatorial co-ordinate system (GeCS) we have:

$$(1) \qquad m\frac{d^2\vec{r}}{d\,t^2} = -\Sigma \vec{f}_k \ ,$$

with initial conditions $\vec{r}_0 = \vec{r}\,(t_0)$, $\frac{d\,\vec{r}}{dt} = \frac{d\,\vec{r}(t_0)}{dt}$, where $\vec{r}$ is the satellite radius-vector; m - its mass and t- the time. The specific form of (1) reflects the accepted motion model. The solution of (1) can be obtained on the basis of analytical or numerical methods [1,2] . In any case, a discretization of the solution of (1) is obtained:

$$(2) \qquad \vec{r}_{t_0} \ , \ \vec{r}_{t_1} \ , \ \vec{r}_{t_2} \ , \ \dots \ , \ \vec{r}_{t_n} \ , \ \dots$$

Usually (2) is obtained in GeCS or in orbital co-ordinate system (OCS). It is necessary to transform the solution of (1) into Greenwich co-ordinate system (GrCS):

$$(3) \qquad \vec{r}_{(GrKS)} = \alpha_{GrG} \cdot \vec{r}_{(GKS)}$$

In (3) α_{GrG} is the transformation matrix [3].

Problems exist in which region V is restricted by a complex outline contour (for example, a state border). There are known methods to present V and to solve the problem for crossing its borders by the sub-satellite trace [4]. Within the terms of different problems, the approximation of region V by a circular spherical segment of the earth surface is completely sufficient and substantiated both physically and of geometrical point of view. The application of such a simplifying situational condition in the discretization of the solution of the artificial earth satellite motion equation requires also considerable computation time.

The verification of the situational condition is made by a step in the time Δt and even within one satellite circle it is connected with a multiple repetition of the respective computation procedure. It is connected with considerable computational expenses. This paper suggests an analytical method to apply the verification procedure once for a whole period of the satellite circle.

2. Formulation of the Problem.

We shall examine the considered region of the earth surface as a spherical segment S (Fig. 1). It is cut out of the earth surface by a straight circular cone with angle ψ between the axis and the generant and its apex is in the earth centre. The crossing point of the cone axis with the earth surface has Greenwich co-ordinates (λ, Θ). Therefore, the segment can be described by the following parameters – angle ψ, earth radius $R_{\oplus}$ and the Greenwich co-ordinates λ and Θ, i.e. $S\ (\Psi, R_{\oplus}, \lambda, \Theta)$. Moving along with the earth surface, the cone tangents with the plane of Keppler's orbit at its two sides at moments t_1 and t_2. (Fig. 2). Between the two moments t_1 and t_2, the Keppler's plane and the conic surface intercross. This means that part of the Keppler's ellipsis is also restricted within the limits of the conic surface and that it is located over segment S.

We shall discuss an approach, allowing to obtain moments $\tilde{t}_1$ and $\tilde{t}_2$ when the satellite crosses the cone generants $\vec{\tau}_1$ and $\vec{\tau}_2$ which tangent with the Keppler's orbit.

The relation between the intervals (t_1, t_2) and $(\tilde{t}_1, \tilde{t}_2)$ on the time axis shows whether the artificial earth satellite passes over segment S (Fig. 3). If the two intervals intercross, then the condition for passing over the examined segment is fulfilled.

3. Construction of an algorithm.

Let's assume that segment S forms a tangent with K. For distance δ from the centre of S to K we can write down [5]:

$$(4)\qquad \frac{\vec{n}}{|\vec{n}|}(\vec{R}_C - \vec{x}) = \delta = \sin\psi . R_\oplus$$

or

$$(4')\qquad \vec{n}^0 \cdot \vec{R}_C = \sin\psi . R_\oplus$$

where $\vec{n}^0$ is the null vector of K, $\vec{R}_c$-is the radius-vector of the segment middle and $R_\oplus = |\vec{R}_c|$- the Earth radius. The radius-vector of the spherical segment centre $\vec{R}_c$ can be presented in the following way:

$$(5)\qquad \left|\begin{array}{l} X_c = R_\oplus \sin\Theta . \cos[\omega_z (t - t_0)] \\ Y_c = R_\oplus \sin\Theta . \sin[\omega_z (t - t_0)] \\ Z_c = R_\oplus \cos\Theta \end{array}\right.$$

In (5) $\omega_\oplus$ is the Earth angular rotation velocity and t_0 is appropriately selected epoch (for example, the moment when the artificial earth satellite passes through the orbit perigee). If we substitute (5) in (4') we'll obtain:

$$(6)\qquad A\cos\varphi + B\sin\varphi + C = 0,$$

where

$A = n_x . \sin\Theta$, $B = n_y . \sin\Theta$, $C = \sin\psi - n_z . \cos\Theta$, $\varphi = \omega_\oplus (t - t_0)$.

By solving (6) we determine $\vec{R}_c$ at the tangenting moments t_1 and t_2 as well as the very moments. Thus, for the tangent vector we can write down:

$$(7)\qquad \vec{\tau} = (\vec{R}_c \times \vec{n}) \times \vec{n}$$

Vector $\vec{\tau}$ is determined in (7) in GeCS . We make a transformation of $\vec{\tau}$ in OCS [3 :

$$(8)\qquad \vec{\tau}_{(OKS)} = \alpha_{OGe} \cdot \vec{\tau}_{(GeKS)}$$

In (8) the transformation matrix α_{OGe} has the following form [3]:

$\alpha_{11} =$ cosω . cosΩ - sin ω . cos i . cosΩ
$\alpha_{12} =$ cosω . sin Ω + sinω . cos i . cosΩ
$\alpha_{13} =$ sin ω . sin i

α_{21}= -sin ω . cosΩ - sinω .cos i . sin Ω
α_{22}= -sin ω . sin Ω + sinω .cos i . cosΩ
α_{23}= cosω . sin i

α_{31}= sin Ω . sin i
α_{32}= -cos Ω . sin i
α_{33}= cos i

After determination of the tangent vector $\vec{\tau}$ in K , we can determine its crossing points with Keppler's ellipse in OCS:

$$(9) \qquad \frac{(\xi+c)^2}{a^2} + \frac{\eta^2}{a^2(1-c^2)} = 1 \;\; , \; \eta = k \cdot \xi$$

In the second equation of system (9) k signifies the tangent's coefficient in OCS. The following relation exists between the orbital co-ordinates (ξ,η) and the eccentric anomaly E [1]:

$$(10) \qquad \left| \begin{array}{l} \xi = a\,(\cos E - c\,) \\ \eta = a\,\sqrt{1-e^2}\cdot\sin E \end{array} \right. ,$$

where a is the large orbital semi-axis, e - is the eccentricity. On the other side, on the basis of Keppler's equation we can write down:

$$(11) \qquad t = t_0 + (E - e \,.\, \sin E\,)/\lambda$$

After we find out the eccentric anomaly E in (10) and substitute it in (11), we determine the moments when the satellite crosses the specified tangents.

4. Estimation of the Method.

The explained method is analytical and it is presented by final formulae. It is reduced to a single application of the respective calculation procedure within the limits of one satellite circle. After correction of the orbital elements, the procedure can be repeated for the next interval of time. The examined method is based on a situational condition whose geometrical model is reduced to the determination of tangents $\vec{\tau}_1$ and $\vec{\tau}_2$ in GeCS. The transformation of the tangents in OCS is equivalent to the transformation of the situational condition in the orbital plane [6].

A structural approach is applied for the method algorithmization. Based on a programme complex for situational analysis, developed for solution of the problems in [6], it was necessary to add two new sub-programmes for ensuring the treated situational problem. This means that the development of algorithms for situational analysis, based on the transformation of the situational conditions to Keppler's plane is facilitated by the presence of common sub-problems. In our case and for these in [6] this is the crossing of a straight line with Keppler's ellipse.

The following cases are possible for one Earth rotation around its axis:

- with sufficient orbital inclination equation (6) has four roots which leads to determination of four tangents connected with two crossings of segment S with Keppler's plane;
- with smaller orbital inclination equation (6) has two solutions which determine two tangents, corresponding to one crossing of segment S with K;
- with small orbital inclination segment S doesn't cross K.

The correction of the orbital elements of each satellite circle on the basis of the selected model of disturbances allows to apply the presented approach for situational analysis within long interval of time. Considering the effectiveness of the computation procedure, even for a long interval of time the computation expenses are much less than by verification along the orbit, performed with a step. The method is applicable in the cases when Keppler's approximation in the terms of the satellite's circle period is admissible with a view to the solved problem. For solving practical problems in many cases this is executed.

The offered method for determination of a satellite pass over a region of the earth surface, represented by a circular segment, as well as the examples, given in [6], are connected with a transformation of the situational condition in the plane of Keppler's orbit. Analogous to these examples, there are others, which allow to develop an analytical computation procedure, applicable within the terms of one period of the satellite circle. Such situational tasks, for example, are connected with a satellite pass through the shadow of the Earth, the Moon (a central body or its natural satellite). Analogous explanation can be made for the situational tasks for determination of a satellite pass through the impact wave, the magnetopause and the neutral layer, which are exceptionally important in the design of experiments of the type of INTERBALL [7].

References

1. Абалакин, В., Е. Аксенов., Е. Гребеников., Ю. Рябов., Справочное руководство по небесной механике и астродинамике, М., "Наука", 1971, 584с.
2. Эльясберг, П., Введение в теорию полета искуственных спутников Земли., М , "Наука", 1965.
3. Эскобал, П., Методы определение орбит., М., "Мир", 1970.

INSTRUCTIONS TO AUTHORS

The Aerospace research in Bulgaria series publishes original articles in the theoretical or applied fields of space and aviation science and practice.

Conditions:

- The articles should be submitted in duplicate in English language. Bulgarian authors should also supply Bulgarian version for verification of the translation.
- Each article should be accompanied by diskette or CD containing text and figures
- Manuscripts (including tables and references) should not exceed 15 standard pages (30 lines per page, 60 strokes per line) typed on font "Times New Roman" , font size 12. Paper in standard office format A4 with margins: top –8.2 cm, bottom- 2 cm, left and right –4 cm.
- Each article should have a summary (up to 15 lines) in English and Bulgarian languages.
- The articles should not be published, neither submitted for publication elsewhere.
- Measurement unites should be used only according to SI.
- Authors have to accomplish one proof–reading within term specified by the publishers. Only type –setting errors are subject of correction.

Arrangement:

- Title page. The first page of each article should indicate the title, the author's names and the Institute where the was conducted.
- Tables and Illustrations. Tables and captions to illustrations should be submitted on separate sheets. The proper place of each figure in the text should be indicated in the left margin of the corresponding page. All illustrations (photos, graphs and diagrams) should be referred to as "figures" and given in abbreviations "Fig.". The author's name, the number of the figure with indication of its proper orientation (top, bottom) should be slightly marked on the back on each figure. All illustrations should be submitted in duplicate too.
- References. They should be indicated in the text by giving the corresponding number in parentheses. The references should be typed on a separate sheet, arranged chronologically by number figuring in the text. The name of the first author should be given with inversion. The title of the article is followed by that of the journal (collection), volume, year of publication, issue number and the pages cited. The titles of the monographs should be followed by the city, year of publication and the cited pages.

Example:

1. Krustanov L., K.Serafimov- Proc.BAS, XX , 1974, vol.2, p. 29
2. Nestorov G. Physics of the low ionosphere. S., BAS,1969, p. 63

Address The authors may submit articles in person or send them to the following address:

Editorial Board
Aerospace Research in Bulgaria
Space Research Institute
Bulgarian Academy of Sciences
6, Moskovska St., 1000 Sofia, Bulgaria

ISSN 0861-1432

УКАЗАНИЯ ЗА АВТОРИТЕ

В тематичната поредица „Аерокосмически изследвания в България" се отпечатват оригинални научни статии от областта на аерокосмическата наука и практика.

Условия:

• Статиите трябва да бъдат представени в 2 екземпляра на английски език. Българските автори трябва да представят статиите си и на български език.

• Статиите на английски език трябва да се представят на дискета или CD.

• Обемът на статията (включително таблиците и литературата) не трябва да превишава 15 стандартни машинописни страници (30 реда на страница, 60 знака на ред). При компютърен вариант – шрифт "Таймс ню роман", 12 пункта. Формат на печатното поле 13/20 см. Отгоре 8.2 см, отдолу 2 см., ляво, дясно по 4 см. Формат А4

• Всяка статия трябва да бъде придружена от резюме (до 1/2 стандартна страница) на български и на английски език.

• Материали, прести за печат или публикувани в други издания, не се приемат.

• Мерните единици задължително да бъдат по СИ.

• Авторите преглеждат една коректура в определен срок. Допускат се само поправки на грешки, направени при набор

Подреждане:

• На първата страница на всяка статия трябва да бъдат написани заглавието, имената на авторите и месторАботата.

• Таблици илюстрации. Таблиците и текстът към илюстрациите трябва да се представят на отделни страници. Мястото им в текста да се посочи в полето на съответната страница. На гърба на илюстрациите (фотоси, чертежи, графики и др.) с молив да се напишат заглавието на статията, имената на авторите, номера на фигурата и да се посочи ориентацията.

• Литература. Цитираната литература се представя на отделен лист по номерация, появяваща се хронологично в текста. Името на първия автор се дава с инверсия. Следват заглавието на статията, заглавието на списанието (сборника), том, година, книжка, страница, а при монографиите — град, издателство, година, страница.

Пример: Нов пример !

1. Кръстанов, Л. К. Серафимов. - Сп. на БАН, XX, 1974, №2, с. 29.
2. Несторов, Г. Физика на ниската йоносфера. С., БАН, 1969, с. 63.

Адрес. Авторите могат да представят лично материалите си или да ги изпратят на адрес:

София 1000
ул. „Московска" № 6
Институт за космически изследвания — БАН
Редакционна колегия на „Аерокосмически изследвания в България"